

**ALMA MATER STUDIORUM - UNIVERSITÀ DI BOLOGNA**

---

**SCUOLA DI INGEGNERIA E ARCHITETTURA**

DICAM

Dipartimento di Ingegneria Civile, Ambientale e dei Materiali

International Master Course in Civil Engineering

**FINAL DISSERTATION**

in

Structural Strengthening & Rehabilitation

**Analysis of an innovative slim floor composite beam conformed  
by a custom GFRP pultruded profile and reinforced concrete.**

CANDIDATO:

*Pedro Ospina*

RELATORE:

*Chiar.mo Prof. Andrea Benedetti*

Anno Accademico 2012/2013

Sessione III



For the ones that remained...



## **Acknowledgments**

Among all the people that have contributed to my education as an engineer and, most importantly, as a human being, my loving family stands high above. Their unconditional support and teaching has paved this long and laborious road to my success and it is for this reason that they deserve this work entirely. Just to give them a piece of pride and a handful of joy, because nobody deserves it more than them.



# Table of Contents

Introduction.....	- 1 -
List of Symbols and Acronyms.....	- 3 -
Chapter 1: Fiber Reinforced Polymers .....	- 6 -
1.1 Literature Review .....	- 6 -
1.2 Mechanical Behavior.....	- 7 -
1.2.1 Micromechanical analysis .....	- 7 -
1.2.2 Macromechanical analysis.....	- 8 -
1.3 Pultruded GFRP cross sections .....	- 14 -
1.3.1 Mechanical and general properties .....	- 14 -
1.3.2 Normal stresses.....	- 14 -
1.3.3 Shear stresses .....	- 16 -
1.3.4 Deflection .....	- 16 -
1.3.5 Connection.....	- 17 -
1.4 Composite steel-concrete structural elements .....	- 18 -
1.4.1 Cross section analysis.....	- 19 -
Chapter 2: The GFRP-RC Composite beam.....	- 24 -
2.1 Description of the element .....	- 24 -
2.2 Analysis of the GFRP-RC beam .....	- 25 -
2.2.1 Material properties.....	- 25 -
2.2.2 Determination of the neutral axis .....	- 25 -
2.2.3 Shear stress distribution at the cross section .....	- 27 -
2.2.4 Loading actions considered .....	- 26 -
2.2.5 Serviceability Limit State .....	- 27 -
2.2.6 Ultimate limit state .....	- 29 -
2.3 Fire analysis.....	- 33 -
2.4 GFRP pultruded deck.....	- 39 -

2.5	The connection .....	- 40 -
Chapter 3: Finite Element Model Simulation.....		- 42 -
3.1	The software .....	- 42 -
3.2	GFRP-RC composite beam and composite slab simulation.....	- 42 -
3.2.1	Two dimensional model .....	- 44 -
3.2.2	Three dimensional model .....	- 47 -
Chapter 4: Comparison of results .....		- 48 -
4.1	GFRP-RC composite beam .....	- 48 -
4.1.1	Neutral axis.....	- 48 -
4.1.2	Flexure effects in the beam.....	- 48 -
4.1.3	Shear stresses .....	- 50 -
4.1.4	Deflection .....	- 52 -
4.1.5	Slip Strain .....	- 53 -
4.1.6	Fire Analysis.....	- 54 -
4.1.7	Bolted connection .....	- 55 -
4.2	GFRP Deck composite slab.....	- 56 -
4.2.1	Neutral Axis.....	- 56 -
4.2.2	Flexure induced stresses .....	- 56 -
4.2.3	Longitudinal shear stress .....	- 57 -
Chapter 5: Conclusions and Recommendations .....		- 60 -
5.1	The GFRP-RC composite beam.....	- 61 -
5.2	The composite slab.....	- 62 -
List of Figures .....		- 63 -
List of Graphs .....		- 63 -
References.....		- 65 -
Books.....		- 65 -
Research publications.....		- 65 -

Design codes and standards.....	- 69 -
Annex.....	- 74 -

# Introduction

Italy, a country which has given birth to so many advances in engineering, has been the scenario for a vast number of constructions that have been left as record of its history, marking forever each overwhelming era. In recent history, the old quarters of many cities are still mostly made up of ancient houses which maintain functioning services. Just as humans, structures are troubled by the effects of time, where, subjected to constant loading, corrosion and accidental actions, its integrity and strength can't be assured forever. Therefore, structural engineers have supplied themselves with the latest technology in materials and science to overcome this issues in the most efficient manner while portraying its historical significance.

Geographically trapped in a seismic region, these ancient constructions are constantly exposed to the lateral loading effects of earthquakes. One famous example is the small town of L'Aquila, which most of its historical center was seriously compromised and forced its inhabitants to evacuate their houses permanently. One of the possible solutions, for those allowed or worth the trouble, was to rehabilitate and strengthen the structures' foundations, its brick walls and its wooden trussed beams. Even more, ancient military and bell towers, with slender structural configurations, absorbed intense seismic forces, resulting into a variety of longitudinal, transversal and diagonal cracks.

Over the last few decades, new materials such as Fiber Reinforced Polymers (FRP) have become the main solution for the strengthening of damaged structures. These materials are mainly used because of their extreme lightness, strength and ease of application. Carbon Fiber Reinforced Polymers (CFRP) have been widely used as an on-site intervention solution, with the scope of increasing the stiffness and ultimate strength of the remaining structural elements. Its excellent mechanical properties are counteracted by its high cost, specialized work force and low productivity; which has ultimately limited its versatility.

As a more monolithically structural element, pultruded profiles made from Glass Fiber Reinforced Polymers (GFRP) have been developed. Due to its process of fabrication, it has opened a door of unlimited possibilities by means of simple shape molding of the profile's cross section, making its customization possible. Called a die, this heated mold joins the glass fibers from a roving and induces the curing of the polymer resin, maintaining the longitudinal direction of the fibers and the desired shape of the profile. As a continuum, this process creates

an infinitely long element with a constant cross section that allows the customer to cut each element to the desired length. The pultrusion technology and its process, has allowed the material to be industrialized by producing structural profiles in marketable quantities at lower costs, thus becoming a competitive product. The mechanical behavior of pultruded elements are ruled by an orthotropic law of mechanics, making it perform differently in function of the direction of the load, and therefore, extra care is needed when using it for structural purposes.

Every structural material has been known to have its strengths and weaknesses. Where steel has great strength and stiffness, it has a high specific weight and is vulnerable to buckling and fire. Reinforced concrete elements are stocky and stiff with great resistance to fire but low strength and excessive volume that translates into weight. Finally, FRP has excellent strength, great stiffness, with extremely low specific weight but a brittle behavior and it is practically useless in case of fire. This has led to develop composite structural elements by joining structural profiles made from different materials and, ultimately, building an eclectic and efficient structural system.

For many years, steel-concrete composite structures have been used all over the world for building frames and limited span bridges. Its efficiency has been widely proven: each material strengthens the weakness of its counterpart providing the final structural product with stiffness, strength, stability, ductility and resistance to fire. Among the different composite profile configurations developed over the years, the Slimflor® system has portrayed an interesting solution, both in an engineering and an architectural point of view, by embedding the entire steel profile in the reinforced concrete. Following this principle, a composite structural element has been proposed, conformed of a customized GFRP pultruded profile and reinforced concrete, following the Slimflor® configuration and structural mechanism.

# List of Symbols and Acronyms

FRP – Fiber reinforced polymer

GFRP – Glass fiber reinforced polymer

CFRP – Carbon fiber reinforced polymer

CLT – Classical laminate theory

FSDT – First-order shear deformation theory

ENA – Elastic neutral axis

PNA – Plastic neutral axis

SLS – Serviceability Limit State

ULS – Ultimate Limit State

ROM – Rule of Mixtures

FEM – Finite Element Method

$L_{cb}$  – Length of the composite beam

$d_{slab}$  – Effective depth of the slab

$b_w$  – Web width of the composite beam

$b_{slab}$  – Width of the composite slab

$A_{tr}$  – Area of transversal reinforcement

$\rho_{tr}$  – Transversal reinforcement ratio

$S_{ij}$  – Stiffness of the lamina

$Q_x, Q_y, Q_z$  – First moment of area

$I_x, I_y, I_z$  – Second moment of area

$A_{cb}$  – Total cross sectional area of the composite beam

$D_{sc}$  – Dowel resistance of a stud

$\tau_{sc}$  – Resistance of the shear stud shank  
 $f_{ck}$  – Characteristic compressive strength of concrete  
 $f_{cd}$  – Design compressive strength of concrete  
 $f_{ct}$  – Tensile strength of concrete  
 $f_{ctm}$  – Means tensile strength of concrete  
 $f_{yk}$  – Characteristic yield strength of steel  
 $f_{yd}$  – Design yield strength of steel  
 $\gamma_c$  – Reduction factor for concrete  
 $\nu_{xy}, \nu_{xz}, \nu_{yz}$  – Poisson ratio  
 $E_x, E_y, E_z$  – Elastic modulus  
 $E_s, E_c, E_p, E_f, E_m$  – Steel, concrete, FRP, fiber, matrix elastic modulus  
 $G_{xy}, G_{xz}, G_{yz}$  – Shear modulus  
 $k$  – Shear deformation amplification factor  
 $n$  – Modular ratio  
 $V$  – FRP Composite total volume  
 $V_m$  – Matrix volume ratio  
 $V_f$  – Fibers volume ratio  
 $V_{xy}, V_{yz}, V_{xz}$  – Tangential shear force  
 $\sigma_x, \sigma_y, \sigma_z$  – Normal axial stress in the global axes  
 $\sigma_1, \sigma_2, \sigma_3$  – Normal axial stress in the local axes  
 $\varepsilon_x, \varepsilon_y, \varepsilon_z$  – Normal axial strain in the global axes  
 $\varepsilon_1, \varepsilon_2, \varepsilon_3$  – Normal axial strain in the local axes  
 $\tau_{xy}, \tau_{xz}, \tau_{yz}$  – Tangential shear stress

$\gamma_{xy}, \gamma_{xz}, \gamma_{yz}$  – Tangential shear strain

$\theta_{xy}$  – Rotational strain due to torsion

$\alpha$  – Angle difference between the local and the global axes directions

$\chi_x, \chi_y, \chi_z$  – Curvature of the middle surface

$y_k$  – Distance to the k-th lamina

$\delta_y$  – Deflection of the beam

# Chapter 1: Fiber Reinforced Polymers

## 1.1 Literature Review

Fiber Reinforced Polymers (FRP) were developed at the mid of the 20<sup>th</sup> century in order to replace metallic materials, where the principle problem in Aerospace Engineering is gravity, these new materials provided the same strength and stiffness at a fraction of the weight. These materials (very similar to reinforced concrete) are formed of continuous aligned fibers embedded in a polymer matrix. The purpose of the matrix is to hold the fibers aligned in order to make them work as a whole, where fibers provide the great majority of the strength and stiffness, the matrix provides resistance to shear stresses. There exists a variety of fibers as well as a variety of matrices, being two the main branches: thermoset and thermoplastic polymers. Inside the thermoset branch, resins are the most widely used, presented as epoxy, phenolic and polyester. It is thanks to the vast options of fibers and polymer matrices that FRP is a highly efficient structural system designed to suit our problems accordingly.

Over the years, Carbon Fiber Reinforced Polymers (CFRP) and Glass Fiber Reinforced Polymers (GFRP) have grown to be the most widely used structural materials over many engineering fields. Starting in Aerospace Engineering and expanding to Mechanical Engineering, to finally introduce its versatility to Civil (Structural) Engineering. These last decades have been a preset for research and development, focusing its use on civil infrastructures strengthening. Currently, pultrusion technology is the most promising FRP structural system to compete with steel and reinforced concrete structures, especially for low height building frames and limited span bridges.

The pultrusion process is simple, efficient and maintains a high level of product quality, this last being crucial for the analysis and design of a structure which relies on its mechanical properties consistency. By means of a mechanical puller, placed at the end of the process, fiber rovings are submerged in a resin bath, guided and aligned to finally enter a heated die that both cures the resin and shapes (or molds) the structural element to the desired shape, exiting as a constant cross section element which is cut by a saw to the desired length. Besides the longitudinal (principal horizontal axis) rovings, a strand mat that surrounds the element is placed as shear reinforcement. The process can be appreciated at Figure 1.

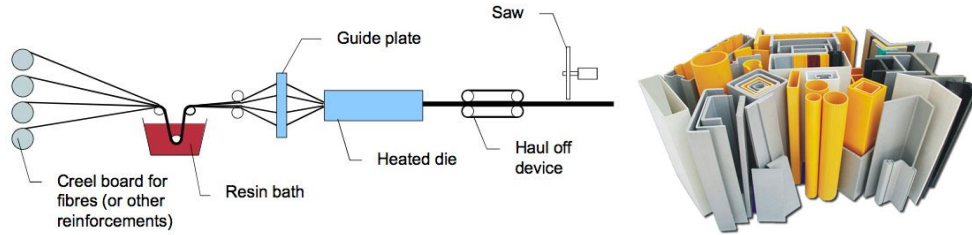


Figure 1. Pultrusion production process and variety of profiles.

## 1.2 Mechanical Behavior

FRP has a particular mechanical behavior, where its properties are divided into two approaches: the micromechanical and the macromechanical level, being both approaches equally important in the understanding and the correct estimate of the resistance of its structural elements. From this point forward, the axes considered will be taken as seen in Figure 2.

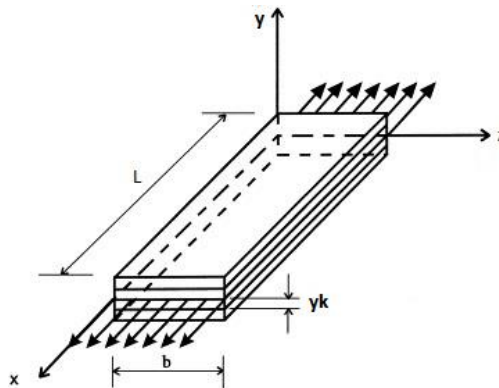


Figure 2. Unidirectional laminate subjected to normal stress.

### 1.2.1 Micromechanical analysis

The micromechanical theory focuses on the interaction between individual fibers and the matrix surrounding them, where the main aspect is the adhesion at their interface, therefore, its main role is to assure a proper transfer of stresses from the matrix to the fibers. This approach is used for lamina design, it being a single row of fibers placed longitudinally and surrounded by a polymer matrix, forming a very thin plate. This is the simplest way of representation of an FRP and is the basis for the design of pultruded FRP elements, taking much attention to its orthotropic mechanical properties that come with it. By means of area ratios (percentage of the

total cross sectional area) between the fiber and the matrix, the elastic properties are calculated. Called the “Rule of Mixture”, the elastic modulus for each axis direction is given by:

$$E_x = E_f V_f + E_m V_m \quad (1.1)$$

$$E_z = \frac{E_f E_m}{V_m E_f + V_f E_m} \quad (1.2)$$

$$\nu_{xz} = \nu_m V_m + \nu_f V_f \quad (1.3)$$

Where:

$$V_f = \frac{A_f}{A} ; V_m = \frac{A_m}{A} \quad (1.4)$$

A is the total area of the lamina’s cross section and the areas of each material inside the composite. The assumptions taken for this analysis to be real are: perfect bonding between the two materials, which permits to assume a uniform strain along the x-axis direction and uniform stress in the z-axis direction.

## **1.2.2 Macromechanical analysis**

### **1.2.2.1 The lamina**

#### **1.2.2.1.1 Stress-strain relationship**

Where an anisotropic material is considered to have a behavior which will vary depending on each possible vector of load application, there is coupling between all of its 36 constants which represent the membrane and bending deformations in each axis by influence of the external loads, keeping in mind that there are no planes of symmetry. The stress-strain relation of anisotropic materials can be represented by its mechanical relationship between the stresses, strains and its 36 independent constants:

$$\begin{Bmatrix} \sigma_x \\ \sigma_y \\ \sigma_z \\ \tau_{yz} \\ \tau_{zx} \\ \tau_{xy} \end{Bmatrix} = \begin{bmatrix} c_{11} & c_{21} & c_{31} & c_{41} & c_{51} & c_{61} \\ c_{12} & c_{22} & c_{32} & c_{42} & c_{52} & c_{62} \\ c_{13} & c_{23} & c_{33} & c_{43} & c_{53} & c_{63} \\ c_{14} & c_{24} & c_{34} & c_{44} & c_{54} & c_{64} \\ c_{15} & c_{25} & c_{35} & c_{45} & c_{55} & c_{65} \\ c_{16} & c_{26} & c_{36} & c_{46} & c_{56} & c_{66} \end{bmatrix} \begin{Bmatrix} \varepsilon_x \\ \varepsilon_y \\ \varepsilon_z \\ \gamma_{yz} \\ \gamma_{zx} \\ \gamma_{xy} \end{Bmatrix} \quad (2)$$

When dealing with two planes of symmetry with a third plane perpendicular to them, we can establish a reduced matrix with only 9 independent constants representing the stiffness of an orthotropic material:

$$\begin{Bmatrix} \sigma_x \\ \sigma_y \\ \sigma_z \\ \tau_{yz} \\ \tau_{zx} \\ \tau_{xy} \end{Bmatrix} = \begin{bmatrix} c_{11} & c_{21} & c_{31} & 0 & 0 & 0 \\ c_{12} & c_{22} & c_{32} & 0 & 0 & 0 \\ c_{13} & c_{23} & c_{33} & 0 & 0 & 0 \\ 0 & 0 & 0 & c_{44} & 0 & 0 \\ 0 & 0 & 0 & 0 & c_{55} & 0 \\ 0 & 0 & 0 & 0 & 0 & c_{66} \end{bmatrix} \begin{Bmatrix} \varepsilon_x \\ \varepsilon_y \\ \varepsilon_z \\ \gamma_{yz} \\ \gamma_{zx} \\ \gamma_{xy} \end{Bmatrix} \quad (3)$$

Introducing the engineering constants: the elastic modulus (E), shear modulus (G) and the Poisson ratio ( $\nu$ ) we obtain:

$$\begin{Bmatrix} \sigma_x \\ \sigma_y \\ \sigma_z \\ \tau_{yz} \\ \tau_{zx} \\ \tau_{xy} \end{Bmatrix} = \begin{bmatrix} E_{xx} & -E_{yy}/\nu_{yx} & -E_{zz}/\nu_{zx} & 0 & 0 & 0 \\ -E_{xx}/\nu_{xy} & E_{yy} & -E_{zz}/\nu_{zx} & 0 & 0 & 0 \\ -E_{xx}/\nu_{xz} & -E_{yy}/\nu_{yz} & E_{zz} & 0 & 0 & 0 \\ 0 & 0 & 0 & G_{xx} & 0 & 0 \\ 0 & 0 & 0 & 0 & G_{yy} & 0 \\ 0 & 0 & 0 & 0 & 0 & G_{zz} \end{bmatrix} \begin{Bmatrix} \varepsilon_x \\ \varepsilon_y \\ \varepsilon_z \\ \gamma_{yz} \\ \gamma_{zx} \\ \gamma_{xy} \end{Bmatrix} \quad (3.1)$$

Where:

$$G_{yz} = \frac{E_{yy}}{2(1+\nu_{yz})} ; G_{zx} = \frac{E_{zz}}{2(1+\nu_{zx})} ; G_{xy} = \frac{E_{xx}}{2(1+\nu_{xy})} \quad (4)$$

$$\nu_{yz} = \frac{\varepsilon_z}{\varepsilon_y} ; \nu_{zx} = \frac{\varepsilon_x}{\varepsilon_z} ; \nu_{xy} = \frac{\varepsilon_y}{\varepsilon_x} \quad (5)$$

For the case of a plate, the normal stress in the y-axis and shear stress resistance in the yz-plane and xy-plane can be neglected since they are considerably smaller compared to the ones in the xz-plane. With this in mind, we consider a lamina as a plate by setting the final matrix to describe its strength under plane stress, with 3 independent constants:

$$\begin{Bmatrix} \sigma_x \\ \sigma_z \\ \tau_{xz} \end{Bmatrix} = \begin{bmatrix} E_{xx} & -E_{zz}/\nu_{zx} & 0 \\ -E_{xx}/\nu_{xz} & E_{zz} & 0 \\ 0 & 0 & G_{xz} \end{bmatrix} \begin{Bmatrix} \varepsilon_x \\ \varepsilon_z \\ \gamma_{xz} \end{Bmatrix} \quad (3.2)$$

To compare it with an isotropic material such as steel (with 2 independent constants), the matrix representation is:

$$\begin{Bmatrix} \sigma_x \\ \sigma_z \\ \tau_{xz} \end{Bmatrix} = \begin{bmatrix} E_x & -E_x/\nu_x & 0 \\ -E_x/\nu_x & E_x & 0 \\ 0 & 0 & G_{xz} \end{bmatrix} \begin{Bmatrix} \varepsilon_x \\ \varepsilon_z \\ \gamma_{xz} \end{Bmatrix} \quad (3.3)$$

### 1.2.2.2 Classical Laminate Theory

In order to determine the stiffness of the lamina, by means of classical laminate plate theory, the relationship between the materials deformations and the external loads applied to it. Paying attention that this theory establishes the axial strains according to the middle surface of the lamina and the shear strains are related to the extremes of the plate, forming the angles of curvature. As the name of the theory says, when considering the element as a plate, some degrees of freedom are not considered, them being:  $\varepsilon_y, \gamma_{xy}, \gamma_{yz}, \chi_y$ . The reason for this assumption is done by reasoning that their values are significantly smaller compared to the main degrees of freedom, resulting into insignificant variations of the final results. The matrix representation of the lamina becomes:

$$\begin{Bmatrix} \varepsilon_x \\ \varepsilon_z \\ \gamma_{xz} \\ \chi_x \\ \chi_z \\ \theta_{xz} \end{Bmatrix} = \begin{bmatrix} a_{11} & a_{31} & a_{51} & b_{11} & b_{31} & b_{51} \\ a_{13} & a_{33} & a_{53} & b_{13} & b_{33} & b_{53} \\ a_{15} & a_{35} & a_{55} & b_{15} & b_{35} & b_{55} \\ b_{11} & b_{31} & b_{51} & d_{11} & d_{31} & d_{51} \\ b_{13} & b_{33} & b_{53} & d_{13} & d_{33} & d_{53} \\ b_{15} & b_{35} & b_{55} & d_{15} & d_{35} & d_{55} \end{bmatrix} \begin{Bmatrix} N_x \\ N_z \\ V_{xz} \\ M_x \\ M_z \\ T_{xz} \end{Bmatrix} \quad (6)$$

Where the axial strain is the variation of deformation over its length in its own axis, the shear strain is due to the angle formed between the ratios of the variation of deformation in function of its perpendicular axis, rotating according to its middle surface. Where two shear strains exist in each plane, the final shear strain is the sum of these two angles. The curvature is the rotation of the middle surface due to the bending moment and the twist is the rotation due to an applied torque. The matrix of constants which does the coupling between the different loads actions have been divided into three sub matrices. The “a” matrix contains the shear-extension coupling coefficients, matrix “b” (symmetric) the bending-extension coupling coefficients and finally the “d” matrix the bend-twisting coupling coefficients. This approach is commonly known as the Kirchhoff-Love Plate theory.

### 1.2.2.3 First-order Shear Deformation Theory

Following the principles of Timoshenko and the original Reissner-Mindlin plate theory, the shear deformations can play a significant role due to the low shear stiffness modulus (G) that FRP materials have and, therefore, the missing factors for shear can be introduced by means of the first-order shear deformation theory (FSDT). This factors account for the two missing shear strains in equation (6) and can be represented in a separate matrix, allowing to have both CLT and FSDT as needed. This type of deformation is important when dealing with shear deformations in a beam, being bending moments and in-plane shear deformation much more crucial that out-of-plane deformations like warping (in the case of torque). Since it has been considered that CLT is an acceptable approach for practical purposes. The additional matrix is:

$$\begin{Bmatrix} \gamma_{yz} \\ \gamma_{xy} \end{Bmatrix} = \begin{bmatrix} h_{44} & h_{64} \\ h_{46} & h_{66} \end{bmatrix} \begin{Bmatrix} V_z \\ V_x \end{Bmatrix} \quad (6.1)$$

Called the transverse shear stiffness matrix, the “h” matrix is used when these two shear strains want to be accounted as part of the total deformation of the laminate. When summing up the contribution of each lamina, the “h” coefficients of the matrix are calculated by equation (8.3).

#### 1.2.2.4 The laminate

The analysis of the laminate, it being the staking of various laminae (a sequence of laminas) and focusing on the mechanical contribution of each lamina to the laminate. This laminate, or even laminates, will eventually take the shape to become a pultruded element, where its resistance is calculated by means of these approach.

To counteract the orthotropic weakness behavior of each lamina, they are combined together at different angles to generate a final laminate that is able to withstand all type of stresses coming from external loading in its three main directions. The sequence of staking depends on the direction of the fibers, the symmetry and the balance of the laminae combination, as seen in Figure 3.

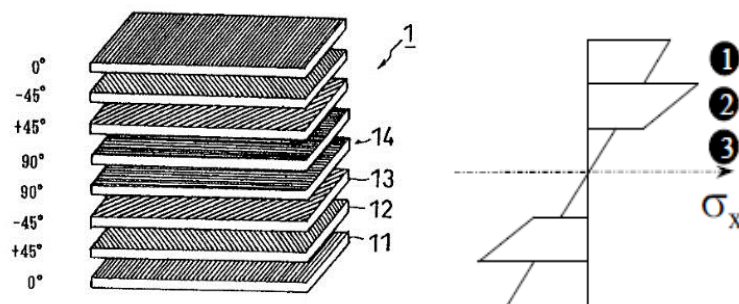


Figure 3. Laminae distribution of a multi-directional laminate.

To account for the contribution of each lamina to a laminate, as well as the contribution from each lamina, a transformation matrix is needed. By means of this matrix we can consider the local direction of each lamina and place its contribution to the global coordinates. By simple trigonometry, a relationship between the vector components in the local axis can be represented to the global axis and hence the transformation matrix is obtained. To avoid confusion, the global axis have been renamed, where the (x,y,z) used to represent the local axis of each lamina, it has been replaced by (1,2,3), and hence we get:

$$\begin{Bmatrix} \varepsilon_1 \\ \varepsilon_3 \\ \gamma_{13} \end{Bmatrix} = \begin{bmatrix} \cos^2 \alpha & \sin^2 \alpha & -2 \sin \alpha \cos \alpha \\ \sin^2 \alpha & \cos^2 \alpha & 2 \sin \alpha \cos \alpha \\ \sin \alpha \cos \alpha & -\sin \alpha \cos \alpha & \cos^2 \alpha - \sin^2 \alpha \end{bmatrix} \begin{Bmatrix} \varepsilon_x \\ \varepsilon_z \\ \gamma_{xz} \end{Bmatrix} \quad (7.1)$$

$$\begin{Bmatrix} \gamma_{23} \\ \gamma_{12} \end{Bmatrix} = \begin{bmatrix} \cos \alpha & -\sin \alpha \\ \sin \alpha & \cos \alpha \end{bmatrix} \begin{Bmatrix} \gamma_{yz} \\ \gamma_{xy} \end{Bmatrix} \quad (7.2)$$

To avoid incompatibility of deformations, involving fracture mechanics, the bonding between laminae must be considered as perfect. With this as a starting point, we can simply sum the stiffness (S) contribution of the k-th lamina to the total stiffness matrix  $\begin{bmatrix} a & b \\ b & d \end{bmatrix}$  and we can get a global matrix system that represents the laminate's stiffness. To do so we use the equations:

$$a_{ij} = \sum_{k=1}^N (S_{ij})_k (y_k - y_{k-1}) \quad (8.1)$$

$$b_{ij} = \frac{1}{2} \sum_{k=1}^N (S_{ij})_k (y_k^2 - y_{k-1}^2) \quad (8.2)$$

$$d_{ij} = \frac{1}{3} \sum_{k=1}^N (S_{ij})_k (y_k^3 - y_{k-1}^3) \quad (8.3)$$

$$h_{ij} = \frac{5}{4} \sum_{k=1}^N (S_{ij}^*)_k \left[ t_k - \frac{4}{t^2} \left( t_k y_k^2 - \frac{t_k^3}{12} \right) \right] \quad (8.4)$$

This final step allows the acquisition of the laminate's stiffness in its global reference axes, which in turn becomes the beam element as a whole, therefore, we can calculate its resistance under different types of loading; just as beams for building frames. Essentially, suppliers of FRP pultruded profiles give an extensive quantity of strength and resistance properties that permit engineers to calculate the required sizing of beam members. This data can be appreciated at the documents located at the Annex.

## **1.3 Pultruded GFRP cross sections**

### **1.3.1 Mechanical and general properties**

The combination of fiber and matrix type permits to design an FRP element with a vast range of possibilities, permitting to control the level of stiffness, strength, ductility, corrosion resistance, fire resistance, etc. Needless to say, the higher the mechanical properties of the material, the higher the costs. For example, GFRP elements range their elastic modulus values between 20 and 30 [GPa], making it very compatible to concrete which has a very similar range of stiffness values. As for the strength, it is unfortunate that its behavior is brittle, which is highly undesired because of its unexpected failure. Nevertheless, the strength values range between 250 and 350 [MPa] which is comparable to the strength of steel. As for the specific weight of this material, the ranging values go from 16 to 19 [kN/m<sup>3</sup>] which is up to seven times lighter than steel and around 50% lighter than reinforced concrete, making the montage quite easy.

The weakest link of this type of members is its resistance to fire, where a diversity of polymeric coatings can reduce the flammability and smoke generation, it doesn't change the effect of temperature to the matrix, which basically turns it useless after 350 degrees Celsius and a reduction of strength of about 50% after only 250 degrees Celsius. The problem arises from the glass transition temperature of the matrix resin, where, once it is reached, the material is decomposed. This leaves the fibers working independently, leading to a progressive failure up to the total failure of the element.

Fortunately, besides the vulnerability of glass fibers to water absorption, the corrosion resistance of these pultruded elements are excellent thanks to the polymer's capabilities to enclose the fibers by not permitting water and other chemicals to degrade the material. This is the reason why it has become highly attractive in the use of bridge girders.

### **1.3.2 Normal stresses**

Over the last decades, a variety of companies have developed an industrialized market that provides pultruded elements made from GFRP with an enormous supply and variety of geometrical profiles, mechanical properties, length, etc. In addition, some companies even provide services for the development of personalized cross sections, fitted to the design and desire of the customer. Each company has accompanied its technology with deep research and testing over their products, in order to assure their mechanical behavior to customers, up to the point of providing design codes and handbooks. The most common cross sections are the ones

commonly used in structural steel, such as I and H-shaped, as well as rectangular and circular hollow tubes, up to the point of hollow sandwich deck slabs. Even through the pultrusion process is not based on joining of separate laminas (to form a laminate), its behavior is analyzed as such. The variety of profiles offered by Creative Pultrusions can be seen at the Annex.

For the case of pultruded structural elements, we can pass from the analysis of a laminate to the simplified theory of resistance of materials; widely used for structural steel and reinforced concrete beam elements. Using the equation of curvature and the relationship that it has to normal strains:

$$\chi_z = \frac{M_z}{E_x I_z} \quad (9)$$

$$\varepsilon_x = \chi_z y \quad (10)$$

Being (M) the bending moment, (y) the distance from the neutral axis to the desired point of analysis and (I) the second moment of area (commonly known as moment of inertia). Equaling these two equations we can get the normal stresses present in each point along the height of the beam:

$$\sigma_x = \frac{M_z \cdot y}{I_z} \quad [MPa] \quad (11)$$

The complexity of the material can make differences in resistance not only for each varying axes but also for the direction of application of the load, meaning that it behaves differently under tensile and compressive stresses. For example, Creative Pultrusions indicate a 10% increase of strength for compressive normal axial stress compared to tensile normal axial stress.

When dealing with the design values of its resistance, some manufactures and general building codes have reduced its characteristic bending moment resistance by 50% but in some cases, such as in deck systems, a reduction factor of 8 is used.

### 1.3.3 Shear stresses

For the case of shear stresses in the cross section, the equation presented by Zhuravskii, where (V) is the vertical shear, (Q) is the first moment of area and (b) the width of the cross section:

$$\tau_{yz} = \frac{V_y Q_z}{I_z b_w} \quad [MPa] \quad (12)$$

In a general case, thin walled cross section beams such as I-beams have the majority of their shear stress concentrated in the web, where its maximum is located at the centroid of the cross section.

The resulting stress from this equation is equal for both the vertical (yz-plane) and the horizontal (xz-plane or longitudinal) shear stress since it must be fulfilled for equilibrium. When analyzing such shear stresses in the longitudinal direction we can find the weakest point of a pultruded beam, since its strength only depends on the strength of the matrix between the lines parallel to the fibers. To counteract this weakness, production companies have included a strand mat of discontinuous fibers that surrounds the longitudinal section to form a 45 degree reinforcement.

The materials sensibility and weakness to shear stress, due to the matrix and not to the fibers, has obliged design guides and codes (either made by manufacturing companies or by government institutions) to reduce its resistance by a factor of 3. For the case of pultruded decks, a massive 75% decrease is introduced, or in other words, the design shear resistance of a pultruded element is one fourth of the calculated resistance value.

### 1.3.4 Deflection

When analyzing the deflection of pultruded beams, flexure beam theory of Euler-Bernoulli is no longer applicable due to the sensitivity of the material to shear deformations. These characteristics coming from shear strains have demonstrated to contribute considerably to the beam's deflection. Therefore, Timoshenko's flexure beam theory is needed to account this effect. The first theory establishes that the angle of rotation of the beam (the first derivative of the deflection function) is equal to the curvature of the cross section (the inverse of the radius of curvature), where Timoshenko's theory establishes that these two angles are not equal, and

thus generating a total deflection from the bending moment alone plus a shear deformation. The beam's differential equation under a distributed load (q) becomes:

$$q(x) = E_x I_z \left( \frac{d^4 y}{dx^4} + \frac{1}{k A_{cb} G_{xy}} \frac{d^2 q}{dx^2} \right) \quad (13)$$

The shear coefficient (k), defined as an incremental factor that is the ratio of the maximum shear stress divided by the mean shear stress in the cross section, can also be calculated by  $k = 10(1 + \nu)/12 + 11\nu$  (Eq.14) for a rectangular solid cross section. Solving the differential equation with the proper boundary conditions with fixed end supports, the deflection equation was obtained and used to calculate its maximum, located at mid-span of the beam:

$$\delta_{y,max} = \frac{qL_{cb}^2}{8} \left( \frac{L_{cb}^2}{48 E_x I_z} + \frac{1}{k A_{cb} G_{xy}} \right) \quad (15)$$

Consider the discrepancy between this calculation and the one used by CLT, which in reality uses the same assumptions as Euler-Bernoulli beam criteria and hence, the use of FSDT is once again needed to keep consistency in the analysis.

### 1.3.5 Connection

There are two types of connections for pultruded elements: a bonded connection by means of an adhesive, a bolted connection with supporting pressure plates or a mixture of the two. Adhesive joints have been proven to have great resistance but of catastrophic sudden failure, which sets engineers into a doubtful thinking. Even though the bonded connection can withstand higher loads than the bolted one, its failure happens in the element and not in the connection; where fracture happens due to shear stresses in the element's layer (thinking of it as the separation between laminas) close to the adhesive. Therefore, the strength of the bonded joint actually depends on the interlaminar shear strength of the GFRP pultruded material.

Bolted connections follow the same type of failure as the one seen in bolted connection analysis for steel profiles, with the difference that the orthotropic characteristics of the material make it more complex to analyze. The principal failure types that need to be calculated to assure the

proper resistance of the connection, and the weakest link of these five possible failures becomes the leading resistance value of the bolted connection:

- Shear failure due to tension, characterized by a perpendicular line passing through the hole.
- Cleavage or splitting of the extremity, occurring parallel or perpendicular to the line of loading.
- Bearing failure due to compressive stress concentration.
- Shear-out failure that follows the line of the hole up to the border of the element.
- Shear failure of the bolt, which can be either made of steel or even of FRP material.

Pultruded GFRP structural elements have proven to have excellent mechanical characteristics, some considerable weaknesses and great manageability (thanks to its very low specific weight), but a reduced experience of its use and real life testing (specially for long-term behavior) has introduced uncertainty in engineers criteria, leading them to punish its strength with massive reduction factors.

#### **1.4 Composite steel-concrete structural elements**

The use of composite structures have been developed with great success as an efficient system, permitting building frames to be light, cover long spans and increase construction productivity. Among a diversity of different steel-concrete composite systems, the Slimflor® beam system has proven to solve not only the basic problems in structural engineering but also increase the fire resistance of the structure, as well as becoming more architecturally appealing. Figure 4 gives a good representation of the final product and its conforming parts.

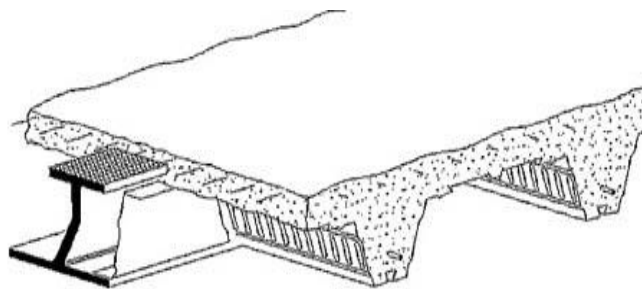


*Figure 4. Steel-Concrete asymmetrical slim floor composite beam.*

The procedure to its construction consists on the placement of the steel beam, called an asymmetric beam due to the difference of size of the flanges' width. Once the beam has been joined properly to the column through a welded or bolted connection, the steel deck can be placed on top of the lower flange, transversal to the beam's axis. The upper steel grid reinforcement is placed and, finally, the concrete is poured. Once the concrete has hardened, the composite beam element is conformed according to the design and it can perform its job accordingly.

#### **1.4.1 Cross section analysis**

When analyzing the behavior of a composite beam a variety of factors must be taken into account, such as: the end support, its performance for negative and positive bending moment, its behavior at the elastic phase as well as for the plastic one. Even more importantly, the composite behavior between the two materials depend of their slipping interaction, which turns it into a key factor. Meaning that, to assure the composite monolithic behavior of the structural element, a proper shear connection must exist between them, otherwise, its real behavior will be very different.

##### **1.4.1.1 Neutral axis**

For the case of a beam with fixed supports, the inversion of flexural stresses make the beam perform in very different ways, where for positive bending moment (sagging) the lower flange is in tension, the concrete, the upper steel beam's flange and the steel reinforcement are working in compression. For negative bending moment (hogging), the lower flange must work in compression with some support from the concrete surrounding the web, these being equilibrated by the top reinforcement and the upper flange of the steel beam (both working in tension). Design guides recommend that the tensile resistance of concrete must be neglected for Ultimate Limit State analysis. Figure 5 shows the location of the two plastic neutral axis in that particular beam since it changes depending on the beam's characteristics.

Considering all of the previously mentioned facts, this type of composite beam has three different neutral axes:

- The elastic neutral axis (ENA) used for Serviceability Limit State (SLS) verifications, set at the centroid of the composite beam's cross section can be calculated by means of area distribution by reaching an equivalent modulated area. This approach homogenizes the cross section as if it was conformed of one single material by means of increasing

the area of the steel elements so to develop the same resistance as if it was made of concrete. This modular ratio is obtained by dividing the materials' elastic moduli:

$$n = \frac{E_s}{E_c} \quad (16)$$

- The plastic neutral axis (PNA-) for hogging bending moment (negative bending moment set at the supports) which is obtained by finding an equilibrium point between the ultimate compressive and tensional forces that provide each material.
- The plastic neutral axis (PNA+) for sagging bending moment (positive bending moment with its maximum at mid-span) it is determined in the same manner as for hogging bending moment but with the stresses inversed and considering the changes resulting from the cracked concrete when it is neglected.

Usually, the PNA(+) is placed at the slab's height of the T-shaped composite beam and the PNA(-) at mid-height of the web. Certainly, the placing of these axes depend on a variety of reasons, but principally on geometric and mechanical properties of the cross section and the materials, respectively. The importance of these factors is high since they are the base for all the continuing calculations which are dealt with next.

#### **1.4.1.2 Shear interaction**

The efficiency of these composite system depends on the shear interaction that both materials have to assure that they are working together, especially considering the fact that, being materials with very different stiffness and strength values, their deformations diversify, resulting in a slip between the two elements. For the Slimflor® system, there is contact shear interaction (along the web's and top flange's perimeter) with a mean value of 0.6 [MPa] according to [4], but in the case of a needed increase in shear interaction, vertical shear studs can be welded on top of the steel beam's top flange or elsewhere. For this purpose, three scenarios are present in any given section:

- Full shear interaction: the whole composite beam works together harmonically as if it was a single homogeneous cross section with a single curvature angle.
- Partial shear interaction: both materials work together with a limited slip that establishes a curvature to each cross section but sharing some of the total deformation. In other words, creating a jointed single second moment of area (inertia) but having

different curvatures. It has been proven that, the loss of shear interaction due to slip, projects into small losses in resistant bending moment.

- No shear interaction: Each material element works independently, having independent curvatures. This system is not possible in reality unless oil or frictionless materials are used at the interface.

When shear studs are present, either on the top flange or in the web, they are resisted by the dowel action resulting from the concrete surrounding it. Obtained as an empirical equation from push-out tests, [3] has estimated the maximum dowel resistance of a single shear stud. Another check must be done to assure that the failure doesn't come from the shearing of the steel rebar. Therefore, the minimum of the two will lead the design:

$$D_{sc,max} = 0.5 A_{sh} \sqrt{f_{cd} E_c} \quad (17.1)$$

$$\tau_{sc,max} = 0.8 A_{sh} f_u \quad (17.2)$$

#### 1.4.1.3 Resistant bending moment

Once the PNA is known, by equilibrium to rotation, the ultimate resistant bending moment of the composite beam can be estimated. Needless to say, separate calculations must be performed for hogging and sagging resistant bending moment, taking into consideration the use of the proper PNA. Figure 5 shows the stress block distribution of the materials at its ultimate (plastic) state, where the concrete's parabolic representation is simplified by a reduced rectangular one.

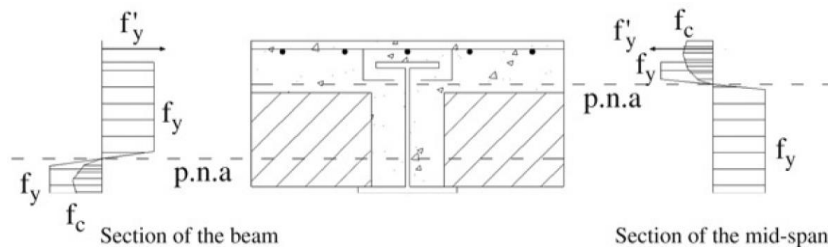


Figure 5. Hogging and sagging plastic stress-block distribution.

#### 1.4.1.4 Resistant shear force

The resistance of the composite beam to shear stress has been simplified by only considering the contribution of the steel beam, and not only that but considering only the contribution of the web. By means of this approach, a big safety margin is achieved, which is highly desirable since shear failure can occur suddenly and in a brittle manner. Some authors have considered possible the contribution of the concrete trapped between the flanges, which, in the case of negative bending moment, not only it is partly in compression but also confined. Some authors and codes consider it to be too unreliable and prefer to focus on the steel section only.

#### 1.4.1.5 Transverse resistance

In the transverse direction (yz-plane), the beam section that conform the composite slab, are part of the T-shaped composite beam's flange, which is submitted to a hogging bending moment. This hogging bending moment is resisted by the slab's transverse shear reinforcement that comes from the reinforcing grid. Equally, the vertical shear resistance of the slab must be verified, considering that it's a resistant element without shear reinforcement. From Eurocode 2, the vertical shear resistance is given by:

$$V_{Rd} = \left[ 0.18 \left( 1 + \sqrt{\frac{200}{d_{slab}}} \right) (100 \rho_{tr} f_{ck})^{1/3} \right] \frac{b_{slab} d_{slab}}{\gamma_c} \quad (18)$$

Where ( $d_{slab}$ ) is the effective depth of the slab, ( $\rho_{tr}$ ) the flexural reinforcement ratio and ( $b_{slab}$ ) the width, which is taken as 1 meter. The safety factor  $\gamma_c$  has a given value of 1.5.

As for other shear resistance verification, the composite T-beam's flange must be checked for transverse resistance (in the xy-plane), specially for the fact that its thickness (the slabs thickness) can be quite low, ranging from around 80 to 100 [mm]. The shear strength verification in the slab is its resistance to longitudinal axial stresses resulting from the bending moment in the yz-plane, where the composite beam's web joins the flanges. To calculate this resistance, [3] has given the equation:

$$V_{xy} = 0.66 f_{ct} d_{slab} + 0.8 A_{tr} f_{yr} + 0.8 \sigma_z L_{cb} \quad (19)$$

Where the first term is the contribution of concrete to shear, the second is the dowel action contribution of the slab's flexural reinforcement and the third is the friction contribution due to the compressive stress ( $\sigma_z$ ) chord in the slab which comes from the bending moment in the transverse direction. This stress has a compressive value and placed at the lower part of the slab/T-beam flange.

## Chapter 2: The GFRP-RC Composite beam

The complete analysis of the proposed beam has been done by comparing the results between a Finite Element Method model (FEM) and simple hand calculations done in an Excel spreadsheet. The objective of this is to understand how reliable hand calculations can be and, therefore, possibly use them as a reliable tool for future designs. Figure 6 shows the representation of the proposed GFRP-RC composite beam and the given name to each geometric property, which follows as well for the Excel calculation program. First, the Excel program will be dealt with in order to calculate a diversity of parameters and mechanical effects. Keeping in mind that the only one which depends entirely on the FEM simulation is the fire situation due to its time-step variable. However, some tools can help predict the resulting effect of fire after a 60 minute exposure.

### 2.1 Description of the element

The proposed composite beam has been formed from a base of a customized pultruded GFRP beam formed of an asymmetric I-beam with a continuous shear connector composed of a vertical extension of the web. For sake of simplicity, this extension of the web ( $hf$ ) will be referred as “the fin” by analogy of a fish, and the final composite beam will be referred as GFRP-RC beam. The top extreme of the fin will give the total height of the GFRP-RC beam, and hence, the slab. To support the transversal steel bars, U-shaped milling or perforated holes can be performed on the fin. The grid reinforcement will consist of transversal steel bars and, supported over these, the longitudinal steel bars.

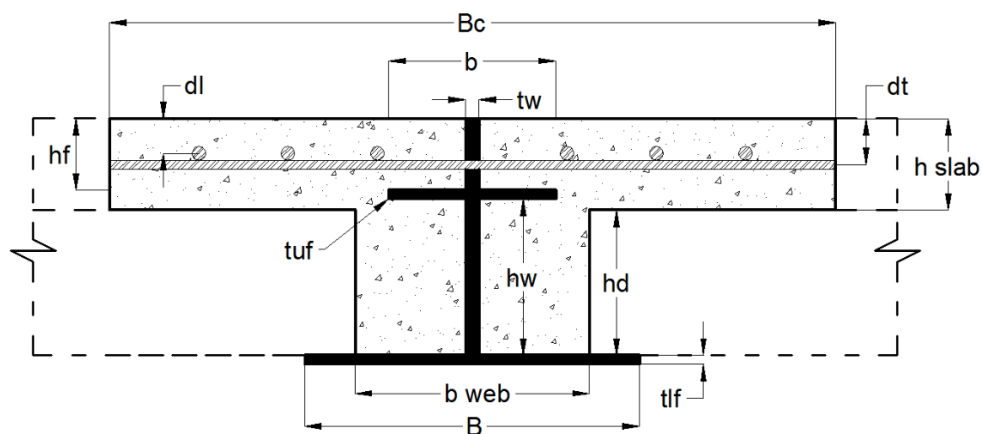


Figure 6. Cross section geometric parameters of the GFRP-RC composite beam.

For the structural analysis, this is the GFRP-RC beam's configuration but the reality of its shape is obtained when a GFRP pultruded deck is placed over the lower flange of the GFRP pultruded beam, which latter will be part of the composite slab. This matter will be dealt with on the next chapters but it's important to keep it in mind to understand the construction process that makes this final composite beam possible.

The type of end support has been considered as fixed-fixed by following the research done by [55]. For hand calculations (Excel), supposing that each space of the cross section at the support connection has no rotation is not real, starting with the fact that the GFRP profile, having a bolted connection in its web and no connection to its flanges, in reality is working as a simply supported structural element. The concrete and steel reinforcement may be considered as part of a fixed connection, but being submitted to a negative bending moment (tensile axial stresses at the top of the beam), makes it quite complex to estimate its real behavior. Therefore, the only part that makes this system work as a fixed system is the longitudinal reinforcement.

Focused in the analysis of the lower bound potential resistance of the proposed composite FRP-RC beam, common pultruded profiles were chosen (from Creative Pultrusions company) and concrete of the lowest acceptable strength,  $f_{ck} = 20 [MPa]$ . The chosen values for the geometric dimensions were chosen according to common limiting distances seen of slim floor examples presented at [4]. Refer to the Annex for the complete data used in the analysis as well as the material data provided by the manufactures of the GFRP pultruded profiles.

## **2.2 Analysis of the GFRP-RC beam**

### **2.2.1 Material properties**

Considering that the GFRP-RC composite beam has three different materials, the ROM approach was used to determine a unique elastic modulus and its mechanical properties. To do so, equations (1.1), (1.2) and (1.3) were used.

### **2.2.2 Determination of the neutral axis**

As mentioned in the literature introduction, the neutral axes of a slim floor composite beam are three. There is one elastic neutral axis and two plastic ones as presented in Figure 7, where the two plastic neutral axes vary for the hogging and sagging bending moment. They are different due to the assumption that the tensile contribution of concrete is zero and only for sagging bending moment the compressive concrete was accounted. For the hogging bending moment, the compressive concrete trapped between the flanges is not accounted. For sake of simplicity, they have been named as PNA(+) and PNA(-) which clearly refers to the sign of the bending

moment at which the beam is subjected to. After obtaining these three axes, we can proceed to the calculation of the beam's mechanical properties for each neutral axes, such as the first and second moment of area and the radius of gyration. It is interesting to notice how close together the PNA(+) and the ENA are, which, in raw words, can be said that the cross section has a “constant” behavior from zero loading up to failure for sagging bending moment. For the analysis of the ENA, the uncracked cross section is considered, which makes a difference in the calculation of the second moment of area.

It is very important to consider that this approach can drastically change if the neutral axes fall into places different to the ones seen in Figure 7, where, if the ENA is placed on the web or the PNA(-) at the flange, will represent unreal results. As an assumption, due to generally seen results, the neutral axes have been expected to be placed at each ranged zone. In other words, the use of these beams for other purposes other than the ones explained, is outside the scope of this thesis.

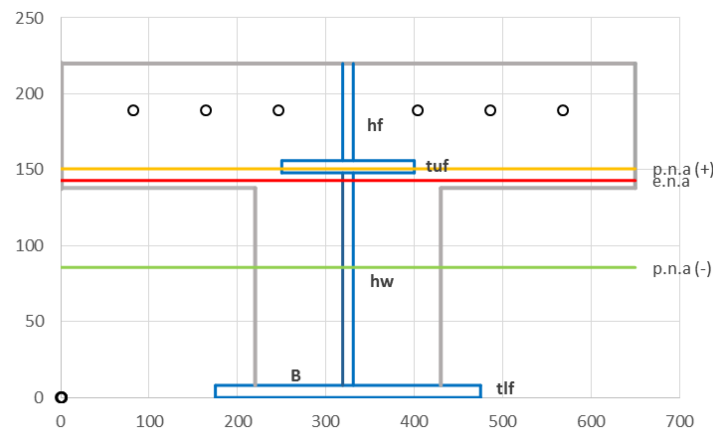


Figure 7. Placing of the neutral axes in the GFRP-RC composite beam.

### 2.2.3 Loading actions considered

Following the code's loading principles, they were estimated for the analysis of the beam. Starting with the permanent actions of the different parts that conform the GFRP-RC composite beam, it was appreciated that the weight of the GFRP pultruded profile is extremely low with just 0.18 [kN/m<sup>2</sup>]. To account for a variety of possible permanent loads such as the gypsum board (dealt with later) and miscellaneous, a 0.5 [kN/m<sup>2</sup>] was given. For the variable actions, a 1.5 [kN/m<sup>2</sup>] is given by the code. To estimate the participating area coming from the slab, a

contributory symmetric length was placed equal to 5 meters. This length will be the same for the composite slab's beam analyzed latter. This analysis can be appreciated at the Excel spreadsheet located in the Annex.

### 2.2.4 Shear stress distribution at the cross section

Using Equation (12) the shear stress distribution over the cross section was estimated, with an expected maximum at the point where the flange and the web meet since it represents a point for concentration of stresses. By looking at Figure 8, the difference between the average shear stress (the vertical line) over the cross section and the maximum are very different, resulting into incremental values of shear deformation. This ratio gives the value of the constant  $k$ , applicable in Equation (15) so to determine the maximum deflection. Since the three axes are placed at different parts of the beam, it can be seen how their maximum values can drastically change. This effect is seen especially at the ULS phase where the plastic neutral axes are very different among each other. As the figures show, the shear stress for the case of sagging bending moment is much higher than for the hogging case.

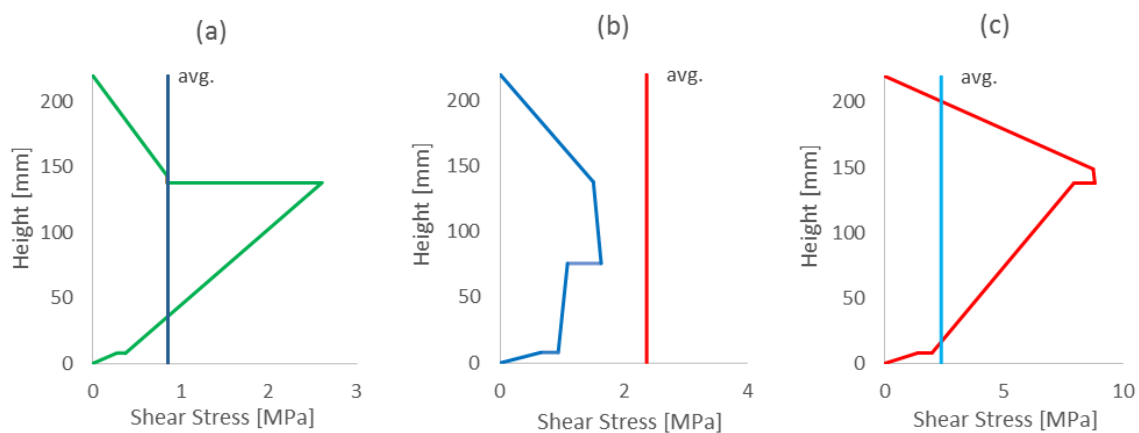


Figure 8. Shear stress flow. (a) Elastic phase, (b) Hogging bending moment plastic phase, (c) Sagging bending moment plastic phase.

### 2.2.5 Serviceability Limit State

The loading value for this verification came from the sum of the permanent and variable actions without any incremental factors. Bending moment and deflection values were calculated, considering the contribution from shear deformation. Even though this problem is applicable

for GFRP, for sake of safety, it has been applied to the GFRP-RC composite beam too. The value of the bending moment at mid-span for a fixed beam and double its value for the end supports (with a changed sign):

$$M_{sd}(+) = \frac{q_{SLS} L_{cb}^2}{24} \quad (20)$$

Using equations (9), (10) and (11), the normal axial stresses along the height of the beam were calculated, checking the values for the three different materials at their respective distances from the neutral axes. Applying this approach, the stresses in every point for each material (GFRP, concrete, steel) was calculated accordingly. For the case of sagging bending moment, the GFRP, the concrete and the reinforcement steel are submitted to lower values of axial stress than the ones allowed by the SLS. A problem arises when we verify the values obtained at the hogging bending moment since the concrete in compression (at the lower part) is well beyond the limiting values. However, this issue can be discarded considering that this contribution of concrete wasn't accounted from the start, and thus, the resistant bending moment of the composite beam doesn't suffer at all. Though, it must be kept in mind that this might bring excessive cracking and unacceptable aesthetic issues.

Maintaining constant the geometrical dimensions of the cross section (as previously stated) and changing only the span length, values for Graph 1 were generated. This will help understand the scope of possible use of this particular GFRP-RC beam in function of the maximum deflection at its mid-span. The horizontal dotted lines represent the limit that the code has considered as safe, and therefore, the beam remains inside the SLS limits even to spans longer than 8 meters. For the case of the analyzed beam, the six meter length span is by far inside the safe side.

Another check done was that of the vibrating behavior of the structural element, which has been introduced by the codes in order to assure a pleasurable function of the floor to people. Infrequent cycles per second of oscillatory motion could turn into perceivable vibrations, becoming an uncomfortable situation for its users. The result obtained at the analysis is well above the minimum value of 4 [Hz] cycles/second set by the code.

### **2.2.6 Ultimate limit state**

The value of the distributed load for ULS received and increment of 35% for permanent loads and a 50% increment for variable loads. Following the assumptions of the code, the cross section was considered as fully plastic (elastic, perfectly plastic materials) with stress block representation of its components and the tension resistance of concrete was neglected.

It should be pointed out the changes that go through the section when it passes from the elastic (uncracked) phase to the plastic phase. The cracking of the element and the distribution of the stresses (due to the change in the neutral axes) will also change the second moment of area of the element and hence, a new one is generated. This new plastic second moment of area is calculated in the same manner as for the elastic one, where a modulated area approach is used, so to account for the proportional provision of each material, keeping in mind the particular situation of concrete, since it is the only one neglected once it has cracked. Both the GFRP and the steel reinforcement keep their original volumes and characteristics all the way from the elastic phase up to failure.

#### **2.2.6.1 Resistant bending moment**

For the hogging bending moment, the contribution of concrete in compression was completely unaccounted as done by [49], making the steel reinforcement bars and the GFRP profile equilibrate all of the forces present in the beam. This was decided due to the connection type with the column, where being (the concrete in compression) discontinuous at this point, the compressive contribution cannot be guaranteed. Only in the case of a concrete or a tube-shaped column there could be some proper interaction, however, for the purpose of this structural system, it is much more likely to be a slender column made of a steel or GFRP profile. Introducing a safety factor that accounts only the 85% of the resistance, the design resistant bending moment was obtained. Interestingly, the resistance for sagging bending moment, besides having the compressive contribution of concrete, it is lightly larger than the resistance for case of hogging bending moment.

#### **2.2.6.2 Shear resistances**

For all the different shear stress planes, there have been a variety of verifications that will help us assure that the beam can work properly. This becomes of major importance since it is the weak point of FRP pultruded elements. Among these shear stresses, there are:

- Vertical shear stress in the xy-plane of the GFRP-RC composite beam.

- Longitudinal shear stress in the  $xz$ -plane in the elastic phase and plastic phase in the case of sagging bending moment, considering that their neutral axes are very close to each other.
- Longitudinal shear stress at the critical  $yz$ -plane in the plastic phase, being the point where the slab joins the web of the GFRP-RC beam.
- Vertical shear stress in the  $yz$ -plane in the plastic phase at the critical point where the slab joins the GFRP-RC web.
- Longitudinal shear stress in the  $xy$ -plane for the transverse reinforcement at the face of the fin.

Following the principle established by [3] and the code, the resistance to vertical shear in the  $yz$ -plane was taken into account only from the vertical elements of the pultruded beam (the web and the fin). Even if some authors consider a possible contribution from the concrete trapped between the flanges, it was decided not to count on it. Besides, the Pultex Design Manual has a very high penalization factor for the resistance to shear, with a reduction of 3 times its characteristic resistance. Even so, the element's web is able to withstand the required shear force coming from the external loads.

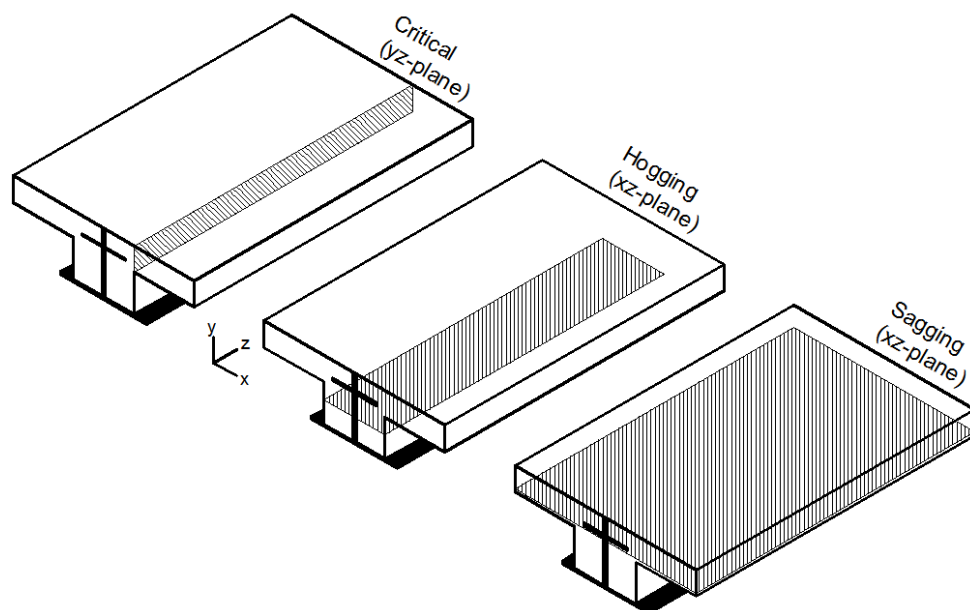


Figure 9. Shear stress planes analyzed for full interaction of the GFRP-RC composite beam.

The three main cases of shear stress planes are represented in Figure 9, where all three must be checked with care, otherwise, the beam can fail in unexpected manners with very dangerous consequences.

### **2.2.6.3 Shear interaction**

For the shear interaction between the GFRP and the reinforced concrete, the section was considered as a homogeneous element, therefore, accounting that it has a full shear interaction. This approach is not only seen at steel-concrete composite slim floor design, but further studying of these effect is presented latter to assure the mentioned assumption. To assure even further the interaction, some particular elements can be considered as contributors. In the case of the GFRP-RC composite beam, some of them are from mechanical characteristics or contact friction between their interfaces. In this particular case of beam, some of the possible contributions are:

- The perimeter of the pultruded beam in contact with the concrete has a friction resistance which may be highly increased by adding an adhesive coating to the pultruded profile. The thesis done by [58] has concluded that a minimum contact shear resistance of 1 [MPa] can be guaranteed when an adhesive coating is used on the walls of the FRP element right before the pouring of the concrete. Besides, the failure happens at the unconfined concrete interface and not at the adhesive.
- The fin, together with the transverse reinforcement, form a shear stud-like mechanical system. The advantage of this factor is that it is continuous, leaving no concentration of stresses as happens on the dowel action in steel studs. It must be taken with care the effect and resistance of the transverse reinforcement, because an excessive number of perforations can weaken the material critically.
- The bolts from the connection of the pultruded profile, with its horizontal configuration, can work as shear studs. Since these bolts will be embedded in the concrete, a possible way to exploit them is by stretching the head of the bolts to form a stud-like mechanical system. This way the beam section can have horizontal shear connectors that contribute in the critical shear zone, exactly where they are needed the most. Fortunately, the resistance of the FRP web to longitudinal shear is higher than for vertical shear (due to the direction of the fibers) and therefore, if it can withstand the forces from the vertical shear, it can easily withstand the longitudinal forces as well. Certainly, it is wise to verify that it is so.

#### 2.2.6.4 Slip

With the assumption of full shear interaction, the slip between the two members is zero. This assumption can be taken with more certainty than in the case of the steel-concrete composite beam since, the reason of the slipping is partly due to the big difference of stiffness among the two materials. For the GFRP-RC beam, the elastic moduli differences is very small, making the deflections of the two much more compatible, therefore, making slip values smaller. The research done by [55] has shown that the values of slip between the steel beam and the surrounding concrete of the slim floor was practically nonexistent.

For the case of the program, a rough calculation was performed to estimate a possible value of slipping that can permit to know (as a secondary approach) the required strength of the shear connection. For this procedure, it was assumed that the curvature obtained for the GFRP-RC beam, with its own elastic modulus, will be used because both elements deflect up to the same point. At a deformed state, the stresses inside this two elements (pultruded beam and RC beam) change since they have different values of elastic modulus, hence, the strains were calculated for each element (each with its own value of E) and the difference between the two would be the slip value. Through some derivation of simple equations a simple way to estimate the longitudinal slip strain and total slip is:

$$\varepsilon_{slip} = \frac{M y}{I} \left( \frac{1}{E_p} - \frac{1}{E_c} \right) \quad (21.1)$$

$$\Delta_{slip} = \varepsilon_{slip} \left( \frac{L}{2} \right) [mm] \quad (21.2)$$

For the case of this equation, (y) is the distance from the neutral axis to the transversal reinforcement, since the concrete cover on top of the GFRP-RC beam is not considered. Through the use of these equations, it was calculated that the maximum slip, it being at the support of the beam, is of 0.62 [mm] which can have some relation to the mentioned results by [55].

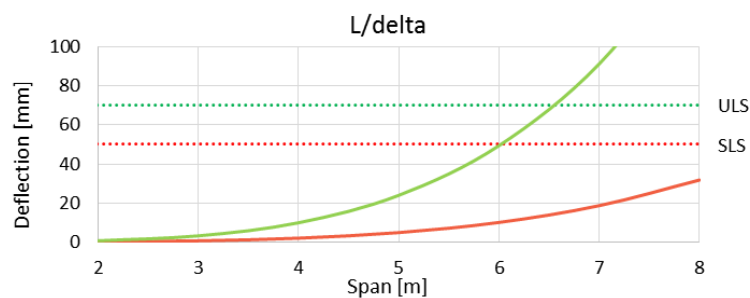
Another approach was used by following the equations of [5]. The author developed an approach by means of the differential equations of beam theory to composite action between a

steel I-beam with the slab on top of the upper flange connected together through shear studs. Even though this composite system is quite different, it was used so to see the outcome of the results. When applying them, the results turned out to be excessive, with a maximum slip of 6.5 [mm], which will contradict the conclusions taken from the research mentioned earlier and therefore, making it inapplicable.

### 2.2.6.5 Deflection

The total deflection at mid-span has shown to be inside the code limitations. As mentioned earlier, Graph 1 shows the increase of the deflection as the span length increases, and therefore, the maximum accepted deflection is at 6.5 meters. This can also be interpreted as an over strength of the beam which may permit to reduce the cross section. Certainly, this factor is not the only one to be considered, and therefore, the deflection is not a fundamental factor inside the design of this beam but it is certainly satisfactory to see its performance.

The new second moment of area ( $I_{plastic}$ ) will be smaller than the elastic one. The mentioned effect can be clearly seen in Graph 1, where the line for ULS has a much steeper slope. Obviously, this effect is also due to the increase in the loading since it is incremented by the factors given by the codes. This factor is really dangerous because it means that the cross section is losing strength as the loading increases, due to the weakness of concrete to tension. It's an intriguing fact since the opposite result would be the safest outcome for the structure.



Graph 1. Deflection-Span Length ratio of the GFRP-RC composite beam.

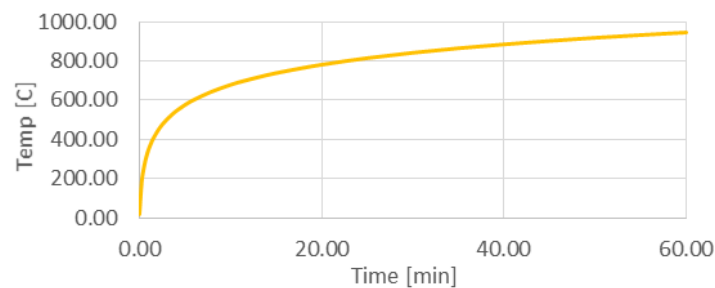
## 2.3 Fire analysis

The transmittance of heat from a fire happens by means of convection and radiation heat fluxes. Where convection heat fluxes happens by expansion of the gases through a fluid (the air in the ambient), radiation heat fluxes are the electromagnetic waves emitted by a fire flame. This two

components give the total heat flux [ $\text{W}/\text{m}^2$ ] which basically translates on the amount of the increasing thermal energy applied on a surface in function of a time increasing temperature. The code gives a value of  $25 [\text{W}/\text{m}^2 \text{ C}]$  as the coefficient for heat transfer by convection which will be useful for the FEM simulation.

For the fire situation analysis, the Standard Fire approach given by the Eurocodes was used. Graph 2 shows the given representation of a fire situation by means of the increasing temperature over time and its equation to calculate it.

$$T_g = 20 + \log_{10} 345 (8t + 1) \quad (22)$$



Graph 2. Standard fire curve from Eurocode 2.

Many factors must be taken into account to assure the integrity of the structure for at least 60 minutes in case of fire. To analyze the behavior of the element through a simulation, three things are needed:

- The thermal conductivity of the material ( $\lambda$ ) with units [ $\text{J}/\text{s}\cdot\text{cm}\cdot\text{C}$ ] which can be simplified to [ $\text{W}/\text{cm C}$ ] since watts is the energy (joules) variation over time. Meaning the vibrational energy ease of travel.
- The specific heat of the material ( $C_p$ ) with units [ $\text{J}/\text{kg}\cdot\text{C}$ ] represents the effect of mass in the transfer of heat as dealt with in thermodynamics.
- The strength decrease rate of the materials in function of the increasing temperature.

Certainly, these three properties change drastically for every material, making the analysis quite complicated. For the case of steel reinforcement and concrete, the known values are well

established by the codes but for FRP, research is still in its beginning steps. Different authors have produced tests of FRP profiles under fire in order to understand thermal properties, its behavior and loss of strength. Graph 3 presents the thermal conductivity of each material considered in the simulation.

Even though the fibers have good resistance to fire, FRP material under fire depends only on the matrix and hence, once the matrix is decomposed fibers are loose and the element loses its mechanical homogeneity. Three main phases exist in the heating process of the matrix: the virgin phase, a transition phase and the decomposing phase. Bay et al. have developed an empirical set of equations to represent the thermal conductivity of the profiles produced by Fiberline Composites. Where the different parameters involving the behavior of these GFRP pultruded profiles are:

- For the virgin phase:

$$\lambda_v = 0.33 + 4.4 \times 10^{-5} T \quad (23.1)$$

- For the decomposed phase:

$$\lambda_d = 0.0585 + 5.5 \times 10^{-13} T^4 \quad (23.2)$$

- For the transition phase:

$$\lambda = F \lambda_v + (1 - F) \lambda_d \quad (23.3)$$

Being:

$$F = \frac{\rho - \rho_d}{\rho_v - \rho_d} \quad (23.4)$$

Where  $T$  is the temperature and  $\rho$  is the density of the matrix at each phase.

The specific heat properties of the GFRP profile was taken from [17] where, after a series of tests and analysis, has obtained some empirical equations that represent the mean behavior of this material under fire conditions. Where  $\alpha$  is a factor that accounts the decomposition of the material,  $M_i$  is the initial mass and  $M_e$  is the final mass (which can be taken as being just the 25% of the initial one),  $f_b$  is the temperature dependent mass fraction and  $R$  is the gas constant equal to 8.314 [J/mol C]. We can finally obtain:

$$C_{p,c} = (1097 + 1.583 T)f_b + (896 + 0.879 T)(1 - f_b) + \frac{11.85}{20} \exp\left(\frac{-26527.86}{RT}\right) (1 - \alpha) 385259 \quad (24.1)$$

$$f_b = \frac{M_i(1-\alpha)}{M_i(1-\alpha)+M_e \alpha} \quad (24.2)$$

To estimate the decrease of strength of the FRP material as the heat increases, the experiments performed by [14] through the use of profiles produced by Fiberline Composites, presented an empirical equation for the stress-strain relationship with an exponential rate of decrease:

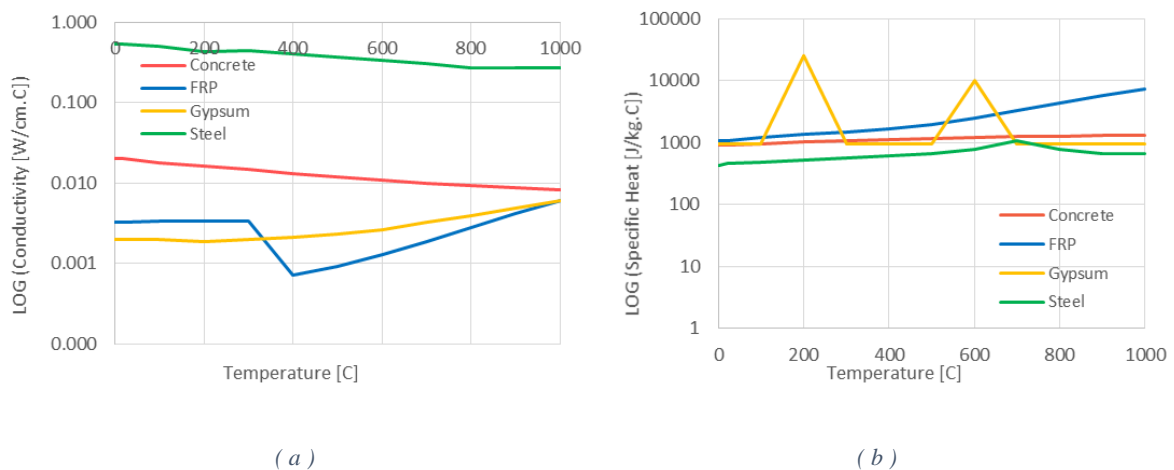
$$\sigma = \sigma_{max} \left[ 1 - \exp\left(\frac{-E \varepsilon}{\sigma_{max}}\right) \right] \quad (25)$$

The factor  $\sigma_{max}$  has been arbitrarily introduced as a very high value impossible to reach as explained by the author. However, the scope of these equation is to understand how the material loses its strength as the temperature increases, where being in a composite system, it can be assumed that the strain is equal than the one of concrete. Strangely, the equation doesn't have the factor of temperature but [14] results can still fall inside his presented equation.

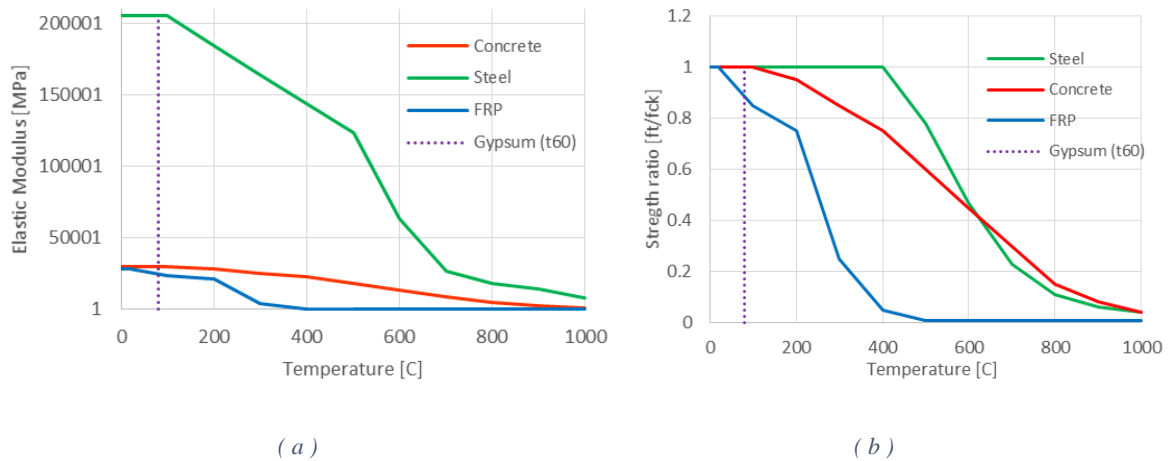
On a first try-out of a 60 minute exposure of the element to fire, it was concluded that about 80% of the GFRP pultruded profile would be completely decomposed, leaving the beam's resistance to the concrete and the reinforcing steel. Since there is no material that contributes for equilibrium in the lower part of the cross section (for hogging bending moment), the

resistance of the beam would decrease to a point that wouldn't even withstand a 30 minute fire situation.

As a solution to the previous problem, instead of following the resistance approach (by adding reinforcement in the lower section), the insulation approach was taken. The insulation was performed by means of a gypsum board that is part of the ceiling's architectural component. To understand the capabilities of gypsum under fire and its efficiency to protect the GFRP profile, a FEM sequential time-step simulation was performed. It was important to account the vulnerability of the whole structural system since the deck that composes the composite slab is also exposed directly to the fire. The research done by [19] has a discontinuous set of equations to model the thermal conductivity of the material, while [15] presents a simple graph of the specific heat values. These factors have been useful for the modelling of its behavior under fire and both can be seen at Graph 3, however, it is important to notice that the properties values are in a logarithmic scale, meaning that gypsum has an extremely low conductivity, about 270 times smaller than steel.

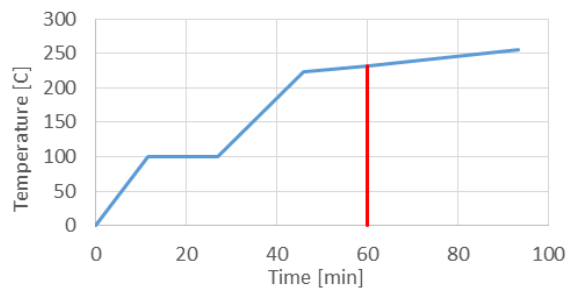


Graph 3. Thermal properties of the materials. (a) Conductivity, (b) Specific heat



Graph 4. (a) Stiffness loss in function of temperature, (b) Normalized strength loss by increasing temperature.

For the case of hand calculations, in [19], a discontinuous equation estimates the temperature of the gypsum board at its internal face. Where the only variable of the equation is the thickness of the board and, having a commercial gypsum boards range from 16 to a 22 [mm], an average 20 [mm] was taken. Graph 5 shows the increase of temperature until the point of burning of the board and, through a simple interpolation, the temperature at 60 minutes was calculated. Having this temperature and knowing the conductivity of the GFRP, an estimated value of the temperature at contact with the gypsum was obtained (presented at the Excel spreadsheet), helping to understand how much the materials have lost in stiffness and strength. It's important to consider that the structural resistance of the gypsum board is out of the scope of this thesis since its contribution has only been considered for fire insulation. However, it was demonstrated that the time at which gypsum burns is after 60 minutes, therefore, the beam is also protected up to that point in time.



Graph 5. Temperature prediction of the gypsum board's internal face.

Once the fire analysis was performed, to calculate the resistance of the GFRP-RC beam at the 60 minutes of the fire some aspects must be considered. The code has introduced a reduction factor for the loads where the simplified value of 0.7 was taken, meaning that the loads accounted will only be the 70% of the SLS loads. Realizing that the temperature at the lower flange of the GFRP profile is barely 80 degrees Celsius, the loss of resistance is extremely low, resulting in just 0.4% for resistant bending moment and 0.1% for shear resistance (since the web is further away from the fire exposure). This values are quite expected if the loss of resistance of the material is minimal (1.4%). All the tabulated data coming from the Excel program can be seen at the Annex.

## 2.4 GFRP pultruded deck

The decking system used for the construction of the GFRP-RC composite beam consists on a system developed by Fiberline Composites which has been intended for the construction of bridges, nevertheless, due to its height of 130 [mm] it became a perfect candidate. The material properties of this profile are quite different than the one of the main beam produced by Creative Pultrusions. For the same reason as for the pultruded beam, this deck section is extremely light and easy to handle, making its assemblage fast and simple. Many authors have gone through a variety of testing that can assure its correct behavior under loading, from which [24] and [25] have done some profound analysis. Figure 11 shows the lateral view configuration of the GFRP-RC composite beam with one meter length. The geometry of the deck surely has undergone a variety of studies to arrive to its optimum performance. Also, being sold as a meter wide section, it is optimal when placing it over the lower flange of the main beam. Once the deck sections have been aligned properly, it leaves the exact free volume to be filled by the concrete that will form the slab.

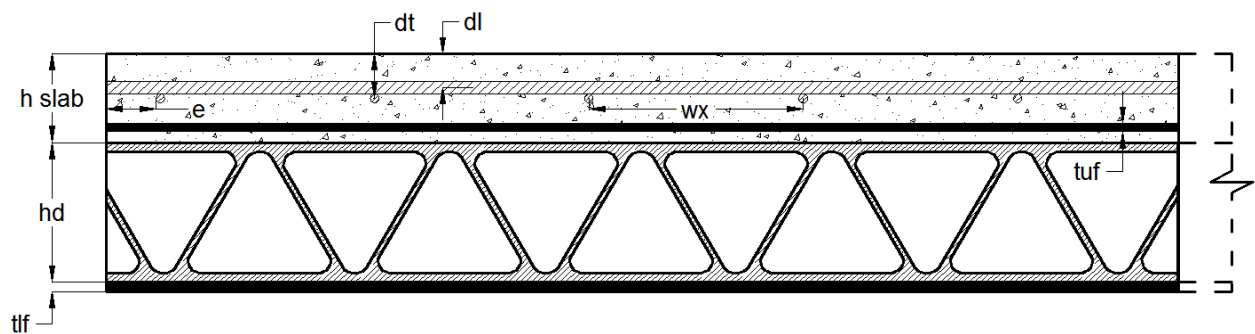


Figure 10. Lateral view and geometric parameters of the GFRP-RC beam.

Just as for the GFRP-RC composite beam, this slab is also a composite structural system and hence, it is referred as a composite slab. To assure a proper shear interaction between the deck and the concrete slab, an adhesive can be placed on the top surface of the deck right before the pouring of the concrete. As mentioned before, [58] has assured an interface shear resistance of 1 [MPa] and, accounting this shear stress resistance, its composite behavior can be assured. With this assumption in mind, the neutral axis of the composite slab was found to be placed at the upper flange of the deck. It is important to mention that, for the calculations done by the Excel program, a simplified geometry of the deck was used taking into account (for bending moment) only the upper and lower flanges and not accounting the contribution of the diagonal elements. Fortunately, the manufacturer has supplied a section modulus of the deck profile, and thus, the real resistant bending moment was determined as well. Once the bending moment was calculated, the difference between the real value and the value coming from the simplified approach (for the Excel spreadsheet) was of only 1.6%. The manufacturer's design manual has very strong reduction factors, where for shear the factor is of 0.5, for bending moment the factor is 0.125, which means that the resistant bending moment is reduced by 8. Due to the complicated type of end support, for sake of safety, the values of the bending moment due to loading was calculated as for a simply supported beam, it being  $M = q L^2 / 8$ .

For the composite slab, there are no variables that could permit changes in its design since all of the used components, such as the reinforcement, are chosen according to the needs of the GFRP-RC composite beam. With this in mind, this section of the analysis just needs to verify that the given values of the different factors permit a proper performance of the composite slab. To understand the differences among different possibilities, another analysis was done with the deck and the slab not working as a composite element. Certainly, the slab's resistance is extremely low, with barely 2.5 [kN.m] and the deck, even though can withstand the needed bending moment by its own, the deflection at ULS surpasses the limits. It is for this reason that the composite action between the two must be guaranteed by means of the adhesive, which has a higher shear strength than the forces coming from the external actions, thus working as desired.

## **2.5 The connection**

When dealing with the connection of the GFRP-RC beam by following [55], the connection was designed as bolted, conformed of two angle profiles to each side of the pultruded profile's web, as recommended by the manufacturer. For FRP connections, it is very important to consider the complex behavior of the material, especially under shear stresses and, even worst,

for concentrated stresses. To make matters less complex, steel bolts were used for the analysis since their theoretical resistance is more reliable than FRP bolts. Based on the same theory developed for steel over many decades, the plate analysis of a bolted connection is checked for the same type of failures. This matter was mentioned at the literature review at the beginning of the thesis. As for the analysis used at the Excel program, the CNR-DT205/2007 code was used as a guide to account for the diverse weaknesses of a bolted connection in FRP.

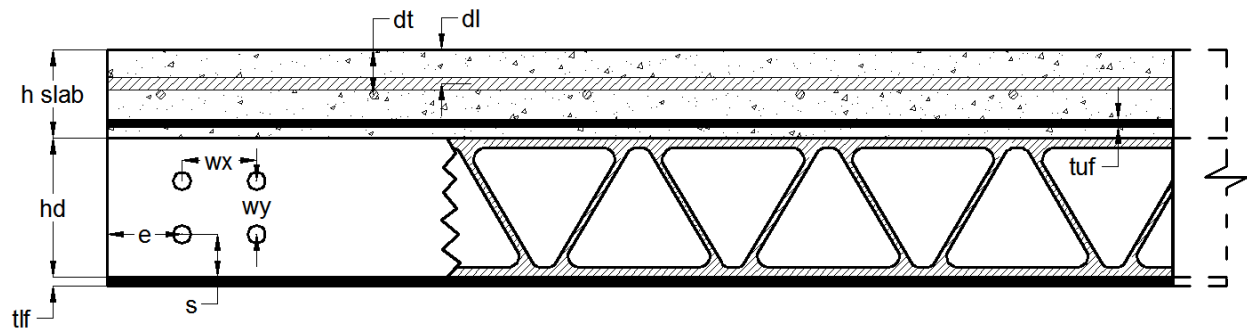


Figure 11. Connection geometric parameters of the GFRP-RC composite beam.

The final design was done by introducing 4 bolts of steel, grade 400 [MPa], and the spacing between them, as well as the spacing to the borders where calculated by the requirements dictated by the code. Even though the upper limit of the web is not a free border, meaning that the top flange and fin are present, for the purpose of the design, it was considered as such and hence making it a safer design. This can be appreciated at Figure 12. As expected, the weakest link in the connection is the interlaminar shear resistance, however, its 27.5 [MPa] of shear strength was sufficient to withstand the requirements from the loading. This resistance has been reduced by a safety factor of 1.3, given by the manufacturers design guide.

Another safety factor can be taken by neglecting the effect of clamping coming from the torque submitted to the bolts when tighten them. This creates a confining effect on surroundings of the FRP's hole which increases its bearing strength, however, it must remain within certain limits considering that excessive torque can crush the material and damage the matrix. A research done by [59] concluded that a lightly clamped bolt with a torque value of 3 [N.m] increased the connection's bearing strength by 45% and a fully clamped bolt with 30 [N.m] torque increased the bearing strength by 80%.

# Chapter 3: Finite Element Model Simulation

Nowadays, its standard procedure to simulate structures by means of FEM models because it is the best tool to solve complicated mechanical analysis by means of dividing, or meshing, its elements. Through its ingenious mathematical procedure and the power of computers, we can calculate with great accuracy the effects of loading in a composite beam formed by different materials with different mechanical characteristics and acknowledge its behavior in reality. The best outcome of this computational tool is to fill the voids left by the hand calculation done at the Excel program, presented over this chapter.

## 3.1 The software

To perform the analysis of the GFRP-RC beam, the FEM software called Straus7 was used. The scope was to obtain resulting values up to the elastic phase of the materials since the simplification of the plastic phase (cracking) is very complicated to introduce inside the model, hence, it is obvious that the results for ULS loading will not be at all similar to the ones calculated in the Excel program. The versatility and ability of the software is well known and, using its different tools, a variety of simulations were performed; not only simulating the structural-mechanical behavior but also the thermal one. Finally, for the ones that can be useful, graphical results were generated by the same software.

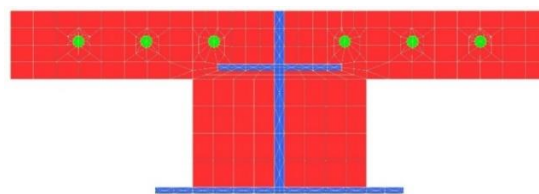
## 3.2 GFRP-RC composite beam and composite slab simulation

Different stages of analysis were created in order to acquire as much results as possible on the behavior of the GFRP-RC composite beam and all its fundamental parts. The different stages are presented in Figure 12 and Figure 13 where:

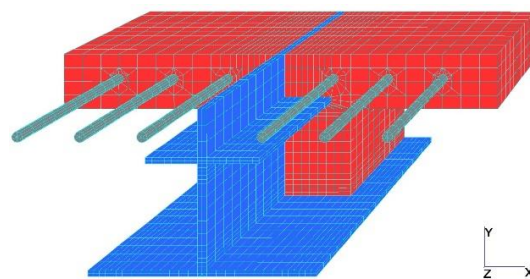
- For the first stage, a two dimension analysis of the cross section was produced by means of Quad4 plate elements, them being finite square elements with four nodes that represent the degrees of freedom. The whole section was meshed to a level of finitude considered to be sufficient for the needed accuracy, since an excess can only lead to unnecessary computational length time and possibly errors.
- For the second stage, a three dimensional model conformed of Hexa8 brick elements was done to understand the beam's deformation under distributed loading and to simulate, in the best way possible (closest to reality), the end supports. This was also a

helpful approach to obtain a variety of normal and shear stresses in all the different axes planes, deflections and natural frequency of vibration.

- A third stage was created to simulate the connection of the element and see its performance closely to the holes, in order to assure that concentration of stresses do not surpass the amounts that the material can withstand. The effect of bolt clamping was also modelled but, considering it as a safety factor, it was later neglected, since it can also have effects on the rotation of the GFRP-RC beam.
- For the fourth stage, the fire simulation was done, including a gypsum board model that will work as insulation, protecting the structural elements to assure a minimum of 60 minute resistance. A transient heat analysis was done by means of a time-step process with the Standard Fire curve given by the code. This analysis can have very heavy computing processing due to the amount of steps needed and therefore it was preferred, for sake of precision, to deal with a two dimensional model.
- One final stage was performed to recreate the simulation of the concrete slab over the GFRP deck which will form the composite slab. The same type of plate and brick elements were used but its properties are different since it is produced by a different manufacturer, however, all the required values of mechanical properties were introduced accordingly. Also, a fire analysis 2D analysis was done to assure that the gypsum board will protect the composite slab properly and secure its safety.

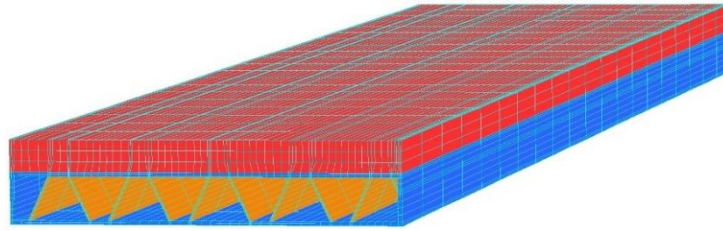


( a )



( b )

Figure 12. FEM simulation models, (a) 2D plate model of the GFRP-RC composite beam, (b) 3D brick model of the GFRP-RC composite beam.



( c )

Figure 13. Three dimensional brick model of the composite slab with a simplified geometry of the GFRP pultruded deck.

For the simulation of the composite slab, the geometry of the deck was changed in order to simplify its meshing and overall analysis. Basically, it is formed of two rectangular flanges and triangular webs where, as sold by the manufacturer, a meter wide pultruded deck profile will form a meter wide composite slab. Since the deck would be simply supported over the lower flange of the GFRP pultruded beam, the composite beam was modelled as being simply supported at its bottom flange, however, being continuous the concrete slab, the concrete section of the composite slab was modelled as fixed. This intends that the nodes inside each mentioned section is limited to the desired degrees of freedom.

### 3.2.1 Two dimensional model

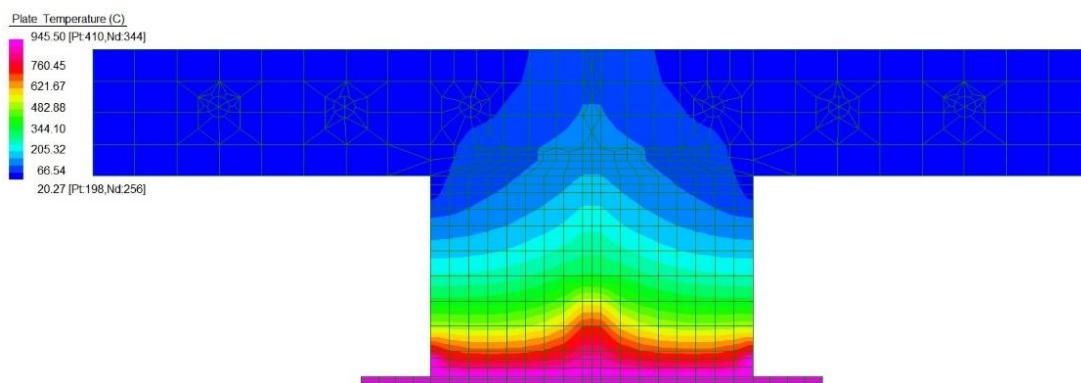
The model used simulated the transverse bending moment and vertical shear suffered by the GFRP-RC beam. The purpose of this procedure was to understand the transversal deformation of the element by considering the deflection of its flange, the tension resultant in the reinforcement and different in-plane stresses inside the cross section due to the complex type of connection that the element has.

#### 3.2.1.1 Fire simulation

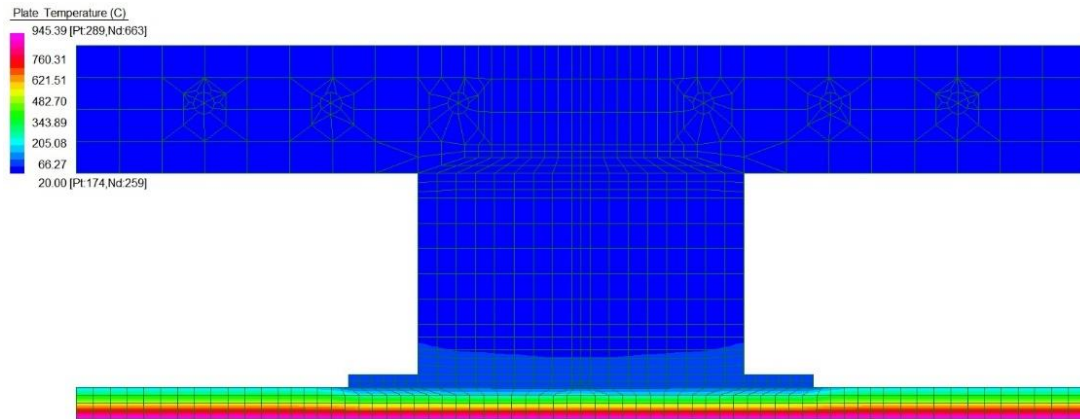
The different values needed to realize the simulation were all mentioned and given in the previous chapter. This factors are the thermal conductivity and the specific heat properties of each material and their variations in function of temperature, where the detailed values can be seen at the tables presented at the Annex. This values where introduced into the program as tables, taking very good care of the units used since it can drastically change the results. Another table introduced into the program was the one of the standard fire curve, which represents the increase of temperature over time in order to simulate a fire situation. With all the needed tables, the two heat fluxes were applied to the beam, them being the convection and radiation fluxes which are represented by means of it coefficients (given on the previous

chapter) and an ambient temperature linked to it. This two steps are needed in order to let the program run its time-step simulation properly. In this procedure the program calculates the temperature distribution of the element at a given time and its effect on each material. For the subsequent step, it will start the procedure with the results obtained in the previous step to later increment the temperature by one step further and continue to calculate the transmission of heat through each material. To obtain accurate results, the simulation was demanded to run for a total fire time of 3600 seconds by means of 900 time-steps. Figure 14 shows the distribution of temperature over the beam after an hour of fire, and for sake of comparison, the first beam represents the situation without insulation, as for the second and third one presents the results with the gypsum insulation. It can clearly be appreciated how drastic the changes of temperature become when a gypsum board is used, and in the same manner, it can be seen how good its thermal properties are.

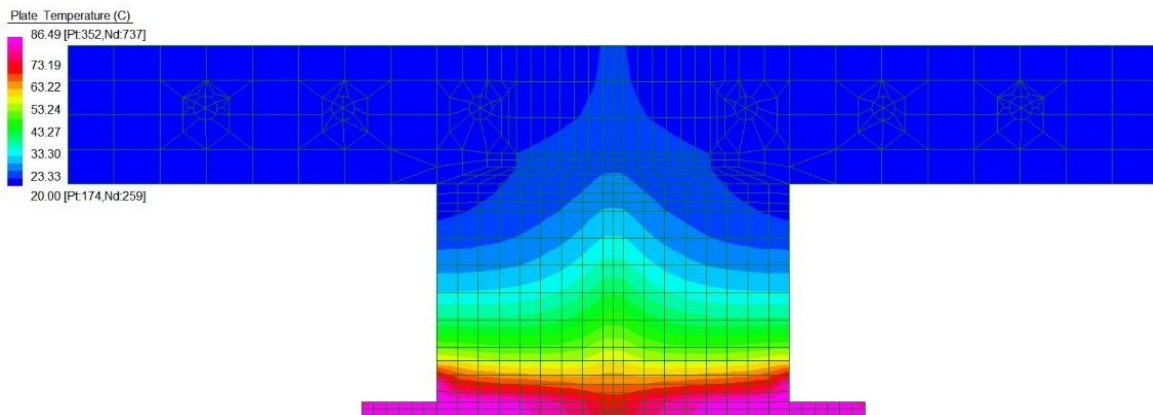
A three dimensional model was also created but it has been discarded for two reasons: first, the time-step procedure of the program requires excessive computing time due to its characteristic way of processing the simulation and, having the 3D model many more elements, it was practically impossible to realize the 900 needed time steps. It can be possible to perform it but became highly impractical because its duration can take many hours. Second, because a simple 16 step simulation was done and, for the final result (at 60 minutes) the temperature distribution was very similar to the 2D model. Therefore, it was decided that a 2D model is more practical and can be much more reliable by means of the number of steps performed by the simulation.



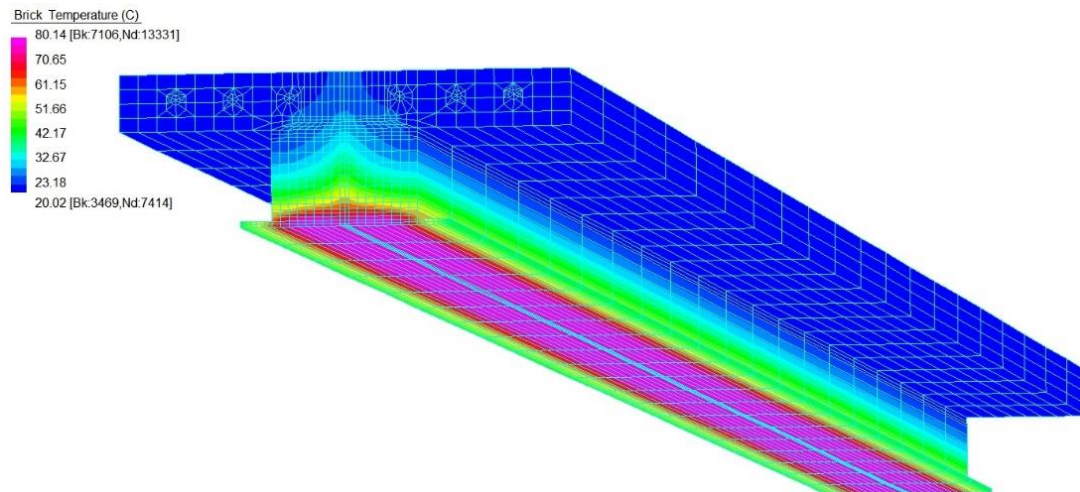
( a )



( b )



( c )



( d )

Figure 14. Fire simulation from the time-step FEM procedure of the GFRP-RC composite beam. (a) Without insulation, (b) With insulation, gypsum board visible, (c) With insulation, gypsum board not visible, (d) 3D simulation.

### **3.2.2 Three dimensional model**

The process to generate the model comprised in taking the 2D model and extrude equal sections until arriving to the desired length of six meters. Since the cross section is constant along the length of the beam, this stretching created the solid beam needed for the analysis. Since the starting geometry was based on plates, the new bricks replacing them needed to be defined, so to keep consistency in the mechanical properties of the materials. Once the geometry and the properties were taken care of, the SLS loading actions were introduced as well as the constraints that can simulate, as close as possible to reality, the end supports. For this purpose, the GFRP pultruded beam's web was constrained only to displacements but the reinforced concrete was constrained also to rotation to simulate it as a fixed-fixed beam.

After running the simulation, the results obtained were very satisfactory, having logical and reasonable values for different aspects of the GFRP-RC beam. The behavior of the beam was that of a normal fixed beam at its end supports, having a maximum deflection of 10.8 [mm] at mid-span which is less than half the limiting value from the codes. Other useful values are the shear stresses analyzed in different planes but especially in the xz-plane that deals with the longitudinal shear. For the case of normal axial stresses, each material could be analyzed with detail along all of its geometrical area, both for tensile and compressive stresses. All the respective values of stresses will be analyzed and compared with the values from the Excel spreadsheet on the next chapter.

#### **3.2.2.1 Connection model**

Through the same base model, the connection was developed to analyze the stress concentrations in the holes. Once the four holes were created in the FEM model, the rest of elements were left equal as the original one. Located at their proper position and size, the constraints were changed by passing from the constraints placed at the web's nodes to the nodes inside the holes. This would represent the reaction of the connection plate coming from the column and for this model, the constraints were placed at the nodes inside the holes. Not only this, but it was applied on a way to realize that the only real part of the hole that is resisting the load is the upper half circle. In some manner, this can be a reasonable assumption, given that the lateral pressure (from the torque of the bolt) and longitudinal axial deformation coming from the beam is neglected.

# Chapter 4: Comparison of results

Having the results from both the Excel spreadsheet and the FEM simulation, a variety of different parameters have been taken to acknowledge how accurate the hand calculations can be. As mentioned at the beginning of the thesis, the scope of this study is to analyze the usefulness of hand calculations when dealing with complex composite beam structures and, therefore, possibly use them for the design of composite structures by joining FRP pultruded profiles and reinforced concrete. It must be acknowledged that tensile stresses have been considered as positive and compressive stresses as negative.

Another important fact to mention is the different approaches used, where the comparison of the main factors are made at the elastic phase of the materials, for the case of longitudinal shear, the stress values were used from the results of the ULS loading situation since it depends on the plastic neutral axis and is the maximum reached value. For the same reason, the bolted connection was also considered under the ultimate value of loading. In addition, for sake of safety, this assures that the element is always performing on the safe side of the demand/resistance ratio; being the shear interaction between materials of the utmost importance.

## 4.1 GFRP-RC composite beam

### 4.1.1 Neutral axis

The program estimated a 141 [mm] distance to the centroid which, at the same time, is the elastic neutral axis. With less than 3 [mm] of difference with the estimated value from the Excel program. For the case of the PNA's they can't be acknowledged since it's not given by the FEM program.

### 4.1.2 Flexure effects in the beam

When dealing with the axial stresses coming from the bending moment we have a variety of factors, where each material has different resulting values due to its elastic modulus, four major axial stresses were analyzed. For both hogging and sagging bending moment, the maximum stresses at the extreme lower and upper fiber were calculated, where there is an inversion of stresses to be considered. Figure 15 clearly shows the changes in normal axial stresses along the beam and its inversion when passing from the hogging bending moment at the supports to the sagging bending moment towards the center of the beam. It is representing only the stress

values of the concrete and the GFRP pultruded beam, nevertheless, the stress value of the reinforcement is presented in Graph 6.

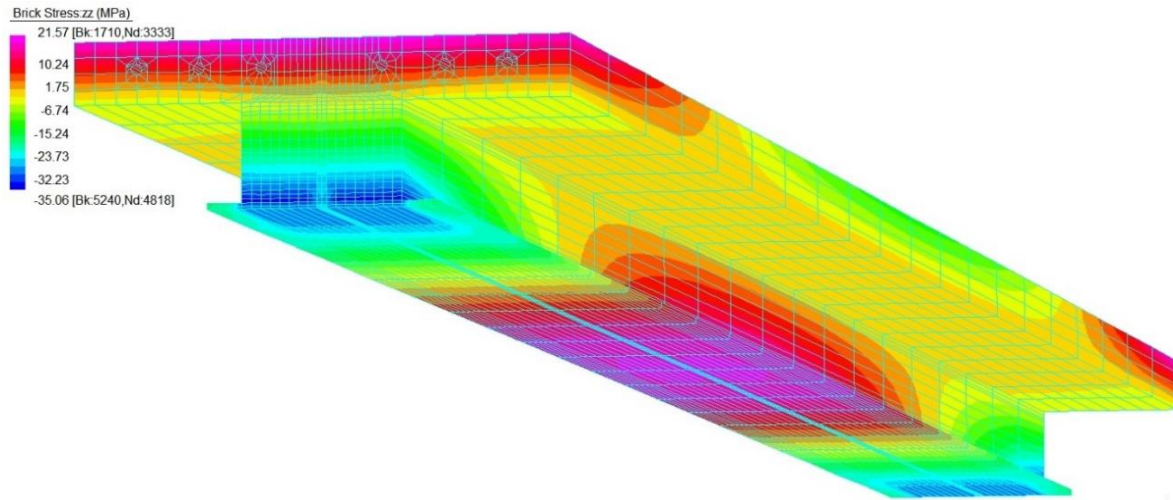
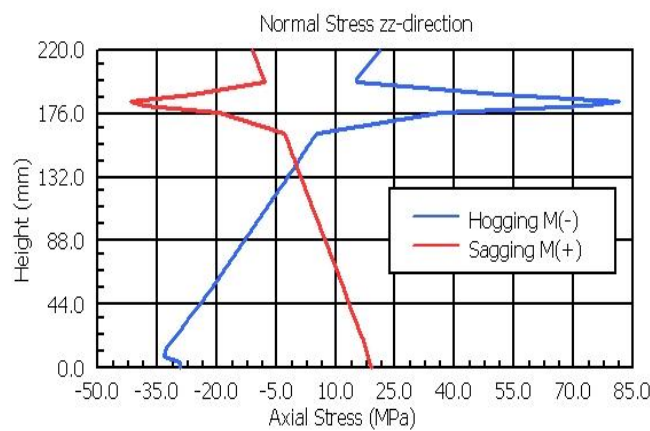


Figure 15. Longitudinal normal stresses of the FEM simulation for the GFRP-RC composite beam at SLS.



Graph 6. Normal stress distribution along the height of the GFRP-RC composite beam.

Graph 6 shows the stress distribution of the beam's cross section in its longitudinal axis. It can be appreciated how the peak values are placed where the steel reinforcement is located, therefore, if we compare with the obtained values from the hand calculations, they are quite similar for both the values at the extreme fibers and at points in between. When dealing with the values obtained from the FEM simulation in the hogging bending moment, it has given a maximum tensile value of the concrete of 20 [MPa] which is the same value as the one obtained

in the spreadsheet, however, for the case of the compressive stress, there is a difference of around 3 [MPa]. This difference could be significant since it represents an 8% error, nevertheless, the fact that its contribution to the resistance of the element is not taken into account can permit us not worry about this fact. The tensile stress at the GFRP pultruded profile is 17.4 [MPa] in the FEM results but a higher 19.6 [MPa] in the spreadsheet and the compressive results have given a bigger difference with 31.7 [MPa] in the FEM simulation and 36.4 [MPa] in the spreadsheet. The reinforcement, which is submitted to a tensile stress has an acceptable difference of around 2.5 [MPa] between the two approaches.

For the case of the sagging bending moment the results are more compatible between the two methods, where the maximum compressive stress of the concrete is 10.3 [MPa] for both analysis and the tensile value has barely a 0.3 [MPa] difference. For the GFRP pultruded profile the tensile stress is 18.7 [MPa] at the FEM model and 18.2 [MPa] in the spreadsheet, where for the compressive value there is no difference, both having a value of 9.8 [MPa]. The compressive stress in the reinforcement is of 41.8 [MPa], while at the spreadsheet we got 42.1 [MPa], again being very similar to each other. Once seen this results, it can clearly be perceived how much more reliable are the results for the case of sagging bending moment over the results from the hogging one.

#### **4.1.3 Shear stresses**

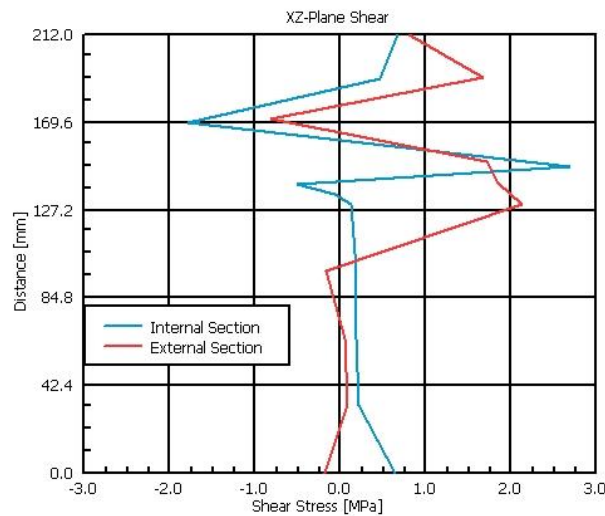
For the analysis of shear stresses in the beam, the way to proceed can be very complex since there is an incredible amount of points to be analyzed inside the FEM simulation. Besides this factor, the three major stresses mentioned at the beginning of the thesis were considered. The needed results were taken graphically from the FEM model to understand its stress distribution and not simply focus on local points at a random section of the element.

The analysis of these type of stresses are worst seen at the point of highest vertical shear which also represents the point where bending moment is at its maximum negative value, however, the code does recommend to analyze the values of this separately when passing from the negative to the positive bending moment. This especial considerations will be dealt with at the slip strain subsection.

##### **4.1.3.1 Longitudinal shear stresses**

The shear stresses analyzed were at the xz-plane since they represent the shear stresses at its highest value inside the cross section. Looking at Graph 7 it can be appreciated how the distribution of the mentioned shear stresses are obtained at the support of the element. They

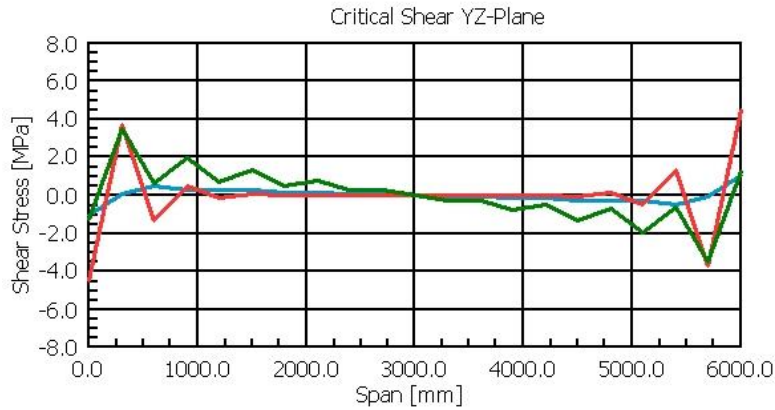
have been represented with two different lines so to see altered results inside the cross section, where one is at the outside (extreme lateral side) and another at the vertical center line of the cross section. When we compare the values with the Excel program, the peak values are not only placed at the same point (where the GFRP-RC web meets its flange) but also the values are very similar; both with a value of 2.6 [MPa]. Most importantly, these values are far away from the limiting values of the material, making it withstand these stresses without any possible vulnerability which is of great importance due to its brittle type of failure.



Graph 7. Longitudinal shear stress along the height of the beam at the end support.

#### 4.1.3.2 Critical Shear Plane

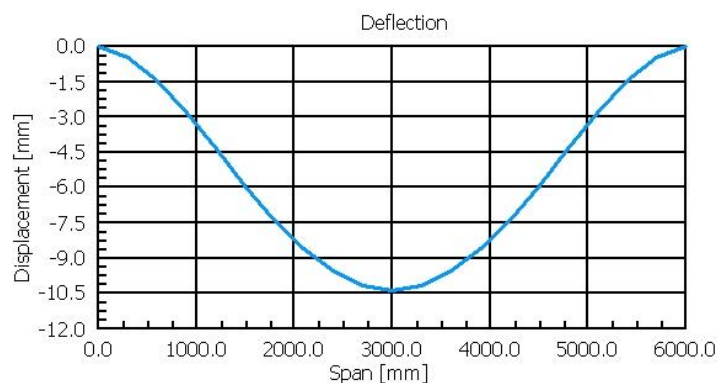
This critical area suffers a shearing stress which can be quite dangerous if not dealt with properly and can have very serious consequences since it places the beam in a vulnerable situation. By looking at Graph 8 it can be seen how the distribution of shear stresses in the yz-plane along the length of the beam at this critical area. Three different lines were taken along the height of the section which, at the same time, is the slab's cross section. The peak values at the supports are not taken into account since those points have node constraints which were placed to simulate the support, hence the real values will be assumed right after this point. By looking at the peak value after the support, which almost reaches 4 [MPa], not only there is a coincidence in the peak value of the two lines but it also has a similar value to the one obtained at the Excel program. With a calculated value of 4.46 [MPa], the spreadsheet is overestimating this plane shear by a small amount.



Graph 8. Plane shear stresses along the GFRP-RC composite beam at its critical plane.

#### 4.1.4 Deflection

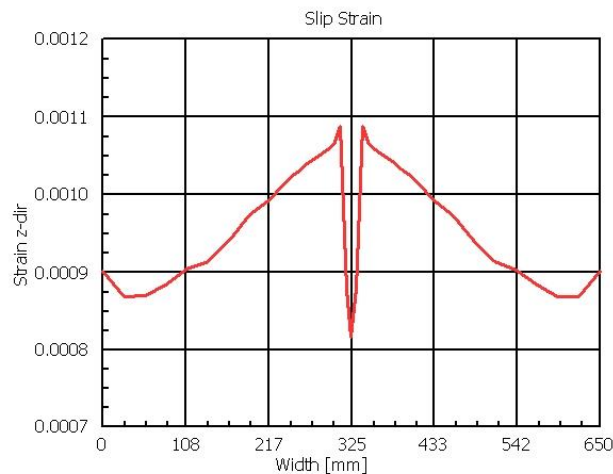
The resulting value of the deflection was taken at the center of the beam at the center of the cross section which will represent the lowest point of the lower flange at the GFRP profile. When comparing the value obtained with the Excel program, it can be valued how close these results are, where for the hand calculations a 10.09 [mm] displacement was calculated, the FEM simulation obtained a 10.5 [mm] (as seen in Graph 9). Also, the distribution of the deflection line has a very normal distribution as expected from a fixed beam with a constant distributed load. The confidence of this similarity is very reassuring since it is one of the most important factors when designing beams and, especially, when dealing with SLS verifications.



Graph 9. Elastic deflection curve of the GFRP-RC composite beam.

#### 4.1.5 Slip Strain

The approximate calculation of the slip strain at the support between the GFRP pultruded profile and the concrete has led to the proper design of their interface. When comparing the results obtained from both studies, it can be understood in Graph 10 that the slip strain is slightly larger than the 0.00021 obtained at the Excel spreadsheet. The jump in strain happens at the interface between the two materials, where it is clear that concrete is more vulnerable to deformation than GFRP. This still can give a good approximation of the required interface strength that will provide the shear interaction level needed so the composite beam can be designed as such and hence, take advantage of its potential.



Graph 10. Slip strain along the width of the beam at the end support.

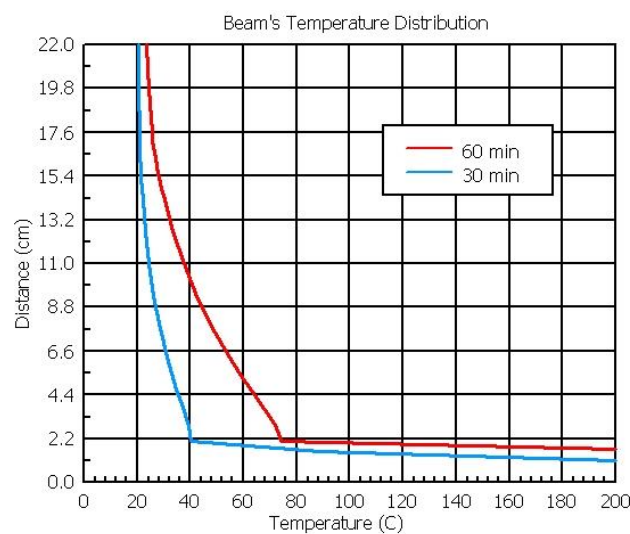
The slip strain between the two structural elements create a complex behavior which must be taken with care in order to provide the proper interface and thus, the correct shear interaction. When talking about shear interaction of a fixed structural element, the analysis will divide the beam into two fundamental parts. The first section will fall inside the negative bending moment and the other at the positive bending moment up to the mid-span (since it has a symmetrical behavior). This is also important since, at the point of zero moment (at around a fourth of its span), the inversion of stresses gives a big change in the plastic neutral axes, resulting in a complete change in the behavior of the beam. Therefore, when providing the shear interaction resistance of the element due to adhesion, the length used to calculate this values is not the entire half span of the beam but, for each of the two mentioned sections, it will be the distance

from the support to the point of zero bending moment and the distance from this point to the mid-span for the first and second section, respectively.

#### 4.1.6 Fire Analysis

When comparing the results of the fire simulation, it is very complex to estimate a real value from single hand calculations, and under this principle, this issue can only be addressed properly by means of the FEM simulation. However, some pointers can be calculated to give an estimate of the final situation of the beam at a given time of the fire, this being at minute 60. Therefore, this comparison will only deal with the values obtained at this given time.

Surprisingly, the obtained values are quite similar between the FEM simulation and hand calculations from the spreadsheet. The temperature at the extreme fiber of the GFRP pultruded beam's lower flange, which is the closest member to the gypsum board, has an average temperature value of 84 [C], which is only 4 degrees more than the estimated value by the Excel program. The maximum obtained value of temperature in the gypsum board at its internal face does have a considering difference, where the hand calculations estimated a 232 [C] temperature, the value obtained by the FEM simulation was of only 178 [C]. The expected maximum value of temperature was adequate by having a peak value of 945 [C] in the Standard Fire curve presented previously in the thesis. Graph 10 shows the temperature distribution in the GFRP-RC beam after 30 and 60 minutes of fire, where it can clearly be seen how the temperature of the first 2 [cm] of the gypsum board protect very well the structural elements.



Graph 11. Temperature distribution of the GFRP-RC composite beam after 30 and 60 minutes in a fire situation.

### 4.1.7 Bolted connection

The comparison of the connection is another complex one since it is very difficult to estimate accurately the behavior, however, the approaches used in the codes can give some safe results and possibly guaranty a proper behavior.

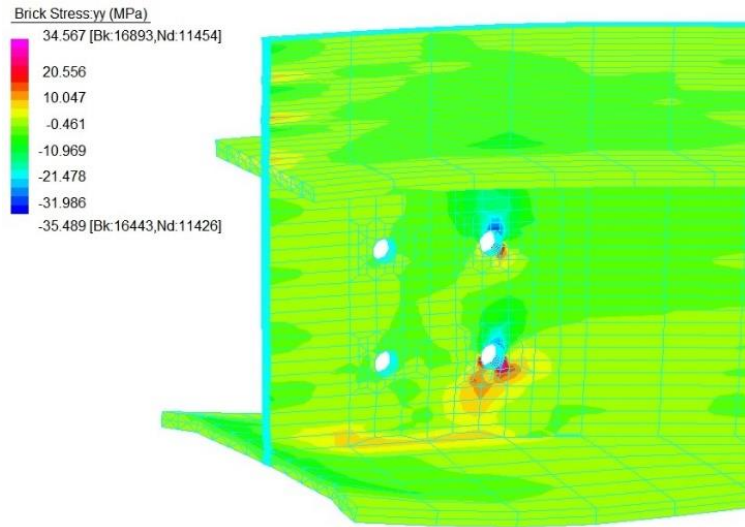
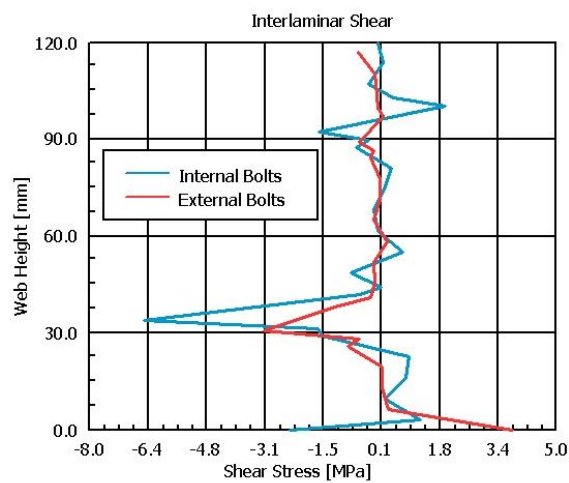


Figure 16. FEM results of the connection: (a) vertical axial stresses. (b) Interlaminar shear stresses along the web.



Graph 12. Interlaminar shear stress ( $xz$ -plane) along the height of the web, passing through the holes at the connection.

When the total reaction force was distributed over the bolts, each bolt has taken a load of 26.9 [kN] which lead to 16 [mm] diameter bolts. The resulting stresses around the holes of the web in the vertical direction (y-axis) has shown a maximum value of 34 [kN] in Figure 16, leaving this value barely inside the estimated one by the hand calculations, which for bearing resistance the result is of 35 [kN]. However, the extreme reduction factors given by the codes would make them change to a point that the design of the connection will change drastically. Even though the material resistance was already reduced by the 1.3 factor given by the manufacturer's code.

Another weak characteristic that needs to be checked is the interlaminar shear resistance of the FRP pultruded material, by which Graph 12 presents this shear stress in the xz-plane along the height of the web for each column of bolts. By looking at this result, the internal columns of bolts take higher values of stresses than the external ones. It can be appreciated how this stress increases where the holes are present, however, the stress values are quite acceptable since the reduced resistance of the material given by the manufacturer is of 21 [MPa] and a calculated connection strength of 27.5 [MPa].

## **4.2 GFRP Deck composite slab**

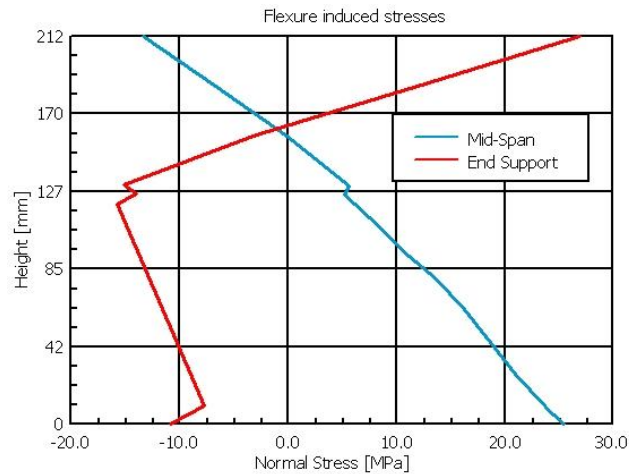
When analyzing the deck, its results are very intricate to analyze but the different approaches described in the previous chapters gave a range of results that permitted the comparison and understanding of the system.

### **4.2.1 Neutral Axis**

The obtained neutral axis from the FEM simulation has given a value of 125 [mm] which is not completely accurate since the model has a simplified geometry. The elastic neutral axis calculate at the Excel program has been calculated to 130 [mm]. This change is present since the computational model has included the diagonal sections of the deck while the hand calculations doesn't.

### **4.2.2 Flexure induced stresses**

The normal stresses from the bending moment have turned into the weakest factors of analysis, where the results are quite unsatisfactory. Graph 13 shows the axial distribution of stresses along the composite slab at its mid-span and at the end support, where a 15.6 [MPa] compressive stress and an 18 [MPa] tensile stress were obtained (at mid-span) with the Excel program. When comparing them, the results are very far from each other, especially the results for the tensile stresses at the bottom of the deck.



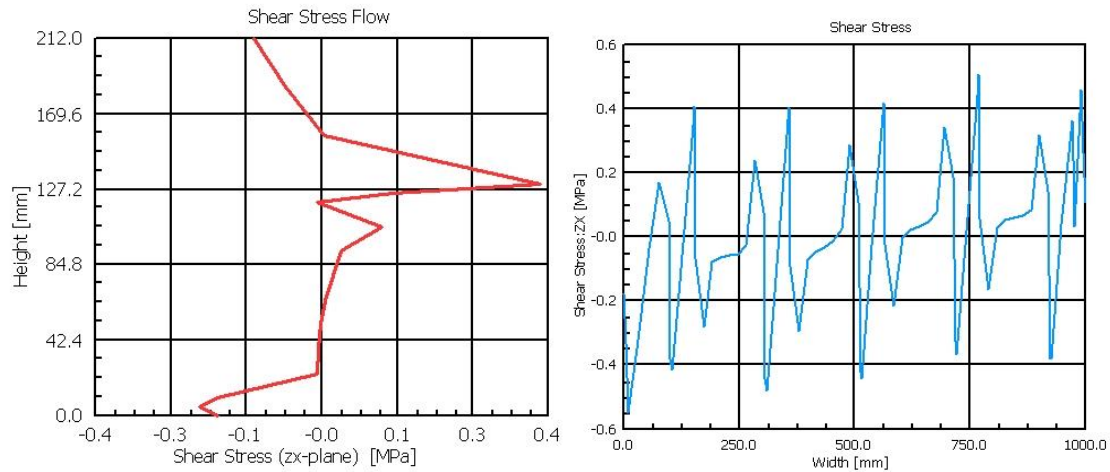
Graph 13. Normal stress distribution along the height of the composite slab.

These differences can have a variety of reasons, from the ones considered relevant we point out the most important ones:

- The complex analysis of the end support, where it has been assumed as simply supported for the Excel program and semi-fixed for the FEM simulation.
- The geometry of the deck's diagonals between the horizontal flanges can change drastically the behavior of the deck and hence, the performance of the composite slab.
- The longitudinal reinforcement, which has not been included into the model, has some influence on the overall behavior of the element, especially if it was taken into account at the Excel program.

#### 4.2.3 Longitudinal shear stress

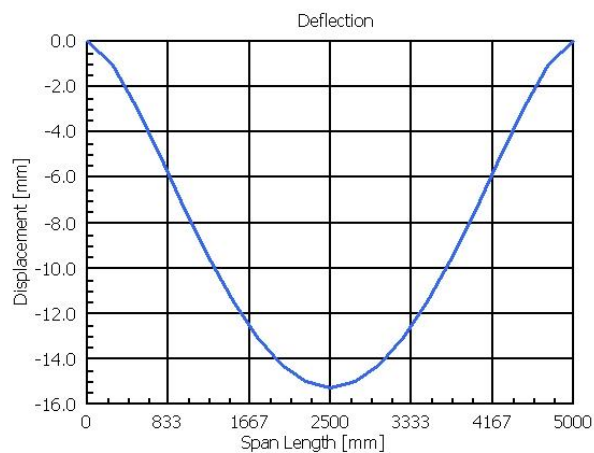
The longitudinal shear analysis presented in Graph 14 is represented by two lines, one from the mid part of the section and the other from the extreme lateral section. When comparing the two values, they can be understood as how the shear stress at the interface of the GFRP deck and the concrete slab is similar to the one predicted by the Excel program. It can be more certain the fact that the adhesive connection between the two can withstand this shearing effect thanks to its reliable 1 [MPa] resistance; assuring that it really works as a composite slab. The hand calculations estimated a maximum value of 0.37 [MPa] which is well below the maximum resistant value, even if the reduction factor of 2 provided by the manufacturer is included.



Graph 14. Shear stress at the interface between the deck and the concrete joined by a polymeric adhesive.

#### 4.2.3.1 Deflection

The deflection of the composite slab from the FEM simulation presented a smaller value than the one from the hand calculations, where it can be seen at Graph 15, its maximum value at mid-span is of 15.3 [mm], where the hand calculation estimated a value of 16.7 [mm]. Both this values have been estimated by means of the simplified deck geometry, however, for the values of the cross sectional area, the second moment of area and the section modulus given by the manufacturer are used, we obtain a 4.7 [mm] deflection of the composite slab. The deck's deflection (no presence of concrete) resulted in 19.5 [mm]. One final calculation was done considering the composite slab as being at a no-shear-interaction situation and the obtained value of displacement was of 10.2 [mm]. This huge dispersion of values can leave a big space for uncertainty.



Graph 15. Deflection curve of the composite slab.

#### 4.2.3.2 Fire situation

For the case of the fire analysis, the results of the simulation has portrayed the same effective outcomes as seen for the main beam, where the gypsum board insulates superbly the slab. This factor is equally important as for the main beam since the GFRP deck is the first element exposed to fire, and it been extremely vulnerable to temperature, it is very important to assure a proper insulation. In addition, the thin concrete slab on top of the deck has a small height that cannot withstand the loading by itself, deriving into a very dangerous situation which can involve partial collapse of the composite slab.

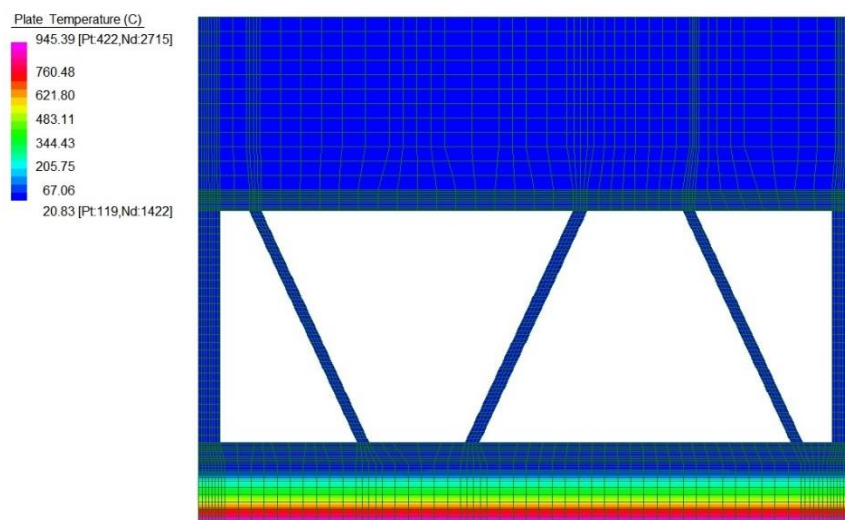


Figure 17. Temperature distribution in the composite slab after 60 minutes of fire.

## Chapter 5: Conclusions and Recommendations

After comparing all the possible aspects that involve the composite behavior of a beam and a slab, many conclusions can be derived when analyzing this particular GFRP-RC composite beam and its composite slab. The approaches taken to analyze the elements, through hand calculations at an Excel spreadsheet and a FEM simulation model, where done with as much precision and care as the tools allowed. For many aspects, the results have been satisfactory and can be a promising subject for future research. However, it is mandatory to proceed to laboratory testing that can corroborate or contradict the conclusions herein presented.

When dealing with the final design of the composite beam, all the different mechanical factors must be satisfied, and complying with all the codes requirements, some guides can be mentioned to assure its resistance. A practical and simple guide is [61] when dealing with pultruded elements, however, for the design of the Slimflor composite beam, it is best to follow [67] with some guidance from [4].

The neutral axes must be taken with much care since they can have drastic changes depending to their placement, where for example, located at the web will be different than if it would be located at the half height of the flange (slab). The resistance of the materials used must be handled with much care, especially for the GFRP pultruded profile which has an orthotropic mechanical behavior and, generally, its resistance in the transverse direction is much lower than in its longitudinal direction and compressive resistance is lightly higher than its tensile strength. Manufacturers are obliged to provide the different factors that represent its properties in each direction and for each type of stress. Fortunately, a variety of design codes and standards have presented the requirements for a safe design and, therefore, following these guides are mandatory; even if safety factors have massive values.

It is of the utmost importance the factor of the fire insulation since FRP is so vulnerable to temperature, and not only for the main composite beam but for the composite slab as well. Gypsum board has proven to have an excellent behavior in the presence of fire, and following the conclusions of the laboratory tests done by Keerthan et al., the FEM simulations recreated in this thesis can be reliable. Taking advantage that it is used as a ceiling covering for the architectural aesthetic design, it can fulfil both purposes accordingly, creating a uniform and continuous protection of all the ceiling.

## 5.1 The GFRP-RC composite beam

All the different stress values obtained from the results have shown that hand calculations done in a spreadsheet can be estimate with good accuracy, which can further allow the proper design of a particular beam. The normal stresses from the cross section flexure and the deflection had great similitude for both approaches, however, the longitudinal shear values may be complex to analyze, especially if so many elements are present, them being: the transverse reinforcement, the bolts from the connection and, above all, the adhesive polymer at the interface between the two materials.

Considering the results from both the elastic phase and the ultimate plastic resistance of the beam, it can be said that the design of such a beam could be done in a proper manner for the scope that has been established. In top of this, the massive strength reduction factors used in FRP pultruded elements (from manufacturers and design codes) can give an adequate safety margin to the final design. The great advantage of this system is the compatibility that the GFRP and concrete can have due to its similarity in their elastic moduli, which is the most important factor when dealing with deformation of the elements.

The analysis for the case of fire has shown that the GFRP-RC composite beam is completely vulnerable to fire, and thus, the insulation approach would be the best solution, especially if the gypsum board was already considered as part of the architectural elements. No other solution was considered because it would go against the scope of the structural system, where the objective is to simplify as much as possible the execution process of the structural floor. Nevertheless, one useful solution can be done by placing longitudinal reinforcement at the lower section of the composite beam. This reinforcement allows equilibrium to remain at the sagging bending moment since it would equilibrate the compressive forces from the slab, which are far from the heating source. Certainly, bending moment resistance will decrease since the lower flange of the pultruded profile would be lost little after the fire had started, at around 200 degrees Celsius.

Another important factor that needs to be addressed by the constructor is related to the process of construction, where it must be verified the possibility that the GFRP pultruded profile might need some propping, otherwise, it is vulnerable to instability such as global or local buckling. The analysis done in this thesis was focused on the behavior of the composite beam, not the pultruded profile by itself. Equally, the process related to the adhesive which will be placed

right before the pouring of the concrete must be performed adequately to assure a homogeneous behavior of the element along its longitudinal direction.

## **5.2 The composite slab**

The results obtained from the analysis of the composite slab were not all that satisfactory, however, considering the complexity of the deck's geometry and hence, the mechanical behavior, the results can give a glimpse of its potential. Fortunately, this GFRP deck can easily be replaced by the well-known steel deck used for many years now, not changing at all the behavior of the GFRP-RC beam since it is the protagonist of this analysis. This simple solution can reduce the uncertainty of the system with a small increase in weight, however, a thorough analysis should be performed to predict its behavior and, therefore, its design. Also, as mentioned for the composite beam, some propping could be required in some particular cases where the deck is not strong enough to hold the loads by itself until the concrete slab hardens and contributes with resistance.

## List of Figures

Figure 1. Pultrusion production process and variety of profiles.....	- 7 -
Figure 2. Unidirectional laminate subjected to normal stress.....	- 7 -
Figure 3. Laminae distribution of a multi-directional laminate.....	- 12 -
Figure 4. Steel-Concrete asymmetrical slim floor composite beam.....	- 18 -
Figure 5. Hogging and sagging plastic stress-block distribution.....	- 21 -
Figure 6. Cross section geometric parameters of the GFRP-RC composite beam.....	- 24 -
Figure 7. Placing of the neutral axes in the GFRP-RC composite beam.....	- 26 -
Figure 8. Shear stress flow. (a) Elastic phase, (b) Hogging bending moment plastic phase, (c) Sagging bending moment plastic phase.....	- 27 -
Figure 9. Shear stress planes analyzed for full interaction of the GFRP-RC composite beam. -	30 -
Figure 10. Lateral view and geometric parameters of the GFRP-RC beam.....	- 39 -
Figure 11. Connection geometric parameters of the GFRP-RC composite beam.....	- 41 -
Figure 12. FEM simulation models, (a) 2D plate model of the GFRP-RC composite beam, (b) 3D brick model of the GFRP-RC composite beam.....	- 43 -
Figure 13. Three dimensional brick model of the composite slab with a simplified geometry of the GFRP pultruded deck.....	- 44 -
Figure 14. Fire simulation from the time-step FEM procedure of the GFRP-RC composite beam. (a) Without insulation, (b) With insulation, gypsum board visible, (c) With insulation, gypsum board not visible, (d) 3D simulation.....	- 46 -
Figure 15. Longitudinal normal stresses of the FEM simulation for the GFRP-RC composite beam at SLS.....	- 49 -
Figure 16. FEM results of the connection: (a) vertical axial stresses. (b) Interlaminar shear stresses along the web.....	- 55 -
Figure 17. Temperature distribution in the composite slab after 60 minutes of fire.....	- 59 -

## List of Graphs

Graph 1. Deflection-Span Length ratio of the GFRP-RC composite beam.....	- 33 -
Graph 2. Standard fire curve from Eurocode 2.....	- 34 -
Graph 3. Thermal properties of the materials. (a) Conductivity, (b) Specific heat.....	- 37 -

Graph 4. (a) Stiffness loss in function of temperature, (b) Normalized strength loss by increasing temperature. ....	- 38 -
Graph 5. Temperature prediction of the gypsum board's internal face. ....	- 38 -
Graph 6. Normal stress distribution along the height of the GFRP-RC composite beam. .	- 49 -
Graph 7. Longitudinal shear stress along the height of the beam at the end support. ....	- 51 -
Graph 8. Plane shear stresses along the GFRP-RC composite beam at its critical plane. ...	- 52 -
Graph 9. Elastic deflection curve of the GFRP-RC composite beam. ....	- 52 -
Graph 10. Slip strain along the width of the beam at the end support. ....	- 53 -
Graph 11. Temperature distribution of the GFRP-RC composite beam after 30 and 60 minutes in a fire situation. ....	- 54 -
Graph 12. Interlaminar shear stress (xz-plane) along the height of the web, passing through the holes at the connection. ....	- 55 -
Graph 13. Normal stress distribution along the height of the composite slab. ....	- 57 -
Graph 14. Shear stress at the interface between the deck and the concrete joined by a polymeric adhesive. ....	- 58 -
Graph 15. Deflection curve of the composite slab. ....	- 58 -

# References

## Books

- [1] R.M. Jones. *Mechanics of composite materials*. Taylor & Francis Group: New York, 1999.
- [2] L.C. Bank. *Composites for construction: Structural design with FRP materials*. Wiley: New Jersey, 2006.
- [3] D.J. Oehlers, M.A. Bradford. *Elementary behavior of composite steel & concrete structural members*. BH: Oxford, 1999.
- [4] D.L. Mullett. *Composite floor systems*. Blackwell: Oxford, 1998.
- [5] R.P. Johnson. *Composite structures of steel and concrete: beams, slabs, columns and frames for buildings, 3<sup>rd</sup> Ed.* Wiley India: New Delhi, 2004.
- [6] S.P. Timoshenko, J.N. Goodier. *Theory of Elasticity, 3<sup>rd</sup> Ed.* Tata McGraw-Hill: New York, 2010.
- [7] L. Hollaway. *Polymer composites for civil and structural engineering*. Blackie Academic & Professional: Glasgow, 1993.
- [8] S. Russo. *Strutture in composito: sperimentazione, teoria e applicazioni*. Hoepli: Milan, 2007.
- [9] E.J. Barbero. *Introduction to composite materials design*. CRC Press: Boca Raton, 2011.
- [10] S. Timoshenko. *Strength of materials – Part 2: Advanced theory and problems, 3<sup>rd</sup> Ed.* CBS: New Delhi, 2002.
- [11] N.L. Hancox. *Fibre composite hybrid materials*. Macmillan: New York, 1981.
- [12] R. Figueiro. *Fibrous and composite materials for civil engineering applications*. Woodhead Publishing: Cambridge, 2011.

## Research publications

- [13] E.J. Barbero, S. Makkapati, J.S. Tomblin. *Experimental determination of the compressive strength of pultruded structural shapes*. Composites Science and Technology (59), pages 2047-2054, 1999.
- [14] R.C. Easby et al. *Failure model for phenolic and polyester pultrusions under load in fire*. Institute of Materials, Minerals and Mining, 2007.

- [15] I. Rahmanian, Y. Wang. *Thermal conductivity of gypsum at high temperatures: a combined experimental and numerical approach*. Czech Technical University Publishing House: Acta Polytechnica, vol. 49 n.1, 2009.
- [16] J.R. Correia, M.M. Gomes, J.M. Pires, F.A. Branco. *Mechanical behavior of pultruded glass fiber reinforced polymer composites at elevated temperatures: Experiments and model assessment*. Composite Structures n.98, pages 303-313, 2013.
- [17] Y. Bai et al. *Fire protection systems for building floors made of pultruded GFRP profiles - Part 2: Modelling of thermomechanical responses*. Composites: Part B n.41, pages 630-636, 2010.
- [18] J.R. Correia, F.A. Branco, J.G. Ferreira. *The effect of different passive fire protection systems on the fire reaction properties of GFRP pultruded profiles for civil construction*. Composites: Part A n.41, pages 441-452, 2010.
- [19] P. Keerthan, M. Mahendran. *Numerical studies of gypsum plasterboard panels under standard fire conditions*. Fire Safety Journal n.53, pages 105-119, 2012.
- [20] P. Makelainen, Z. Ma. *Fire resistance of composite slim floor beams*. Journal of Constructional Steel Research n.54, pages 345-363, 2000.
- [21] J. Cai, I.W. Burgess, R.J. Plank. *Modelling of asymmetric cross section members for fire conditions*. Journal of Constructional Steel Research n.58, pages 389-412, 2002.
- [22] W. Sebastian, G. Gegeshidze, S. Luke. *Positive and negative moment behaviours of hybrid members comprising cellular GFRP bridge decking epoxy-bonded to reinforced concrete beams*. Composites Part B n.45, pages 486-496, 2013.
- [23] T. Keller, H. Gurtler. *Quasi-static and fatigue performance of cellular FRP bridge deck adhesively bonded to steel girders*. Composite Structures n.70, pages 484-496, 2005.
- [24] W.M. Sebastian, J. Ross, T. Keller, S. Luke. *Load response due to local and global indeterminacies of FRP-deck bridges*. Composites Part B n.43, pages 1727-1738, 2012.
- [25] T. Keller, H. Gurtler. *In-plane compression and shear performance of FRP bridge decks acting at top chord of bridge girders*. Composite Structures n.72, pages 151-162, 2006.
- [26] H. Nordin, B. Taljsten. *Testing of hybrid FRP composite beams in bending*. Composites Part B n.35, pages 27-33, 2004.

- [27] Y. Kim, A. Fam. *Numerical analysis of pultruded GFRP box girders supporting adhesively-bonded concrete deck in flexure*. Engineering Structures n.33, pages 3527-3536, 2011.
- [28] A.B. Neto, H.L. Rovere. *Composite concrete/GFRP slabs for footbridge deck systems*. Composite Structures n.92, pages 2554-2564, 2010.
- [29] W.M. Sebastian, T. Keller, J. Ross. *Influences of polymer concrete surfacing and localized load distribution on behavior up to failure of an orthotropic FRP bridge deck*. Composites Part B n.45, pages 1234-1250, 2013.
- [30] T. Keller, H. Gurtler. *Design of hybrid bridge girders with adhesively bonded and compositely acting FRP deck*. Composite Structures n.74, pages 202-212, 2006.
- [31] Q.S. Yang, Q.H. Qin, D.H. Zheng. *Analytical and numerical investigation of interfacial stresses of FRP-concrete hybrid structure*. Composite Structures n.57, pages 221-226, 2002.
- [32] K.V. Subramaniam, C. Carloni, L. Nobile. *Width effect in the interface fracture during shear debonding of FRP sheets from concrete*. Engineering Fracture Mechanics n.74, pages 578-594, 2007.
- [33] R. Seracino, M.R. Saifulnaz, D.J. Oehlers. *Generic debonding resistance of EB and NSM plate-to-concrete joints*. Journal of Composites for Construction, ASCE January/February, 2007.
- [34] J.G. Dai, W.Y. Gao. *Bond-slip model for FRP laminates externally bonded to concrete at elevated temperature*. Journal of Composites for Construction, ASCE March/April, 2013.
- [35] C.A. Coronado, M.M. Lopez. *Experimental characterization of concrete-epoxy interfaces*. Journal of Materials in Civil Engineering, ASCE April, 2008.
- [36] J.R. Correia, F.A. Branco, J.G. Ferreira. *Flexural behavior of GFRP-concrete hybrid beams with interconnection slip*. Composite Structures n.77, pages 66-78, 2007.
- [37] S.K. Ha, S. Na, H.K. Lee. *Bond characteristics of sprayed FRP composites bonded to concrete substrate considering various concrete surface conditions*. Composite Structures n.100, pages 270-279, 2013.
- [38] H. Toutanji, G. Ortiz. *The effect of surface preparation on the bond interface between FRP sheets and concrete members*. Composite Structures n.53, pages 457-462, 2001.

- [39] J.T. Mottram. *Analysis and design of connections for pultruded FRP structures*. Composites in Construction, ASCE.
- [40] S.J. Smith, I.D. Parsons, K.D. Hjelmstad. *Experimental comparisons of connections for GFRP pultruded frames*. Journal of Composite Construction, ASCE February, 1999.
- [41] L.C. Bank. *Flexural and shear moduli of full-section fiber reinforced plastic (FRP) pultruded beams*. Journal of Testing and Evaluation, January, 1989.
- [42] T.M. Roberts. *Influence of shear deformation on buckling of pultruded fiber reinforced plastic profiles*. Journal of Composites for Construction, ASCE November, 2002.
- [43] R. Haj-Ali, H. Kilic. *Nonlinear behavior of pultruded FRP composites*. Composites Part B n.33, pages 173-191, 2002.
- [44] Y. Bai, T. Keller. *Shear failure of pultruded fiber-reinforced polymer composites under axial compression*. Journal of Composites for Construction, ASCE May/June, 2009.
- [45] L.C. Bank. *Shear properties of pultruded glass FRP materials*. Journal of Materials in Civil Engineering, ASCE, 1990.
- [46] V. Nagaraj, V.S. GangaRao. *Static behavior of pultruded GFRP beams*. Journal of Composites for Construction, ASCE August, 1997.
- [47] E.J. Barbero, S.H. Fu, I. Raftoyiannis. *Ultimate bending strength of composite beams*. Journal of Materials for Civil Engineering vol.3, ASCE, 1991.
- [48] S.J. Hicks, R.E. McConnel, M.D. Weerasinghe. *The testing of a full-scale stub-girder floor beam using Slimdek® construction*. Composite Construction in Steel and Concrete, pages 189-200.
- [49] Y. Wang, L. Yang, Y. Shi, R. Zhang. *Loading capacity of composite slim frame beams*. Journal of Construction Steel Research n.65, pages 650-661, 2009.
- [50] U. Kuhlmann, G. Hauf. *Efficient design for the calculation of the deflection and shear force capacity of slim-floor girder*. International Conference on Composite Construction in Steel and Concrete VI, ASCE, pages 185-198, 2011.
- [51] G.J. Kennedy, J.S. Hansen, J. Martins. *A Timoshenko beam theory with pressure corrections for layered orthotropic beams*. Elsevier, 2011.
- [52] P. Makelainen, J. Zhang, S. Peltonen. *Vertical shear resistance in a slim floor composite section*.

- [53] M. Savoia, N. Tullini. *Beam theory for strongly orthotropic materials*. Int. J. Solids Structures vol.33, n.17, pages 2459-2484, 1996.
- [54] S. De Nardin, A.L. El Debs. *Study of partially encased composite beams with innovative position of stud bolts*. Journal of Constructional Steel Research n.65, pages 342-350, 2009.
- [55] S. De Nardin, A.L. El Debs. *Composite connections in Slim-floor systems: An experimental study*. Journal of Constructional Steel Research n.68, pages 78-88, 2012.
- [56] K.D. Tsavdaridis, D. D’Mello, B.Y. Huo. *Experimental and computational study of the vertical shear behavior of partially encased perforated steel beams*. Engineering Structures n.56, pages 805-822, 2013.
- [57] C. Maraveas, T. Swailes, Y. Wang. *A detailed methodology for the finite element analysis of asymmetric slim floor beams in fire*. Nordic Steel Construction Conference 12<sup>th</sup>, pages 191-198, 2012.
- [58] H.N. Honickman. *Pultruded GFRP sections as stay-in-place structural open formwork for concrete slabs and girders*. Queen’s University: Ontario, 2008.
- [59] C. Cooper, G.J. Turvey. *Effects of joint geometry and bolt torque on the structural performance of single bolt tension joints in pultruded GRP sheet material*. Composite Structures n.32, pages 217-226, 1995.

## **Design codes and standards**

- [60] Fiberline Composites. *The Fiberline Design Manual*. Denmark, 2003.
- [61] Consiglio Nazionale Delle Ricerche. *Istruzioni per la progettazione, l’esecuzione ed il controllo di strutture realizzate con profili sottili pultrusi di materiale composito fibrorinforzato*. CNR-DT 205/2007: Rome, 2007.
- [62] Creative Pultrusions. *The Pultex® Pultrusion Design Manual*. USA, 2004.
- [63] The European Structural Polymeric Composites Group. *Structural design of polymer composites, EUROCOMP Design Code and Handbook*. E&FN SPON: London, 1996.
- [64] Tata Steel. *Slimdek® Manual*. CDM, 2007.
- [65] J.W. Rackman, S.J. Hicks, G.M. Newman. *Design of Asymmetric Slimflor beams with precast concrete slabs*. SCI: Ascot, 2006.
- [66] Eurocode 4: *Design of composite steel and concrete structures – Part 1-1: General rules and rules for buildings*. CEN, 2004.

- [67] Eurocode 4: *Design of composite steel and concrete structures – Part 1-2: General rules – Structural fire design*. CEN, 2003.
- [68] Eurocode 2: *Design of concrete structures – Part 1-1: General rules and rules for buildings*. CEN, 2004.

# MATERIAL PROPERTIES

## Pultex® Fiber Reinforced Polymer SuperStructural Profiles Wide Flange Sections and I-Sections Metric Version

1500 Series - Thermoset Polyester – Olive Green  
1525 Series - Thermoset Polyester Class 1 FR – Slate Gray (Dark Gray)  
1625 Series - Thermoset Vinyl Ester Class 1 FR – Beige

Pultex® SuperStructural Profiles are identified with veil-imprinted symbols.

The following data was derived from ASTM coupon and full section testing. The results are average values based on random sampling and testing of production lots. Composite materials are not homogeneous; and therefore, the location of the coupon extraction can cause variances in the coupon test results. Creative Pultrusions publishes an average value of random samples from production lots.

Property (coupon values)	ASTM Test	Units	1500/1525 Series	1625 Series
<b>Full Section</b>				
Modulus of Elasticity (12.7mm thick profiles)	Full Section <sup>2</sup>	GPa	26.8-27.6	26.8-27.6
(6.4mm & 9.5mm thick profiles)	Full Section <sup>2</sup>	GPa	26.8	26.8
Shear Modulus (Modulus of Rigidity)	Full Section <sup>2</sup>	GPa	27.6	27.6
Flexural Stress	Full Section <sup>2</sup>	GPa	3.4	3.4
	Full Section <sup>2</sup>	MPa	226.9	226.9
<b>Flange Section - Mechanical</b>				
Tensile Strength (LW)	D638	MPa	275.0	317.3
Tensile Modulus (LW)	D638	GPa	28.6	28.6
Compressive Strength (LW)	D695	MPa	315.7	362.1
Compressive Strength (CW)	D695	MPa	122.4	140.2
Compressive Modulus (LW)	D695	GPa	26.5	26.5
Compressive Modulus (CW)	D695	GPa	13.1	13.1
Flexural Strength (LW)	D790	MPa	295.2	339.3
Flexural Modulus (LW)	D790	GPa	13.7	13.7
Interlaminar Shear (LW) <sup>5</sup>	D2344	MPa	27.5	30.9
Shear Strength By Punch (PF)	D732	MPa	37.8	41.2
Notched Izod Impact (LW)	D256	J/m	1,494.6	1,708.1
Notched Izod Impact (CW)	D256	J/m	1,121.0	1,281.1
Maximum Bearing Strength (LW)	D953	MPa	226.9	261.2
Maximum Bearing Strength (CW) <sup>3</sup>	D953	MPa	158.1	182.2
Poisson's Ratio (LW)	D3039	mm/mm	0.35	0.35
Poisson's Ratio (CW)	D3039	mm/mm	0.12	0.12
<b>Web Section – Mechanical</b>				
Tensile Strength (LW)	D638	MPa	208.3	240.6
Tensile Strength (CW)	D638	MPa	72.2	82.5
Tensile Modulus (LW)	D638	GPa	21.3	21.3
Tensile Modulus (CW)	D638	GPa	9.6	9.6
Compressive Strength (LW)	D695	MPa	257.8	296.5
Compressive Strength (CW)	D695	MPa	97.6	112.3

Additional properties located on back



### CREATIVE PULTRUSIONS, INC.

214 Industrial Lane, Alum Bank, PA 15521  
814.839.4186 · Fax: 814.839.4276 · Toll free 888.CPI.PULL  
Email: crpul@pultrude.com · www.creativepultrusions.com

Creative Pultrusions, Inc. reserves the right to edit and modify literature, please consult the web site for the most current version of this document.

CPM61-1099r6.50  
Revision Date: 07.02.13

# MATERIAL PROPERTIES

## Pultex<sup>®</sup> Fiber Reinforced Polymer **SuperStructural** Profiles Wide Flange Sections and I-Sections Metric Version (cont'd)

Property (coupon values)	ASTM Test	Units	1500/1525	
			Series	1625 Series
<b>Web Section - Mechanical</b>				
Compressive Modulus (LW)	D695	GPa	19.2	19.2
Compressive Modulus (CW)	D695	GPa	13.1	13.1
Flexural Strength (LW)	D790	MPa	297.8	342.4
Flexural Strength (CW)	D790	MPa	119.3	136.8
Flexural Modulus (LW)	D790	GPa	13.1	13.1
Flexural Modulus (CW)	D790	GPa	12.0	12.0
Interlaminar Shear (LW) <sup>5</sup>	D2344	MPa	23.4	26.8
Shear Strength By Punch (PF)	D732	MPa	37.8	41.2
Notched Izod Impact (LW)	D256	J/m	2,028.4	2,295.3
Notched Izod Impact (CW)	D256	J/m	1,014.2	1,174.3
Maximum Bearing Strength (LW)	D953	MPa	233.6	268.1
Maximum Bearing Strength (CW) <sup>3</sup>	D953	MPa	206.2	237.2
Poisson's Ratio (LW)	D3039	mm/mm	0.35	0.35
Poisson's Ratio (CW)	D3039	mm/mm	0.12	0.12
In-plane Shear (LW)	Modified D2344 <sup>4</sup>	MPa	48.3	48.3
<b>Physical</b>				
Barcol Hardness <sup>1</sup>	D2583		33	39
Water Absorption	D570	% Max	0.6	0.6
Density	D792	Mg/m <sup>3</sup>	1.66-1.93	1.66-1.93
Specific Gravity	D792		1.66-1.93	1.66-1.93
Coefficient of Thermal Expansion (LW)	D696	10 <sup>-6</sup> K <sup>-1</sup>	8	8
Thermal Conductivity (PF)	C177	W/mK	0.58	0.58
<b>Electrical</b>				
Arc Resistance (LW)	D495	seconds	120	120
Dielectric Strength (LW)	D149	kV/mm	1.58	1.58
Dielectric Strength (PF)	D149	kV/mm	7.9	7.9
Dielectric Constant (PF)	D150	@60Hz	5.2	5.2

LW = lengthwise

CW = crosswise

PF = perpendicular to laminate face

<sup>1</sup>Pultex<sup>®</sup> uses a synthetic veil that reduces the Barcol Hardness, but does not reflect lack of cure.

<sup>2</sup>Full section testing is based on a 3-point bend with simply supported end conditions (Reference [The New and Improved Pultex<sup>®</sup> Pultrusion Global Design Manual](#) Appendix for details).

<sup>3</sup>Crosswise bearing strength of the Web sections of 1/4" profiles = 20,500 psi.

<sup>4</sup>Follow ASTM D2344, but rotate coupon 90° (cut section of coupon length faces up).

<sup>5</sup>Tested on a 3:1, span to depth ratio.

Property	ASTM Test	Value	
		1525	1625
Flammability Classification	UL94	(VO)	(VO)
Tunnel Test	ASTM E-84	25 Max	25 Max
Flammability Extinguishing	ASTM D635	Self extinguishing	Self extinguishing
NBS Smoke Chamber	ASTM E662	650	650

Creative Pultrusions, Inc. believes the information put forth in this property sheet to be as accurate and reliable as of the date of publication.

However, we assume no obligation or liability which may arise as a result of its use. While Creative Pultrusions, Inc. has no knowledge that the information put forth infringes any valid patent, it assumes no responsibility with respect thereto and each user must satisfy oneself that one's intended application process or product infringes no patent.

*"No portion of this Material Properties Sheet may be reproduced in any form without the prior written consent of Creative Pultrusions, Inc."*

Copyright © 1999 by  
Creative Pultrusions, Inc.  
All Rights Reserved

Flowgrip<sup>®</sup> and Pultex<sup>®</sup> are registered trademarks of Creative Pultrusions, Inc. Creative Pultrusions<sup>®</sup>, Shaping the Future<sup>®</sup>, Superstud<sup>®</sup>, Superstud<sup>®</sup>/Nuts<sup>®</sup>, Superstik<sup>®</sup>, SUPERTUF<sup>®</sup>, Superplank<sup>®</sup>, Superdeck<sup>®</sup>, Supergrate<sup>®</sup>, Tuf-dek<sup>®</sup>, SuperLoc<sup>®</sup>, SuperWale<sup>®</sup>, SuperCap<sup>®</sup>, SuperRod<sup>®</sup>, Pultrusion Dynamics<sup>®</sup>, DYNARUL<sup>®</sup>, Pulshaping<sup>®</sup>, TOPSCAN<sup>®</sup> and TOPDIE<sup>®</sup> are trademarks of Creative Pultrusions, Inc.

**Pultex® Fiberglass Standard Structural Profiles and Superstud!™/Nuts!  
Metric Product Availability List**

All Items are available upon request in standard resin series:						Delivery:											
Series 1500 = Isophthalic Polyester (I) - Olive Green						Stocked Items: 1-3 days											
Series 1525 = Isophthalic Fire Retardant (IFR) - Slate Gray (Dark Gray)						Items Out of Stock: 2 weeks											
Series 1625 = Vinyl Ester Fire Retardant (VFR) - Beige						Non-Stocked Items: 2-4 weeks											
x = Stocked Items (All items stocked in 6.1m lengths unless otherwise noted.)																	
Equal Leg Angle						Unequal Leg Angle						I-Beam					
Size (mm)	I	F	V	Mill Run (m)	Wt. (kg/m)	Size (mm)	I	F	V	Mill Run (m)	Wt. (kg/m)	Size (mm)	I	F	V	Mill Run (m)	Wt. (kg/m)
25 x 3	x	x		910	0.25	102 x 152 x 10				210	4.38	76 x 38 x 6♦				430	1.50
25 x 6				760	0.46	102 x 152 x 13				210	5.58	102 x 51 x 6♦		x		400	2.43
38 x 3				820	0.37	127 x 254 x 13				210	8.70	152 x 76 x 6♦	x	x		240	3.56
38 x 5				670	0.57							152 x 76 x 10♦		x		240	5.62
38 x 6	x	x	x	610	0.76							203 x 102 x 10♦	x	x		180	7.05
51 x 3				760	0.52	<b>Channel</b>						203 x 102 x 13♦		x		210	9.60
51 x 5				610	0.83							254 x 127 x 10♦				210	9.02
51 x 6	x	x	x	550	1.01	Size (mm)	I	F	V <td>Mill Run (m) <td>Wt. (kg/m) <td>254 x 127 x 13♦</td> <td></td> <td>x*</td> <td></td> <td>180</td> <td>11.80</td> </td></td>	Mill Run (m) <td>Wt. (kg/m) <td>254 x 127 x 13♦</td> <td></td> <td>x*</td> <td></td> <td>180</td> <td>11.80</td> </td>	Wt. (kg/m) <td>254 x 127 x 13♦</td> <td></td> <td>x*</td> <td></td> <td>180</td> <td>11.80</td>	254 x 127 x 13♦		x*		180	11.80
76 x 3				610	0.79	38 x 25 x 5				670	0.71	305 x 152 x 13♦				120	14.63
76 x 5				460	1.16	51 x 14 x 3				850	0.40	*Stocked in 7.62m lengths only.					
76 x 6	x	x	x	460	1.58	70 x 25 x 3				1,520	0.62	<b>Wide Flange Beam</b>					
76 x 10	x*	x	x	370	2.59	76 x 22 x 6	x***	x		520	1.16						
102 x 6♦		x	x	400	2.37	76 x 25 x 5				550	0.94						
102 x 10♦		x	x	270	3.39	76 x 38 x 6			x	400	1.46						
102 x 13♦	x	x		400	4.48	102 x 27 x 3				580	0.80						
152 x 6♦				270	3.41	102 x 3 x 44 x 5		x		460	1.29	Size (mm)	I	F	V <td>Mill Run (m) <td>Wt. (kg/m) </td></td>	Mill Run (m) <td>Wt. (kg/m) </td>	Wt. (kg/m)
152 x 10♦		x		240	5.31	102 x 29 x 6		x	x	370	1.52	76 x 6♦	x	x		300	2.74
152 x 13♦		x	x	210	6.93	127 x 35 x 6				400	2.04	102 x 6♦	x	x*	x	240	3.63
*Stocked in NSF Olive Green Only.						152 x 41 x 6	x	x	x	370	2.48	152 x 6♦		x*		210	5.42
						152 x 43 x 10	x**	x	x	300	3.73	152 x 10♦		x	x	180	8.23
						178 x 51 x 6				370	3.06	203 x 10♦		x		120	10.80
						203 x 57 x 6		x***	x***	300	3.30	203 x 13♦		x*		120	14.86
						203 x 56 x 10	x***	x	x	240	4.88	254 x 10♦				120	13.49
						254 x 70 x 3				460	2.14	254 x 13♦		x*		120	17.90
						254 x 70 x 13			x	180	8.58	305 x 13♦		x**		90	22.20
						292 x 70 x 13♦				180	9.61	*Stocked in 6.1m and 7.62m lengths only.					
						610 x 76 x 6				180	8.35	**Stocked in 7.62m lengths only.					
						356 x 152 x 13♦				150	15.54	<b>Round Tube</b>					
						610 x 102 x 13				150	16.68						
						**Stocked in 6.12m, 9.17m and 12.22m lengths only.						Size (mm)	I	F	V <td>Mill Run (m) <td>Wt. (kg/m) </td></td>	Mill Run (m) <td>Wt. (kg/m) </td>	Wt. (kg/m)
						***Stocked in 6.12m, 7.65m and 9.17m lengths only.						19 x 2				610	0.25
						****Stocked in 6.12m lengths only.						25 x 3	x	x		610	0.42
						+Stocked in Light Gray: 7.47m, 8.89m and 9.45m Lengths.						32 x 2				580	0.40
						+**Stocked in 1525 Light Gray and 1625 Beige Only. Call for availability.						32 x 3				580	0.51
						+Also available in SUPUR TUF™ Polyurethane Resin. Consult factory.						38 x 3	x	x		580	0.62
												38 x 6	x			460	1.15
												44 x 3				490	0.74
												44 x 6			x	460	1.35
												51 x 3				460	0.95
												51 x 6		x*		430	1.61
												63 x 3¹				460	0.92
												63 x 6				300	1.96
												76 x 6				270	2.47
												102 x 88²				213	3.84
												*Stocked in Dark Gray and Yellow Only.					
												¹Reference Part Drawings for Actual Dimensions.					
												²Part Construction is Special. Consult Factory for Special Properties.					

Creative Pultrusions, Inc. reserves the right to edit and modify literature, please consult the web site for the most current version of this document.

	<p><b>CREATIVE PULTRUSIONS, INC.</b> 214 Industrial Lane, Alum Bank, PA 15521 814.839.4186 · Fax: 814.839.4276 · Toll free 888.CPI.PULL Email: crpul@pultrude.com · www.creativepultrusions.com</p>	<p>CPSALM-0111.1C DLR: 05.30.13</p>
---	---	---

Square Tube						Solid Round Rod						Special Shapes							
Size (mm)	I	F	V	Mill Run (m)	Wt. kg/m	Size (mm)	I	F	V	Mill Run (m)	Wt. kg/m	Size (mm)	I	F	V	Mill Run (m)	Wt. kg/m		
25 x 3	x	x	x**	550	0.49	6				3,050	0.06	Toe Plate							
32 x 6 <sup>1</sup>				300	1.13	10	x			1,520	0.14	102 x 13 x 3		x'	x'	760	0.79		
38 x 3	x	x		550	0.71	13	x			1,070	0.26	152 x 13 x 3					760	1.07	
38 x 6			x**	760	1.37	16				730	0.41								
44 x 3 <sup>1</sup>				760	0.80	19	x			610	0.59	Curb Angle							
44 x 6 <sup>1</sup>		x'	x'	490	1.67	25	x			460	1.02	25 x 38 x 6				x**	430	1.34	
51 x 3	x	x'	x'	490	1.03	32	x			370	1.64	38 x 38 x 6				x**	400	1.52	
51 x 6	x****	x'	x'	370	2.08	38	x			270	2.28	51 x 38 x 6				x**	370	1.64	
54 x 5 <sup>1</sup>	x	x'	x'	460	1.61	51				180	3.81								
63 x 6				300	2.66	All Rods Stocked in Natural Color.						Gate Guide							
76 x 6		x		240	3.21	Solid Square Bar						63 x 57 x 6	x***			760	1.80		
89 x 10				210	5.51	Size (mm)	I	F	V	Mill Run (m)	Wt. kg/m	Sludge Flight							
102 x 6		x		210	4.40	6				3,050	0.06	152 x 3 x 63 x 6	x**				300	2.26	
132 x 10				210	8.66	25		x		490	1.20	203 x 3 x 63 x 6	x**				300	2.48	
152 x 10				210	11.62	32 (Actual 812.8mm) <sup>1</sup>		x'		300	1.89	U-Trough							
*Stocked in Yellow Only.						38 (Actual 965.2mm) <sup>1</sup>	x**	x'		240	2.74	216 x 235 x 6					300	7.36	
**Stocked in Dark Gray and Yellow Only.						*Stocked in Yellow Only.						305 x 305 x 6					300	9.40	
***Stocked in Dark Gray, Yellow and Beige.						**Stocked in Yellow and Green						Square Tube with Round Hole							
****Stocked in 6, 12m Lengths Only.						Reference Part Drawings for Actual Dimensions.						25 x 19 dia.	x***	x***		1,520	0.70		
Reference Part Drawings for Actual Dimensions.						Flat Strip						Door Frame							
Flat Sheet						Flat Strip						152						460	2.44
Size (mm)	I	F	V	Mill Run (sheets)	Wt. kg/m <sup>2</sup>	Size (mm)	I	F	V	Mill Run (m)	Wt. kg/m	Fluted Ladder Rung							
3 x 1219 x 2438	x	x	x	188	5.71	3 x 63				3,050	0.36	31 x 3				x'	610	0.48	
5 x 1219 x 2438	x			140	8.25	3 x 102		x**		1,830	0.58								
6 x 1219 x 2438	x	x'	x	94	11.08	5 x 63		x'		1,830	0.55								
10 x 1219 x 2438		x	x	63	16.89	6 x 102				910	1.13								
13 x 1219 x 2438		x	x	47	22.65	6 x 152				610	1.64								
16 x 1219 x 2438				40	28.17	6 x 229				460	2.83								
19 x 1219 x 2438				30	32.08	10 x 76				910	1.29								
25 x 1219 x 2438				20	46.14	10 x 152				460	2.41								
**Stocked in Light Gray and Slate Gray.						13 x 51				910	1.12								
Rectangular Tube						Note: Many other Flat Strips are available. Consult factory for other sizes.													
Size (mm)	I	F	V	Mill Run (m)	Wt. kg/m	*Stocked in Yellow 6.4m Lengths Only.						+* Stocked in NSF Light Gray Only.							
32 x 19 x 3 <sup>1</sup>				500	0.39	**Stocked in Yellow 6.82m Lengths Only.						+** Stocked in 1525 Light Gray and 1625 Beige Only: 7.62m Lengths. Call for Availability.							
102 x 3 x 44 x 6 <sup>1</sup>				600	2.04	Superstud™/Nuts! Fasteners and Isoplast™ Hex Nuts						Adhesive Epoxy							
113 x 37 x 3 <sup>1</sup>				750	1.53							1/2 Gallon Kit (includes 1 quart base and 1 quart hardener)							
121 x 44 x 3 <sup>1</sup>				750	1.74													Stocked	
127 x 51 x 3 <sup>1</sup>				750	2.14													x	
152 x 51 x 3 <sup>1</sup>				800	2.98														
203 x 25 x 2 <sup>1</sup>				300	2.74	Size (mm)	Superstud	Wt. m	Nuts/Hexnuts	Wt. m	Wt. m (Hex nuts)								
*Shapes contain internal webs.						3/8 - 16 UNC	x	0.11	x	0.25	0.20								
Reference Part Drawings for Actual Dimensions.						1/2 - 13 UNC	x	0.19	x	0.50	0.41								
Rectangular Box Beams						5/8 - 11 UNC	x	0.31	x	0.45	0.41								
Size (mm)	I	F	V	Mill Run (m)	Wt. Ft.	3/4 - 10 UNC	x	0.47	x	0.57	0.57								
152 x 102 x 6				300	5.73	1 - 8 UNC	x	0.88	x	0.61	0.59								
178 x 102 x 6				300	6.07	Superstud™ is stocked in 1.22m and 2.44m Lengths and is made with Series 1625 VFR resin.						Flowgrip® and Pute® are registered trademarks of Creative Pultrusions, Inc. Creative Pultrusions™, Shaping the Future™, Superstud™, Superstud™/Nuts!, Superstik™, SUPUR TUF™, Superplank™, Superdeck™, Supergate™, Tuf-dek™, SuperLoc™, SuperWale™, SuperCa							
178 x 102 x 10				240	8.91	Isoplast™ Flanged Hex Nuts are also stocked in all sizes. Please specify square or hex nuts when ordering.													
203 x 102 x 6				300	6.67														
203 x 102 x 9				240	8.70														

Creative Pultrusions, Inc. reserves the right to edit and modify literature, please consult the web site for the most current version of this document.



**CREATIVE PULTRUSIONS**

**CREATIVE PULTRUSIONS, INC.**  
 214 Industrial Lane, Alum Bank, PA 15521  
 814.839.4186 · Fax: 814.839.4276 · Toll free 888.CPI.PULL  
 Email: crpul@pultrude.com · www.creativepultrusions.com

CPSALM-0111.1C  
DLR: 05.30.13

## Mechanical properties of structural profiles

When using Fiberline structural profiles for load-carrying purposes, typical ultimate strength and deflection calculations are made. Complete calculations are carried out in accordance with the Fiberline Design Manual which takes the anisotropic properties of the materials into account.

All values listed below are based on measurements carried out in Fiberline's own laboratories or by independent testing institutes.

### Material parameters

Characteristic stiffness values and transverse contraction			
Elasticity modulus	GPa	E0°	17/23/28*
Elasticity modulus	GPa	E90°	8,5
Shear modulus	MPa	G	3,00
Poisson's ratio	-	V0°,90°	0,23
Poisson's ratio	-	V90°,V0°	0,09

\* The E-modulus varies from 17-28 GPa depending on geometry and reinforcement - See profile tables here for specific values

The E-modulus of the profiles varies from 23 - 28 GPa depending on the geometry and reinforcement. See Fiberline Design Manual for the load-carrying capacities of the individual profiles.

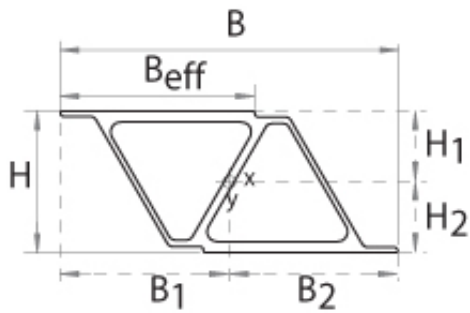
The material values stated are valid for temperatures between -20°C and 60°C (dry condition).

Characteristic strength values		[MPa]
Bending strength, 0°	$f_{b,0^\circ}$	240
Bending strength, 90°	$f_{b,90^\circ}$	100
Tensile strength, 0°	$f_{t,0^\circ}$	240
Tensile strength, 90°	$f_{t,90^\circ}$	50
Compressive strength, 0°	$f_{c,0^\circ}$	240
Compressive strength, 90°	$f_{c,90^\circ}$	70
Shear strength	$f_t$	25
Pin-bearing strength, longitudinal direction	$f_{cB,0^\circ}$	150
Pin-bearing strength, transverse direction	$f_{cB,90^\circ}$	70

Note: For temperatures exceeding 60°C, strengths and stiffnesses must be reduced in accordance with the Fiberline Design Manual.  
The Fiberline Design Manual provides dimensioning guidelines, including tables of load-carrying capacities and more specific geometric properties.



## FBD450 Clap Bridge Deck - Product data



### Specifications

#### Dimensions:

H	130,00 mm
B	310,70 mm
B <sub>eff</sub>	178,80 mm
B <sub>1</sub>	155,35 mm
B <sub>2</sub>	155,35 mm
H <sub>1</sub>	65,00 mm
H <sub>2</sub>	65,00 mm

#### Geometrical data - the profile:

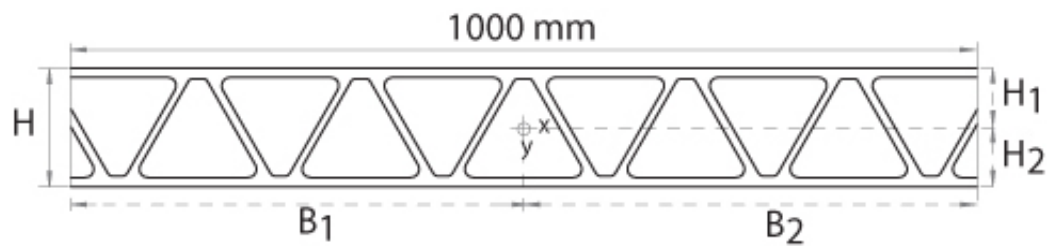
A	6156 mm <sup>2</sup>
I <sub>x</sub>	16,0x10 <sup>6</sup> mm <sup>4</sup>
W <sub>x</sub>	246,2x10 <sup>3</sup> mm <sup>3</sup>
I <sub>y</sub>	30,0x10 <sup>6</sup> mm <sup>4</sup>
W <sub>y</sub>	193,1x10 <sup>3</sup> mm <sup>3</sup>

**Stiffness:**

E <sub>0°</sub>	21,5x10 <sup>3</sup> MPa
-----------------	--------------------------

**Weight:**

Weight	11480 g/m
--------	-----------



**Dimensions:**

H	130,0 mm
B <sub>1</sub>	500,0 mm
B <sub>2</sub>	500,0 mm
H <sub>1</sub>	66,2 mm
H <sub>2</sub>	63,8 mm

**Geometrical data - the module:**

A	35312 mm <sup>2</sup> /m
---	--------------------------

$I_x$  91,1x10<sup>6</sup> mm<sup>4</sup>/m

$W_x$  1376,1x10<sup>3</sup> mm<sup>3</sup>/m

**Stiffness:**

$E_0$  21,5x10<sup>3</sup> MPa

**Weight:**

Weight 65850 g/m<sup>2</sup>

Data	
Geometric	
Bc [mm]	650
B [mm]	300
b [mm]	150
hF [mm]	64
hw [mm]	140
tw [mm]	12
tuf [mm]	8
tlf [mm]	8
H [mm]	220
bD [mm]	220
hD [mm]	130
diam. L [mm]	12
diam. T [mm]	8
nl [uni]	6
dl2[mm]	150
L [m]	6
Contr. L [m]	5
Material	
fpc [Mpa]	278
fpt [Mpa]	244
fcd [Mpa]	11
fyd [Mpa]	391
Ec [Mpa]	29962
Ep [Mpa]	28600
Es [Mpa]	205000
E [Mpa]	27551
G [Mpa]	12334
$\gamma_p$ [kN/m3]	19
$\gamma_c$ [kN/m3]	25
$\sigma_{adh}$ [Mpa]	1
Distributed Loads	
q SLS [kN/m]	25.7
q ULS [kN/m]	35.9
Results	
ad [mm]	45
dl [mm]	31
dt [mm]	41
Asl [mm2]	113.1
Ast [mm2]	402.1
S [mm]	108.3
r SLS [mm]	59.08
r ULS [mm]	26.26
nc	0.95
ns	0.14
As [pc]	0.8%
H slab [mm]	82
b web [mm]	210

### Material Properties

Concrete	fck [Mpa]	20
	fcd [Mpa]	11.3
	fctm [Mpa]	2.2
Steel	fyk [Mpa]	450
	fyd [Mpa]	391.3

GFRP	
fpc [Mpa]	362
fpcd [Mpa]	278
fptk [Mpa]	317
fptd [Mpa]	244

GFRP-RC Composite Beam				
Material	V	E [Mpa]	$\nu$	G [Mpa]
Concrete	0.933	29962	0.2	12484.1
Pultruded	0.067	28600	0.35	10592.6
Steel	0.001	205000	0.28	80078.1

### Neutral Axes and Second Moment of Area

Elastic neutral axis			
Qp	467424	Ap [mm2]	6048
Qc	12394294	Ac [mm2]	83940
QT	12861718	AT [mm2]	89988
HU	77.1	Acs [mm2]	44215
HL	142.9	Ach [mm2]	10718

Elastic Ix		
Material	Initial	M. ratio
lxp	5.78E+07	5.78E+07
lxc	2.35E+08	2.46E+08
lxs	1.45E+06	1.04E+07
lxT	2.94E+08	3.14E+08

Plastic for Sagging B.M (+)		
(HU, HL)	69.30	150.70
lxp	64370457	64370457
lxc	17058319	17870647
lxs	1001628	7179500
lxT	8.243E+07	8.942E+07

Plastic for Hogging B.M (+)		
(HU, HL)	134.34	85.66
lxp	32200304	32200304
lxc	0	0
lxs	7252208	51982611
lxT	3.95E+07	8.42E+07

### Loading Actions

SLS			
M (-) [kN.m]	77.14	Curv.	8.914E-06
M(+) [N.mm]	38.57		4.457E-06
V SLS [N]	77136		

ULS		
Mu [kN.m]	53.8	107.7
M=0 (x1,x2)	1.27	4.73
V ULS [kN]	10.8	107.7

Permanent	[kN/m2]	[kN/m]
Conc.	2.29	11.93
FRP	0.18	0.11
Deck	0.65	3.25
Gypsum	0.5	2.61
Total	3.62	17.90

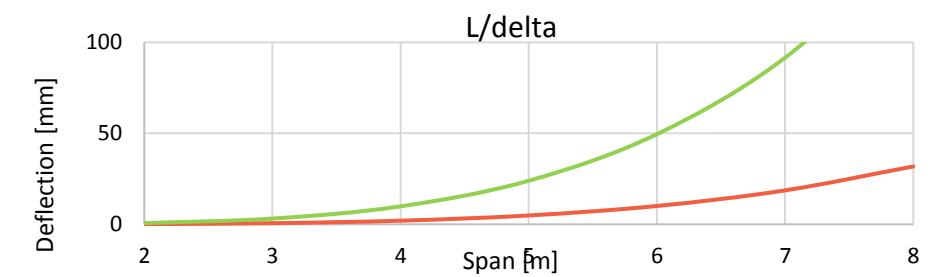
Variable	[kN/m2]	[kN/m]
	1.5	7.8
	[kN/m2]	[kN/m]
<b>Total Load</b>	5.1	25.7
q SLS	4.9	25.7
q ULS	6.9	35.9

### SLS Verification

$\delta$ (Deflection at mid-span) SLS			
B.M.	Shear	Total	(L/ $\delta$ )
10.03	0.06	10.09	595

Vibration check	
$\delta_{sw}$ [mm]	7.02
fsw [c/s]	6.8
fsls [c/s]	5.7

Stress limit control for SLS				
	Hogging M(-)		Sagging M(+)	
	$\epsilon^*$	$\sigma$ [Mpa]	$\epsilon^*$	$\sigma$ [Mpa]
Steel	0.00041	84.20	-0.00021	-42.10
Concrete (U)	0.00069	20.59	-0.00034	-10.29
Concrete (L)	-0.00120	<b>-36.04</b>	0.00060	18.02
P-beam (U)	0.00069	19.65	-0.00034	-9.82
P-beam (L)	-0.00127	-36.44	0.00064	18.22

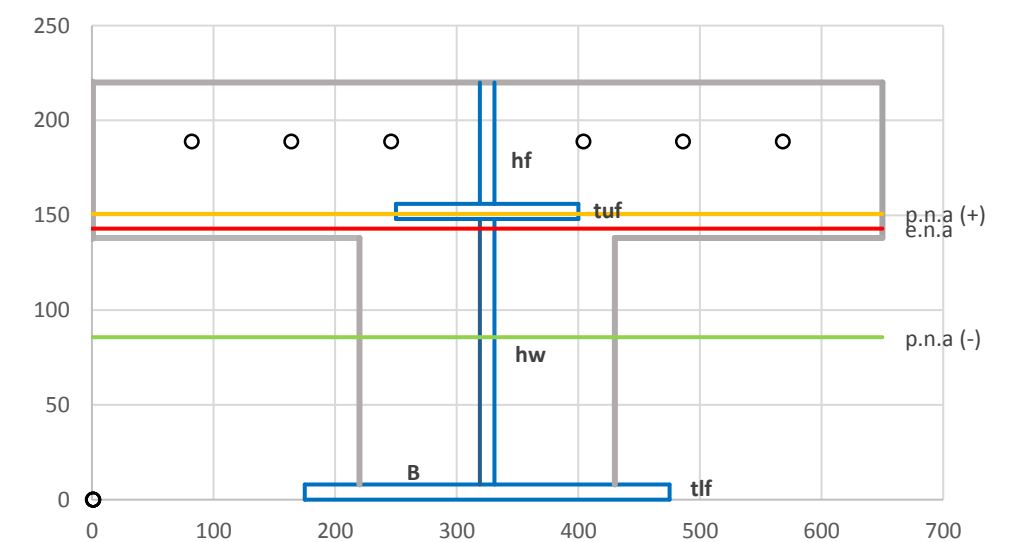


### ULS Resistance

ULS bending moment		
Forces [kN]	Sagging - M(+)	Hogging - M(-)
Rs	265532.9	
Rc	564420.7	0.0
Rpp[c]	565729.7	685702.3
Rpp1	417555.8	259518.3
Rpp2	307421.5	269206.2
Rpp3	585230.8	668307.7

Resistant bending moment		
Mcp	49731731	64654534
Mtp	115644244	91354151
MRd [kN.m]	165375975	156008685
	<b>141</b>	<b>133</b>
Shear Resistance		
VR [kN]	453.1	
VRd [kN]	<b>151</b>	

$\delta$ (Deflection at mid-span) ULS			
B.M.	Shear	Total	(L/ $\delta$ )
49.16	0.19	49.34	<b>122</b>

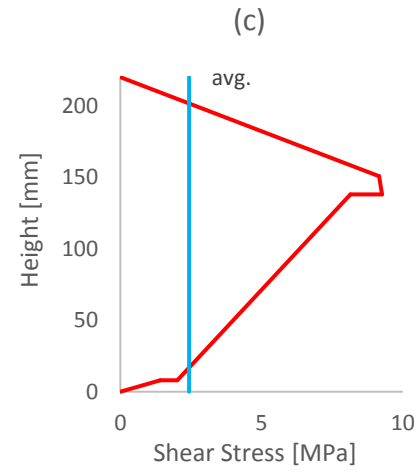
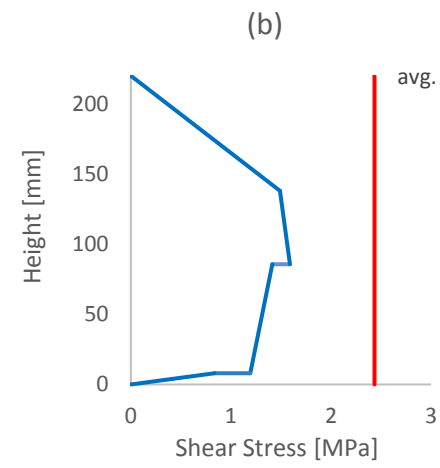
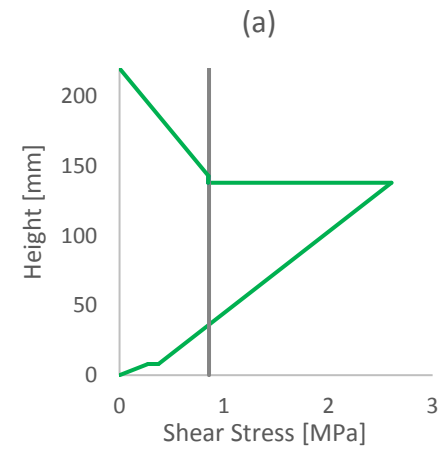


## Shear Stress Flow

Elastic				
Section	Q [mm <sup>3</sup> ]	sum Q	$\tau_c$ [Mpa]	
1	1836458	-	0.66	
2	8259.06	2336412	0.85	
3	-	-	0.85	
4	1994727	2328153	2.61	
5	-	-	0.37	
6	333425	-	0.27	
			$\tau$ ave. [Mpa]	0.86
			k	3.04

Plastic hogging b.m.				
Section	Q	Sum Q	$\tau_c$ [Mpa]	
4	244680	-	0.5	
3-4	-	-	1.5	
3	16434	261114	1.6	
2	36190	232185	1.4	
1-2	-	-	1.2	
1	195994	-	0.8	
			$\tau$ ave. [Mpa]	0.86
			k	1.85

Plastic sagging b.m.				
Section	Q	Sum Q	$\tau_c$ [Mpa]	
4	1508505	-	3.0	
3-4	-	-	9.2	
3	16930	1525435	9.3	
2	1069040	1421115	8.1	
1-2	-	-	2.0	
1	352075	-	1.4	
			$\tau$ ave. [Mpa]	2.43
			k	3.80



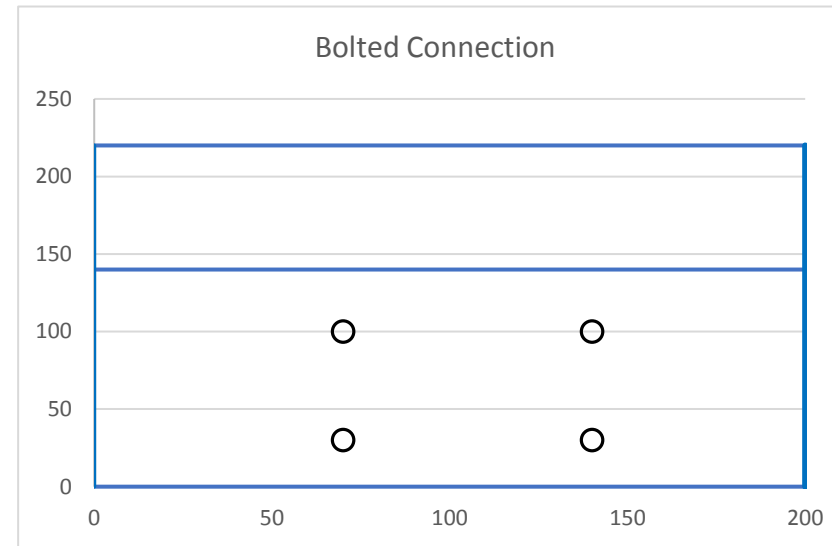
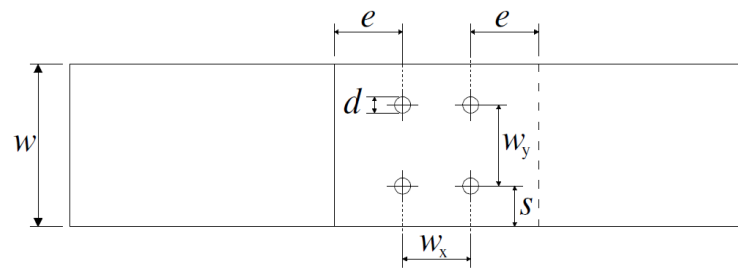
## Connection Design

Data	
Ncol [uni]	2
Nrow [uni]	2
d [mm]	16
Bolt Design	
d bolt [mm]	12
n bolt [uni]	4
V/bolt [kN]	26.9
VRd [kN]	193.0
VRd/bolt [kN]	48.3
FRP Properties [Mpa]	
ft,0	185.1
fc,0	228.1
ft,90	63.5
fc,90	86.4
f <sub>T</sub>	20.6
fc <sub>b,0</sub>	206.2
fc <sub>b,90</sub>	182.5
fy,s	240
Steel Bolt Strenght [Mpa]	
fub	500
τ <sub>u</sub>	240

CNR-DT205		
12.0	< db = 16 <	18.0
Dist. [mm]	Exact	Design
w <sub>x</sub> , w <sub>y</sub>	68	70
e	64	70
s	34	40
Total y	136	<b>150</b>

FRP Stregth (Vsd)	
Direction	
0°	90°
Shear [Mpa]	
214.0	73.4
Intralaminar [Mpa]	
27.5	
Bearing [Mpa]	
39.6	35.0

Shear at last bolt	
Vuls,sc [kN]	100
dist.sc [mm]	210.0



## Transverse Reinforcement Design

Data	
q ULS [kN/m]	35.9
Lslab [mm]	220
I [mm <sup>4</sup> ]	1.11E+07
nt [uni]	8
d [mm]	8

Design	
Ast Tot [mm <sup>2</sup> ]	150.7
Ast/bar [mm <sup>2</sup> ]	18.8
d [mm]	6
$\rho_1$	0.79%

Slab Trans. Resistance	
X [mm]	0.42
MRd (-) [kN.m]	3.21
VRd [kN]	16.31

Shear Resistance	
$\tau_{bar}$ [Mpa]	226
Vr,b/bar [kN]	11.4
Vr,b Tot [kN]	273
Vxz FRP [kN]	245
Vxz,c [kN]	475
Vyz CRIT [kN]	886

Splitting resistance	
hc [mm]	64
P,FRP [kN]	70.9
P,bar [kN]	92.7

FRP Stregth, Vsd	
Direction	
0°	90°
Shear [Mpa]	
111.0	38.1
Intralaminar [Mpa]	
13.6	
Bearing [Mpa]	
19.8	17.5

Transverse Actions	
	ULS
Vy [kN]	4.13
Mz [kN.m]	0.87
$\delta_{max}$ [mm]	0.032
$\chi$	2.62E-06
$\epsilon_x$	5.37E-05
$\sigma_x$ [Mpa]	2.00

CNR-DT205		
6	< db = 8 <	8
Dist. [mm]	Exact	Design
wx	125	125
wy	36	40
e	32	40
s	18	20
Total y	45	49



## Longitudinal Shear

XZ-Plane		
	Hogging	Sagging
L eff [m]	1.3	3.5
Fsc [kN]	928	1101
$\tau_{xz}$ [Mpa]	4.42	1.69

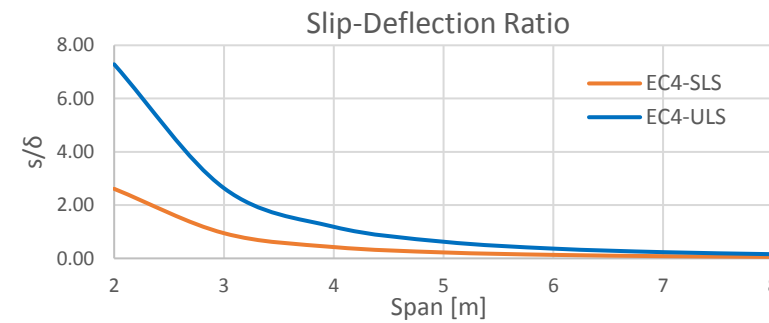
Resistance		
	Hogging	Sagging
Trans.	149	218
Conn.	234	-
Adhesive	671	917
<b>Total [kN]/[Mpa]</b>	1054	1135
	5.02	1.75

Critical YZ-Plane		
Fsc,crit [kN]	464	551
VRd,crit [kN]	886	
$\tau_{yz,crit}$ [Mpa]	4.46	1.94
$\tau_{yz,rd}$ [Mpa]	8.52	3.12

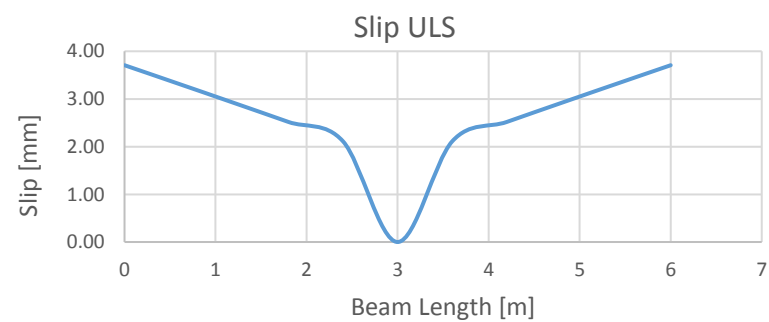
## Slip

Slip	
$\epsilon_{slip, end}$	0.00021
$\tau_{slip,c}$ [Mpa]	5.8
$\tau_{slip,s}$ [Mpa]	43.1
Slip flow [mm]	0.21
Slip Total [mm]	0.63

FRP - Concrete Slip - ULS		
Section	L [m]	sULS [mm]
0	0	3.71
1	0.60	3.31
2	1.20	2.92
3	1.80	2.52
4	2.40	2.11
5	3.00	0.00
6	3.60	2.11
7	4.20	2.52
8	4.80	2.92
9	5.40	3.31
10	6.00	3.71



Slip Deflection Ratio						
L [m]	$\delta$ SLS [mm]	s SLS [mm]	s/ $\delta$ SLS	$\delta$ ULS [mm]	s ULS [mm]	s/ $\delta$ ULS
2	0.13	0.34	2.61	0.65	0.95	7.29
3	0.64	0.61	0.95	3.17	1.69	2.64
4	2.01	0.85	0.43	9.88	2.38	1.19
5	4.88	1.09	0.22	23.98	3.05	0.63
6	10.09	1.33	0.13	49.55	3.71	0.37
7	18.67	1.56	0.08	91.60	4.36	0.23
8	31.81	1.79	0.06	156.05	5.01	0.16

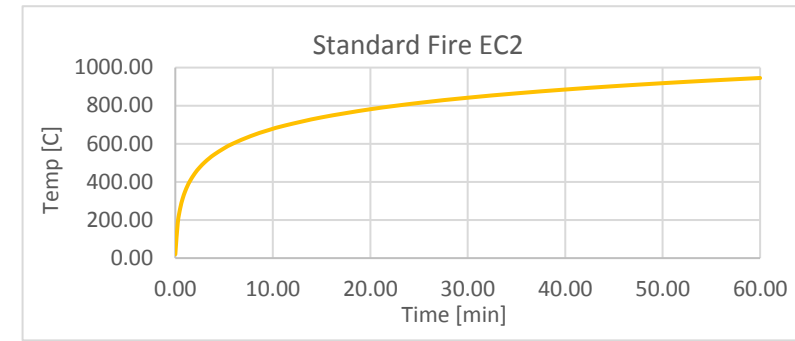
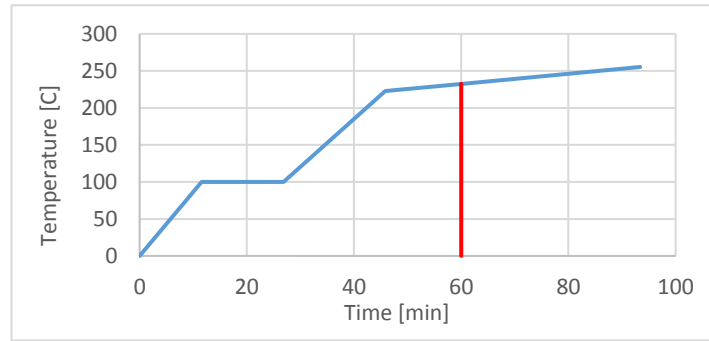


	SLS	ULS
A0	5.66E+03	5.66E+03
Io	3.04E+08	8.42E+07
A'	1.35E-05	4.50E-05
$\alpha$	9.64E-07	1.00E-06
$\beta$	1.77E-02	3.54E-02
k [kN/mm]	13.6	
Prd [kN]	12.6	

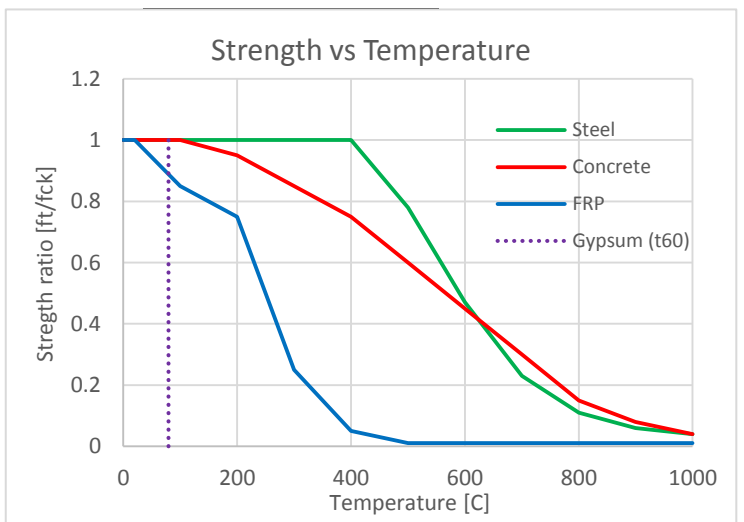
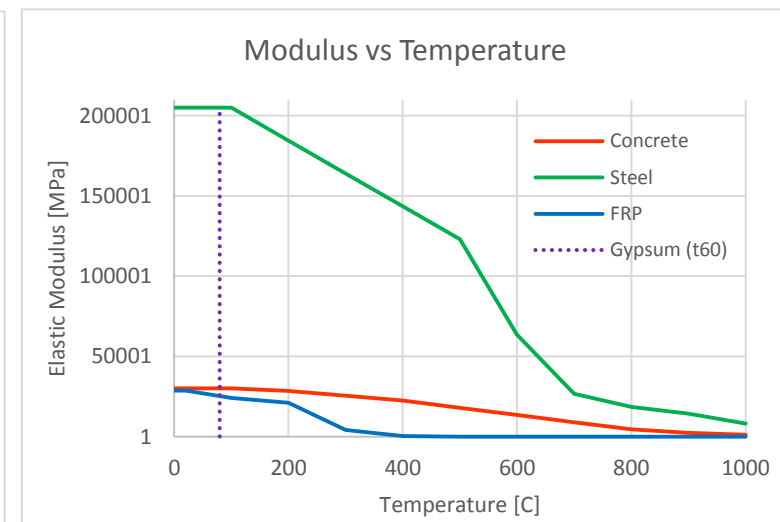
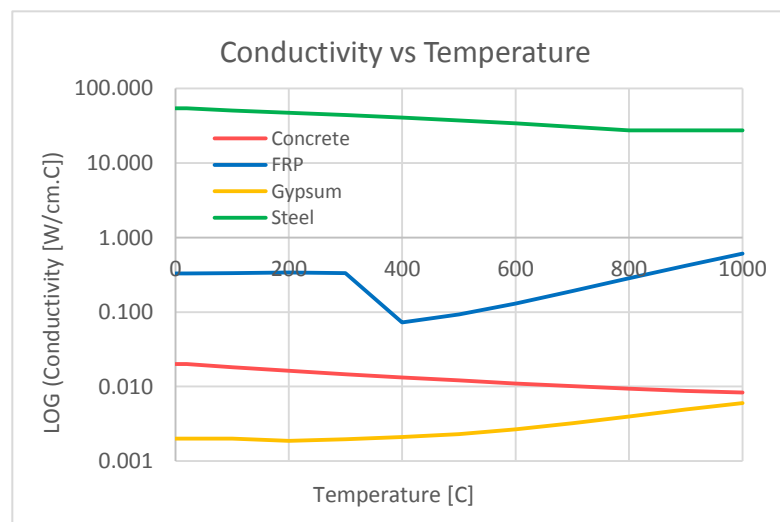
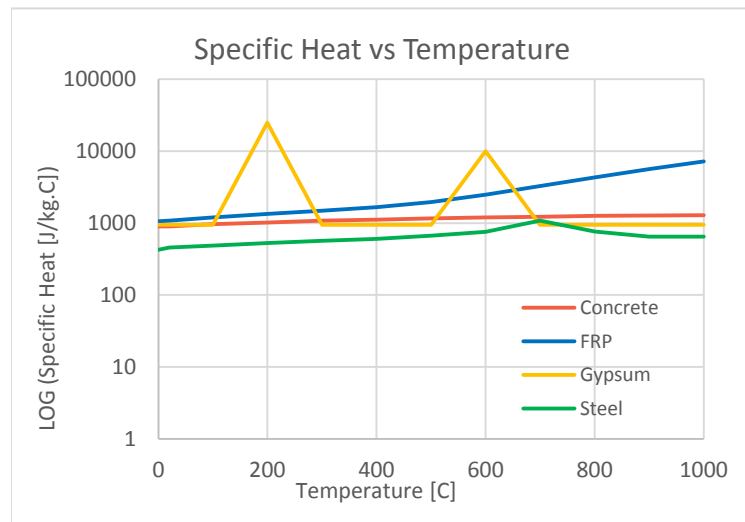
### Analysis in case of fire

Actions	
Ed [kN/m]	25.7
$\gamma_{fi}$	0.7
Ed,fi [kN/m]	18.0
Ed,fi [Mpa]	3.5
Results	
Vfi [kN]	54
Mfi [kN.m]	81
Ex,fi [Mpa]	
Concrete	29962
FRP	25154
E,fi	20895
G,fi	12203

Time - Temp prediction for Gypsum			
tp [mm]	20		
Time [min]		Temp [C]	
t0	0	0	T0
t1	12	100.0	T
t2	27	100.0	T
t3	46	222.8	T1
t60	60	232.5	T60
tBurn	93	255.3	TBurn
Results			
FRP Temp [C]			79.6
Mrd,fi / Mrd			0.8%
Vrd,fi / Vrd			33.4%



Temp [C]	Concrete						Steel					FRP								Gypsum	
	fc,t / fck	$\epsilon_{c1,t}$	Ec [Mpa]	$\epsilon_{cu1,t}$	$\lambda_c$ [W/cm.C]	Cc [J/kg.C]	f <sub>sy,t</sub> / f <sub>yk</sub>	E <sub>s,t</sub> / E <sub>s</sub>	E <sub>s</sub> [Mpa]	$\lambda_s$ [W/cm.C]	C <sub>s</sub> [J/kg.C]	f <sub>p,t</sub> / f <sub>pk</sub>	E <sub>p</sub> [Mpa]	$\sigma_{curv}$	$\sigma_{p,fi} / \sigma_p$	$\sigma_{p,fi}$	E <sub>p,fi</sub>	$\lambda_p$ [W/cm.C]	C <sub>p</sub> [J/kg.C]	$\lambda_g$ [W/cm.C]	C <sub>g</sub> [J/kg.C]
0	1.00	0.002	29962	0.020	0.0200	900	1	1	205000	54.0	425	1	28600	242.8	1	278.4615	28600	0.330	1056.8	0.0020	950
20	1.00	0.003	29962	0.020	0.0200	900	1	1	205000	54.0	457	1	28600	242.8	1	278.4615	28600	0.331	1085.6	0.0020	950
100	1.00	0.004	29962	0.023	0.0181	964	1	1	205000	50.7	488	0.85	24310	239.4	1.0	274.6	23974	0.334	1201.0	0.0020	950
200	0.95	0.006	28464	0.025	0.0163	1020	1	0.9	184500	47.3	530	0.75	21450	237.9	1.0	272.9	21018	0.339	1345.3	0.0019	25000
300	0.85	0.007	25468	0.028	0.0147	1080	1	0.8	164000	44.0	565	0.25	7150	141.0	0.6	161.8	4154	0.333	1492.2	0.0020	950
400	0.75	0.010	22471	0.030	0.0133	1120	1	0.7	143500	40.7	606	0.05	1430	39.8	0.2	45.6	234	0.073	1672.9	0.0021	950
500	0.60	0.015	17977	0.033	0.0121	1160	0.78	0.6	123000	37.4	667	0.01	286	9.1	0.0	10.5	11	0.093	1971.1	0.0023	950
600	0.45	0.025	13483	0.035	0.0110	1200	0.47	0.31	63550	34.0	760	0.01	286	9.8	0.0	11.3	12	0.130	2481.7	0.0027	10000
700	0.30	0.025	8989	0.038	0.0101	1230	0.23	0.13	26650	30.7	1080	0.01	286	10.5	0.0	12.1	12	0.191	3262.5	0.0032	950
800	0.15	0.025	4494	0.040	0.0093	1260	0.11	0.09	18450	27.4	767	0.01	286	11.2	0.0	12.9	13	0.284	4325.3	0.0040	950
900	0.08	0.025	2397	0.043	0.0088	1280	0.06	0.07	14350	27.3	650	0.01	286	11.9	0.0	13.6	14	0.419	5648.7	0.0049	950
1000	0.04	0.025	1198	0.045	0.0083	1290	0.04	0.04	8200	27.3	650	0.01	286	12.6	0.1	14.4	15	0.609	7194.6	0.0060	950

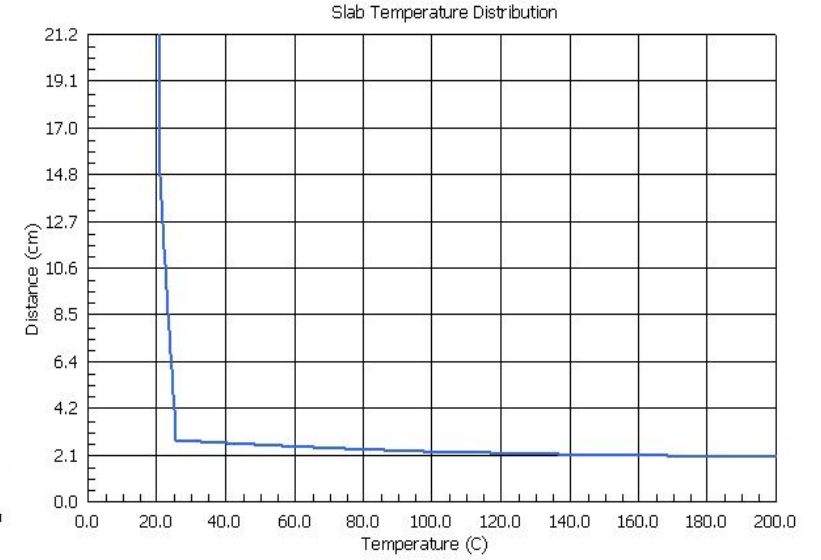
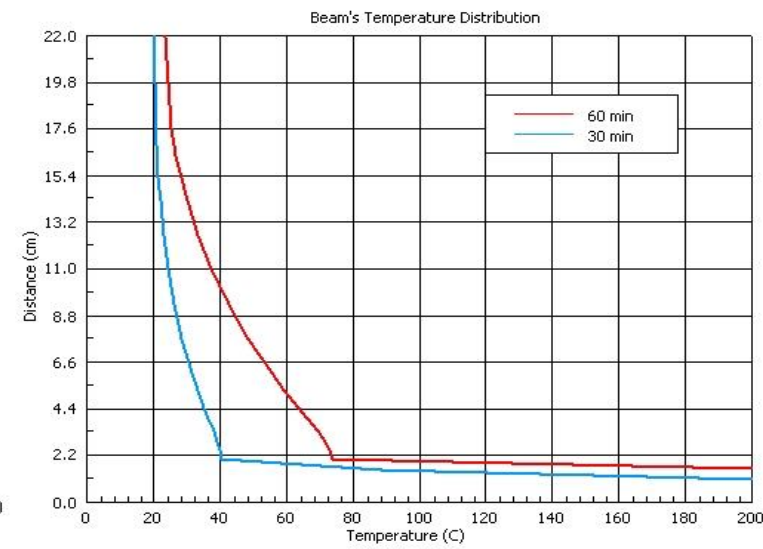
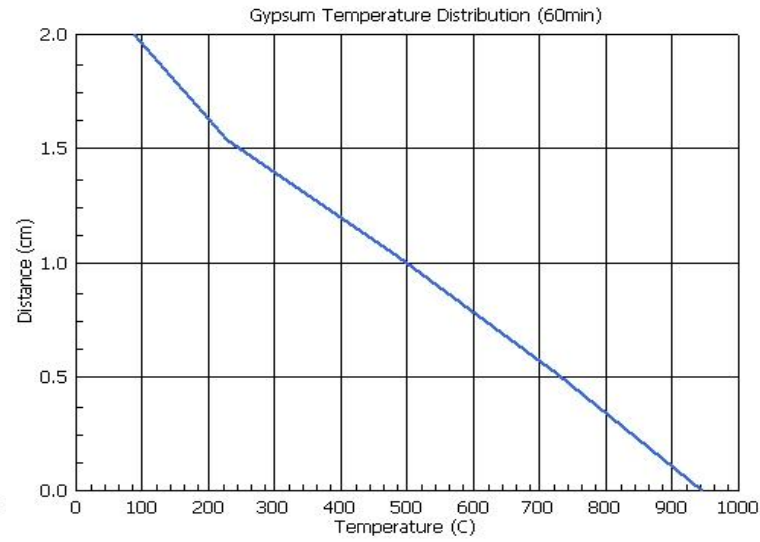
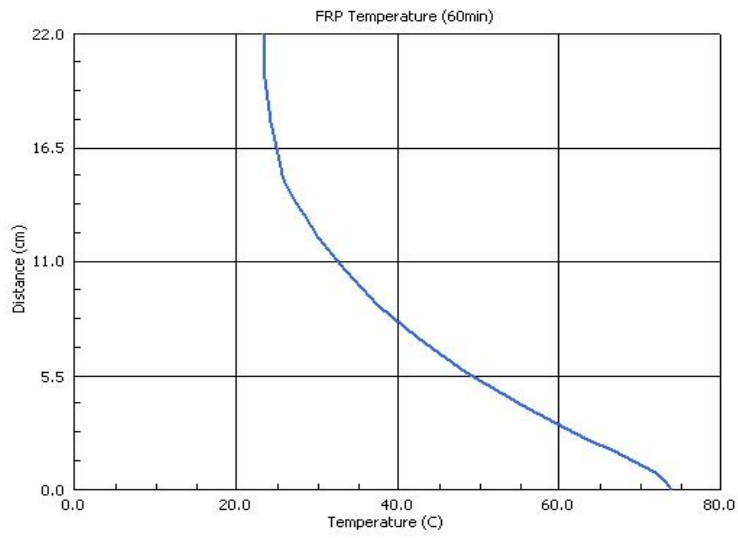


## Beam Resistance for R60

Material Properties	
fpc [Mpa]	276
fpt [Mpa]	241
fcd [Mpa]	11.3
fyd [Mpa]	391
Ec [Mpa]	29962
Ep [Mpa]	25154
Es [Mpa]	205000
E [Mpa]	20895
G [Mpa]	12203
Load	
q,fi [kN/m]	18
Material Properties	
E,fi	G,fi
29962	12484.1
25154	9316.2
205000	80078.1

ULS bending moment		
Forces [kN]	Sagging - M(+)	Hogging - M(-)
Rsp	265533	
Rcp	564421	0
Rpp[c]	565730	685702
Rpp1	417556	259518
Rpp2	0	266433
Rpp3	579202	661423
Resistant bending moment		
Mcp	49331418	64092334
Mtp	114759876	91170195
MRd [kN.m]	164091294	155262529
	164	155
Design bending moment [kN.m]		
Mu [kN.m]	27	54
M=0 (x1,x2)	1.3	4.7
Shear Resistance		
V ULS [kN]	5	54
VR [kN]	453	
VRd [kN]	113	

## FEM Model Results



## Composite Slab Design

Data	
tf,dek [mm]	10
tweb [mm]	6
Ast [mm <sup>2</sup> ]	402.1
H tot [mm]	212
Slab Properties	
Aslab [mm <sup>2</sup> ]	82000
Ix [mm <sup>4</sup> ]	4.59E+07
Deck Properties	
ft,0	185
ft,90	40
fc,0	185
fc,90	75
f <sub>T</sub>	20
fc <sub>b,0</sub>	115
fc <sub>b,90</sub>	54
Ex [Mpa]	21500
Ey [Mpa]	8500
Gxy [Mpa]	3000
Ix [mm <sup>4</sup> ]	9.11E+07
Qx [mm <sup>3</sup> ]	1376100
Adeck [mm <sup>2</sup> ]	35312
FEM Model	
Adeck (2) [mm <sup>2</sup> ]	29240
Ix (2) [mm <sup>4</sup> ]	8.35E+07

Loads [kN/m <sup>2</sup> ]	
qdek	0.65
qc	2.05
q other	0.5
qvar	1.5
q SLS	4.7
q ULS	6.6
Actions	
Vxy SLS [kN]	11.8
Vxy ULS [kN]	16.4
Vsc, xz SLS [kN]	325.6
Vsc, xz ULS [kN]	835.7
Vsc, crit [kN]	929.3
M SLS [kN.m]	14.7
M ULS [kN.m]	20.5
Reduction Factors	
kM	0.125
kV	0.5
ns	6.8
np	0.72

Composite Slab [mm]	
Hu, elast [mm]	81.0
HI, elast [mm]	131.0
yp, tfdek [mm]	7.3
Hup [mm]	89.3
A comp [mm <sup>2</sup> ]	117312
Ix,elast [mm <sup>4</sup> ]	2.96E+08
Ix,plast [mm <sup>4</sup> ]	3.37E+08
E comp [Mpa]	27415
δ SLS [mm]	4.72
δ ULS [mm]	5.80
FEM Model	
δ SLS [mm]	16.72
δ ULS [mm]	23.38
Forces [N]	
Fc	929333
Fs	157353
Fp1	1342492
Fp2	507508
Fp3	1850000
ULS Resistance	
Mrd(+) (2) [kN.m]	34.5
Vrd, (2) [kN]	292.4
Vrd, xy [kN]	369.4
Vsc, xz [kN]	1250

Elastic		τ [MPa]
Q	Sum Q	SLS
3277213		0.13
541	2521353	0.10
1260406	2520812	0.10
1260406		0.05

τ ave. [Mpa]	0.10
k	1.30

Axial stress	Real	FEM
σ <sub>c</sub> [Mpa]	4.40	15.57
σ <sub>p</sub> [Mpa]	5.11	18.08

Plastic		τ [MPa]
Q	Sum Q	ULS
6702950		0.33
147831	6850781	0.33
3763	846330	0.04
842567		0.04

τ ave. [Mpa]	0.14
k	2.39

No shear interaction	
y slab [mm]	41
Ix,tot	1.37E+08
δ SLS [mm]	10.18
δ ULS [mm]	14.24
Uncracked Slab	
σ <sub>s</sub> [Mpa]	0
fctm [Mpa]	2.21
Fc,t [N]	45313.6
Fc,c [N]	45313.6
Fs [N]	0
M elast [kN.m]	2.5
δ uncrk[mm]	4.69
Deck Resistance	
Vrd,deck [kN]	353.1
Mrd(+) [kN.m]	31.8
δ SLS [mm]	19.53
δ ULS [mm]	<b>27.31</b>

